Seasonal Evolution of Supraglacial Lakes on a Major East Antarctic Outlet Glacier

LANGLEY, EMILY,SUSAN

Emily Langley

Seasonal Evolution of Supraglacial Lakes on a Major East Antarctic Outlet Glacier

Supraglacial lakes (SGLs) are ponds of water that develop in topographic undulations on glaciers and ice sheets during the ablation season. They have been extensively studied in Greenland and, to a lesser extent, the Antarctic Peninsula, where they are thought to influence ice motion and ice shelf stability. In East Antarctica, however, we have limited understanding of SGLs and very few reports of their existence. Using 153 optical satellite scenes and meteorological records from 2000-2013, this study provides a multi-year analysis of the evolution of SGLs and associated melt features on an East Antarctic outlet glacier - Langhovde glacier - in Dronning Maud Land (69˚11'S, 39˚32'E). The focus is on four variables (number of lakes, total lake area, mean lake area, and number of surface channels) which are mapped at a temporal resolution of just a few days to a few weeks over the 13 ablation seasons. The results demonstrate that the surface hydrological network of Langhovde Glacier is highly dynamic, with significant inter-annual variability in the four measured variables. SGLs are shown to exist on both the floating ice tongue and the grounded ice sheet, developing up to 18.1 km inland of the grounding line and at an elevation of ~670 m. Three pathways of lake evolution are identified: (i) refreezing of SGLs, (ii) *in situ* drainage on the floating ice tongue during peak temperatures, and (iii) overspilling of SGLs into supraglacial channels located on the grounded and floating ice. The possibility of lakes draining on the grounded ice sheet is also explored and tentatively suggested. Thus, the behaviour of these SGLs show strong similarities to those observed on Greenland and the Antarctic Peninsula, suggesting that they may currently (or in the near future) affect surface energy balance and seasonal ice sheet dynamics in some regions of East Antarctica.

Seasonal Evolution of Supraglacial Lakes on a major East Antarctic Outlet Glacier

Emily Langley

Thesis submitted for the degree of Master of Science

Department of Geography

University of Durham

January 2016

Table of Contents

List of Figures

List of Tables

Statement of Copyright

Acknowledgements

Firstly, I would like to thank Prof Chris Stokes and Dr Stewart Jamieson for their advice and endless support throughout this Master's degree. I would also like to thank Dr Amber Leeson for generating hydro-routing and RACMO2.3 data, and for her continued enthusiasm for this project.

Finally, I would like to thank my fellow postgraduate students and the Geography department as a whole; it has been an amazing year. In particular, I would like to thank those who lived with me in the GIS-lab; we always made the long hours in a window-less room somehow enjoyable.

Introduction

1.1 Significance of Supraglacial Lakes

Supraglacial lakes (SGLs) are ponds of water that form on top of glaciers and ice sheets. They develop from the pooling or runoff of meltwater in topographic undulations during the ablation season (Echelmeyer et al., 1991). The accumulation and drainage of SGLs represents an important component of an ice sheet's response to climate change (Shepherd et al., 2009; Banwell et al., 2013). Research has shown that the drainage of SGLs and the transfer of meltwater to the subglacial environment can alter the effective pressure of the ice-bed interface, which is defined as ice overburden minus subglacial water pressure (Bartholomew et al., 2012). Consequently, during the ablation season, increased meltwater input to the subglacial system may result in transient periods where the ice-bed interface is more highly pressurized than the pressure caused by the weight of ice above, resulting in enhanced basal sliding (Bartholomew et al., 2011).

To date, the majority of research has focused on SGLs on the Greenland Ice Sheet (GrIS) where lake drainage events have been reported to be synchronous with transient acceleration, ice-sheet uplift, and horizontal displacement, followed by subsidence and deceleration once meltwater has been dispersed (Das et al., 2008; Zwally et al., 2002). However, more recent reports have questioned the consistent positive relationship between ice velocity and meltwater discharge, with the efficiency of the drainage system playing a crucial part in determining the seasonal and long-term impact on annual ice motion (Rothlisberger, 1972; Rothlisberger and Lang, 1987; Schoof, 2010). Where meltwater flux through the subglacial drainage system is low, it is thought that a spatially distributed system with low capacity dominates, meaning meltwater is inefficiently transported, raising water pressures and therefore increasing basal sliding (Bartholomew et al., 2011). However, for systems that have a high subglacial water flux, drainage conduits can become enlarged, developing efficient 'R-channels', increasing effective pressure and reducing basal sliding (Schoof, 2010). It is therefore possible that an efficient drainage system can develop throughout the ablation season, with the quantity of meltwater supplied having a different effect (Bartholomew et al., 2012). This theory has been extrapolated to demonstrate the long-term, decadal slowdown of ice velocity in Greenland, despite an increase in supraglacial meltwater (Tedstone et al., 2015). Due to the strong coupling between SGLs and surface air temperatures (e.g. Hoffman et al., 2011), SGLs have been reported to be migrating

further inland, with higher elevations experiencing longer and more intense melt seasons (Fitzpatrick et al., 2014; Steffan et al., 2004).

Research on the role of SGLs on ice shelf stability has been focused on the Antarctic Peninsula (AP), which has been subject to unprecedented ice shelf deterioration over the past two decades (Domack et al., 2005). SGLs can promote ice-shelf instability by assisting crevasse penetration and by generating tensile flexure stresses in response to the loading and unloading of meltwater (MacAyeal and Sergienko, 2013). Disintegration of ice shelves can reduce the buttressing forces that usually reduce ice flow above grounding lines (Scambos et al., 2004), causing an acceleration of glaciers inland (Glasser et al., 2011). The rapid breakup of Larsen B ice shelf in the AP in 2002 (and subsequent acceleration of its tributary glaciers) has been associated with the widespread drainage of ~ 3000 SGLs (Glasser and Scambos, 2008). This dramatic movement of meltwater was potentially instigated by one lake, which generated a ripple effect of fracturing and drainage across the ice shelf (Banwell et al., 2013).

Despite the potential influence of SGLs to transient ice sheet acceleration and ice shelf dynamics on the GrIS and in the AP, SGLs are not currently incorporated into mass balance calculations and sea level rise models (Das et al., 2008; Sundal et al., 2009; Bartholomew et al., 2011). Warming ocean temperatures, reduced sea ice concentrations, and sub-ice shelf melting are considered key components of climate change that influence the mass balance and stability of ice sheets (Cook et al., 2005). However, a recent report on 178 marine-terminating glaciers in Greenland demonstrates that 84% of the increase in the rate of mass loss since 2009 has been due to increased surface melting and runoff (Enderlin et al., 2014). Therefore, an improved understanding of SGL prevalence and intensity across all ice sheets and shelves is necessary to discern ice stability and future sea level rise.

1.2 East Antarctica

Despite the potential importance of SGLs on seasonal ice sheet dynamics, research on their evolution in Antarctica has been mostly constrained to the warmer and more maritime AP. East Antarctica is remote and has often been considered less vulnerable to melt based on its relative isolation from climatic variability (Sugden et al., 1993; Alley and Whillans, 1984). However, more recent studies have questioned these ideologies, with laser altimetry and glacier terminus readings detecting dynamic thinning of

glaciers along the East Antarctic coastline (Pritchard et al., 2009; Miles et al., 2013). Surface meltwater has been detected in satellite radar backscatter, with temporal variations in air temperature causing variability in melt intensity and duration (Trusel et al., 2012; Liston and Winther, 2005). In particular, there have been reports of lakes and channels near the grounding line of the Nivlisen ice shelf, Dronning Maud Land (Kingslake et al., 2015), and along the coastline of Victoria Land (Miles et al., 2013). However, a detailed multi-year study of the evolution of SGLs in East Antarctica is currently lacking. For example, we do not know the spatiotemporal characteristics, geometry and behaviour of SGLs on East Antarctic outlet glaciers that are known to be climatically sensitive (Miles et al., 2013). Figure 1.1 highlights the vast difference in the number of publications on SGLs on Greenland, the Antarctic Peninsula and East Antarctica.

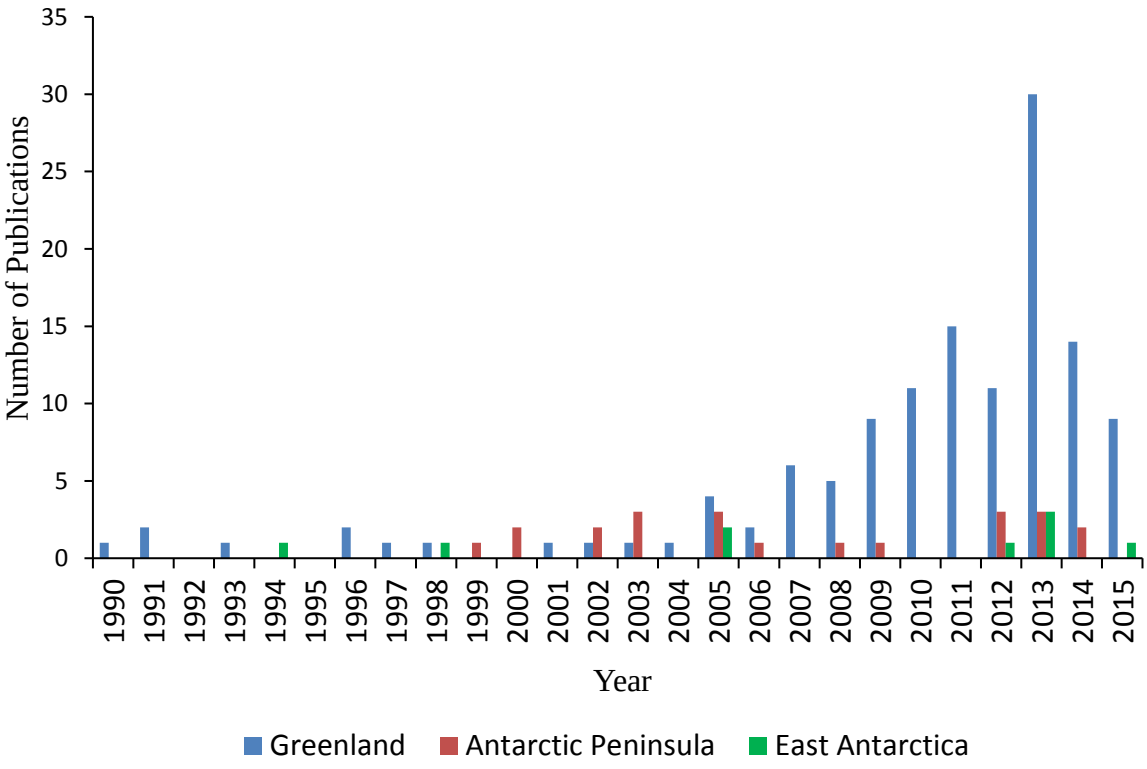

Figure 1.1: The number of published studies on SGLs on Greenland, the Antarctic Peninsula, and East Antarctica. Data were obtained from detailed searches on 'Web of Knowledge', using search terms 'Greenland supraglacial lakes' OR 'Antarctic Peninsula supraglacial lakes' OR 'East Antarctic supraglacial lakes'.

1.3 Thesis Aims and Objectives

This project aims to present the first multi-year quantitative data on the evolution and distribution of SGLs on an East Antarctic outlet glacier between 2000 and 2013. This will involve mapping the annual and inter-annual variability of SGLs, investigating their relationship to surface air temperatures, and examining whether they show behavioural similarities to lakes that potentially generate seasonal change in ice motion and ice shelf stability in Greenland and the AP. To achieve this, the following specific objectives have been addressed:

- To identify and map SGLs over each ablation season on Langhovde Glacier between 2000 and 2013.
- To examine the spatiotemporal characteristics of SGLs and surface hydrological features over this period.
- To assess the relationship between SGLs and local climate data.
- To explore whether the surface hydrological network at Langhovde Glacier demonstrates ability to influence seasonal changes in ice velocity/uplift and ice shelf stability.

1.4 Study Area

Langhovde Glacier (Figure 1.2) is 3 km wide and drains into Lützow-Holm Bay on the Soya Coast (69°11'S, 39°32'E), Dronning Maud Land. The lower 10 km of the glacier flows in a channel confined by bedrock to the west and by relatively slow moving ice to the east (Sugiyama et al., 2014). Surface velocities exceed 100 m a^{-1} within 10 km of the terminus (Fukuda et al., 2014), discharging ice into the ocean via a short (~ 1.6 to 3.3 km) ice shelf. This particular glacier was chosen because: (i) it offers over 150 cloud-free satellite images during the study period, thereby allowing more frequent observations, (ii) its proximity to Syowa research station (20 km) provides daily mean air temperature records, and (iii) widespread meltwater activity was found in satellite imagery at the start of this study.

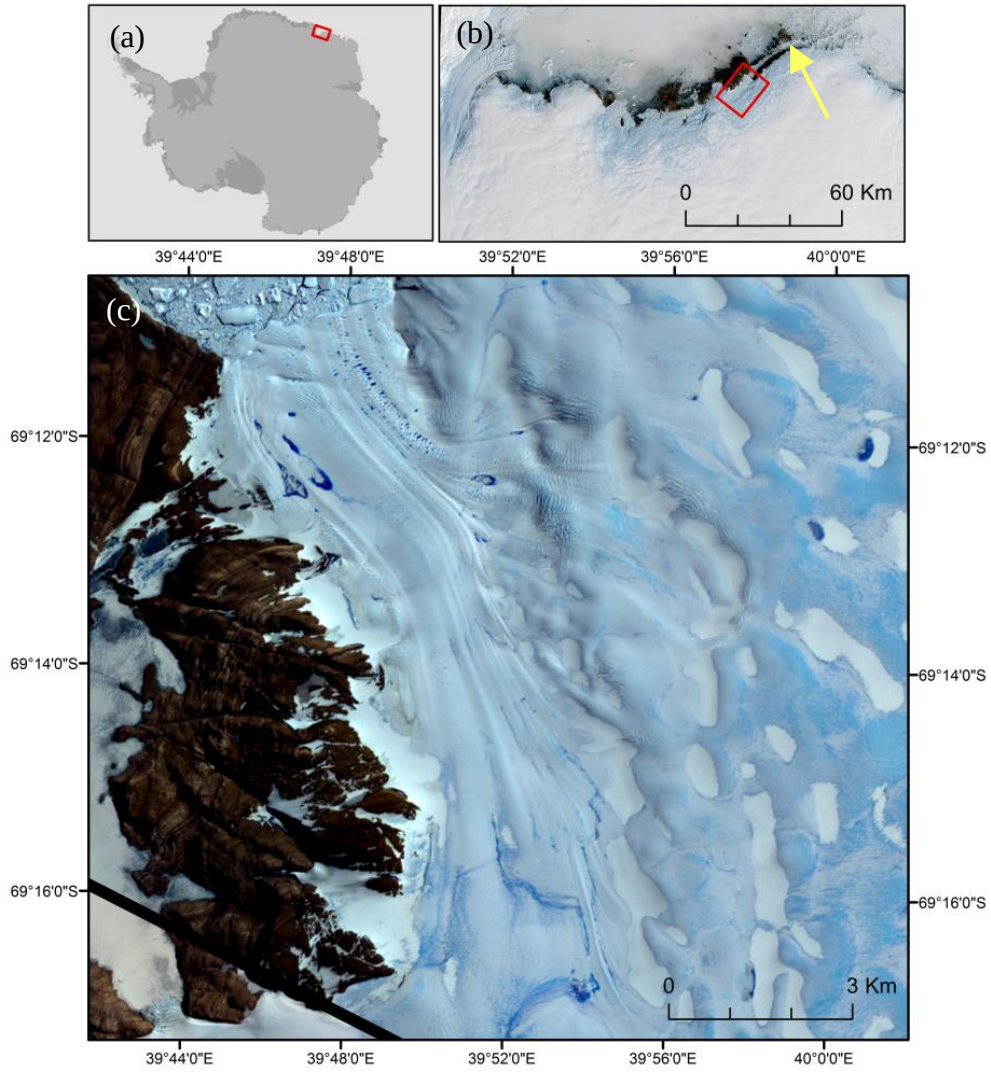

Figure 1.2: (a) Location of Soya Coast Dronning Maud Land (red box). (b) Landsat-7 image of Syowa Coast region with Langhovde Glacier (red box) and Syowa Research Station (yellow arrow). (c) ASTER image of Langhovde Glacier (4th January 2013).

A Review of Supraglacial Lakes and their Impact on Ice Sheet Dynamics

2.1 Introduction

SGLs have become a growing focus of glaciological research, with an increasing number of studies revealing their prevalence and significance across ice sheets (Leeson et al., 2014). As noted in the Introduction, they are potentially able to generate dramatic temporary ice sheet acceleration and uplift (Zwally et al., 2002; Das et al., 2008). However, although this phenomenon has been documented on the GrIS and the AP, our understanding of SGL behaviour on the East Antarctic Ice Sheet (EAIS) remains primitive. This chapter will first review the mechanisms behind lake presence and growth. This is followed by a review of SGL evolution and significance for ice sheet dynamics. Thirdly, this chapter will synthesise the methods currently used to identify and map SGLs.

2.2 Supraglacial Lake Growth

2.2.1 Governing Factors for Supraglacial Lake Occurrence

Although ephemeral (i.e. their lifespan is short-lived), SGLs can grow to substantial size over the course of the summer months, with lakes as large as 9 km^2 and 12 m in depth documented on the GrIS (Box and Ski, 2007) (Figure 2.1a). The principle factors governing the size, appearance and location of lakes are topography and induced melt energy (which typically decreases with latitude and elevation) (McMillan et al., 2007).

It is often possible to determine where SGLs will form by looking at the topography of the ice (e.g. Leeson et al., 2012). Meltwater will naturally accumulate in surface depressions or areas with restricted outflow (Lampkin and Vanderberg, 2011). In addition, meltwater will be routed to these undulations via channels which follow the topography of the ice surface (Figure 2.1b) (Das et al., 2008). Therefore, the surface topography plays an important role in determining where meltwater can accumulate and where channels are directed. This can be simulated using computational flow routing on a digital elevation model (DEM). Studies on Greenland have been able to pinpoint likely SGL locations based on where surface undulations exist and where modelled runoff accumulates (Leeson et al., 2012). The sinks (surface depressions) need to be artificially filled in order to allow meltwater to 'run off' towards the ice sheet edge (Arnold, 2010).

On the grounded ice sheet (ice in contact with the bedrock), SGLs often form in the same locations each year (Echelmeyer et al., 1991). This is because the surface topography is strongly linked to the basal topography below the ice (e.g. Serigienko, 2013; Darnell et al., 2013). Consequently, where bed perturbations exist there will often be a surface undulation to match. As bed perturbations tend to be stationary, the surface undulations usually appear in the same location each year. Therefore, processes unrelated to surface air temperature, such as ice-flow physics and bedrock properties, can control the location and size of lakes (Banwell et al., 2014).

On an ice shelf, however, ice is no longer in contact with the bed. Therefore, SGLs on floating ice shelves are not defined by bedrock topography (McGrath et al., 2012). The lack of consistent surface grooves means that lakes often appear in different locations each year, based on a different set of processes (Banwell et al., 2014). For example: suture-zone voids (Glasser et al., 2009); surface and basal crevasses (McGrath et al., 2012); and surface troughs and grooves (flow-stripes caused by acceleration and extension of ice flow) (Glasser and Gudmundsson, 2012), play an important role in determining the location and size of lakes. In addition, the flexure and fracturing of the floating ice from the loading and unloading of surface melt will also help determine the size and positioning of SGLs (e.g. MacAyeal and Sergienko, 2013).

If topographic undulations or areas with restricted outflow exist, SGLs are likely to form, assuming that surface air temperatures are sufficient (McMillan et al., 2007). Surface air temperature is a proxy for incoming shortwave/longwave radiation and sensible heat flux, which are the primary variables that govern melting (Trusel et al., 2012). Once surface melting has begun, the rate of SGL formation is often quicker due to feedback mechanisms (Tedesco et al., 2011; Morriss et al., 2013). For example, surface albedo change. The albedo is the amount of solar energy (shortwave radiation) reflected from the Earth's surface. In glaciated environments, the albedo is high due to the highly reflective nature of glacial ice (Box, 1997; Bøggild et al., 2010). The albedo of snow is approximately 0.8, meaning that 80% of incoming radiation is reflected (Tedesco et al., 2011; Konzelman, 1995). However, once surface air temperatures increase and snow begins to melt, the albedo decreases (newly melted snow has an albedo of ~ 0.7) (Bøggild et al., 2010). The reduction in albedo allows more solar radiation to be absorbed and increases the energy available for melt. Once lakes form, the albedo of standing water is even lower (~ 0.4) and this positive feedback means that

the water will heat up more quickly than the surrounding ice and begin to melt the ice upon which it sits (Box and Ski, 2007; Georgiou et al., 2009).

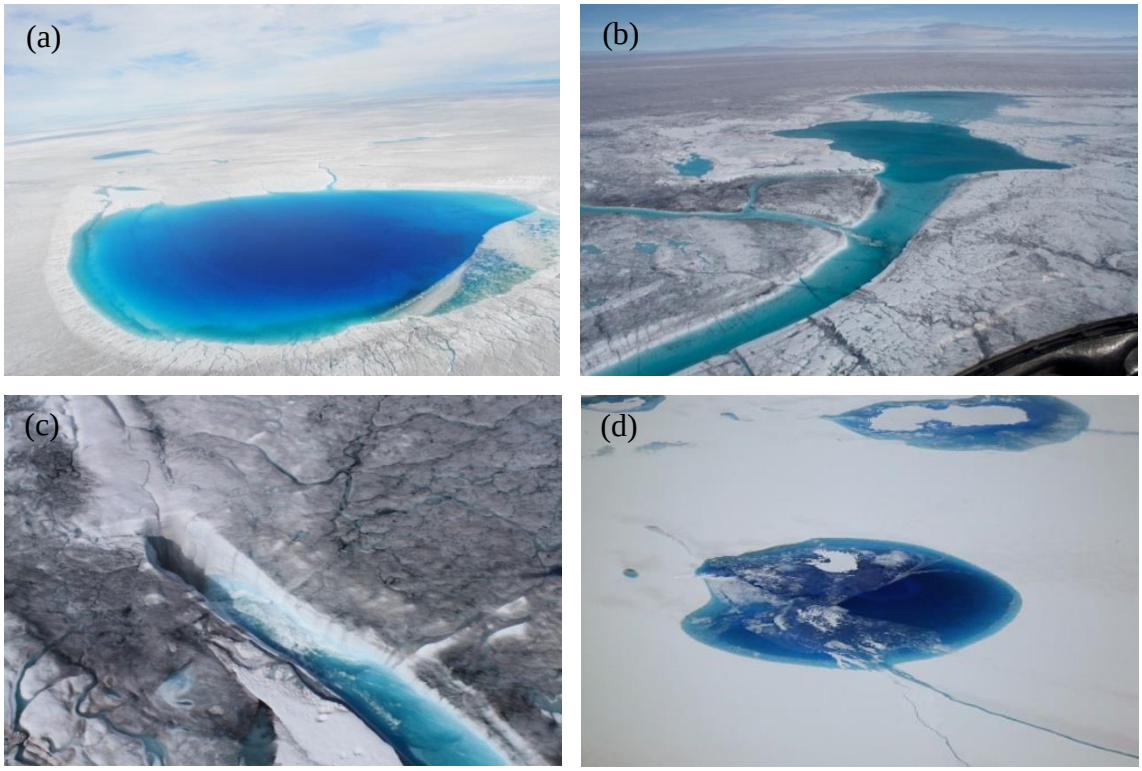

Figure 2.1: Aerial photography of supraglacial meltwater features on the Greenland ice sheet. (a) Supraglacial lake (courtesy of Malin Johansson). (b) Supraglacial lake feeding a surface channel (courtesy of Malin Johansson). (c) Supraglacial channel draining into a moulin in the ice sheet surface (courtesy of Sam Doyle). (d) Supraglacial lake refreezing at the end of the melt season (courtesy of Ed Stockard).

2.2.2 SGLs and Regional Climate

There are a number of factors which influence the surface air temperature experienced in glaciated regions. Consequently, surface air temperature variations can be large even over short distances (McMillan et al., 2007), which affects the distribution and geometry of SGLs (Selmes et al., 2011). The prevalence and duration of SGLs over an ablation season will be dependent on the meteorology of a region; key examples of external forcings are detailed below.

- **The latitude** of a region affects the amount of incoming solar radiation. Close to the poles where latitudes are highest, solar insolation reaches the surface at a low angle of incidence, so that solar energy is spread over a larger area. Therefore, at higher latitudes, the energy available for melting is lower. This has been

demonstrated on the GrIS, with an estimated decrease of 0.78^{o}C per degree latitude (Steffen and Box, 2001). The higher mean annual temperatures estimated for lower latitudes suggest a longer SGL season and intensity at these locations (e.g. McMillan et al., 2007). On the GrIS, the majority (66%) of SGLs are located at lower latitudes in the Southwest region (Selmes et al., 2011).

- **The elevation** of a region affects atmospheric pressure and therefore surface air temperature. As elevation increases, the atmospheric pressure decreases, and therefore particles expand and lose energy. This results in decreasing surface air temperatures for increasing elevations (Mernild et al., 2008). Consequently, SGL formation is elevation-dependent, with SGLs having a longer and more intense melt season at lower altitudes (Fitzpatrick et al., 2014; McMillan et al., 2007). In recent years, there has been growing concern over climate-driven migration of SGLs, with higher altitudes experiencing greater surface air temperatures and thus increased melting (e.g. Leeson et al., 2015).
- **Adiabatic warming of katabatic winds (foehn wind)** is responsible for increasing localised surface air temperatures on Greenland (e.g. Sneed and Hamilton, 2007) and Antarctica (e.g. Luckman et al., 2014). When an air mass is forced upwards on the windward slide of a slope it cools due to reduced air pressure (Parizek et al., 2004). This encourages adiabatic cooling, which forces all of the moisture onto the windward side of the slope (Speirs et al., 2011). Once the air mass passes the slope, the dry air descends and gets warmer (adiabatic warming). Because there is no moisture, the air warms up faster, causing greater surface air temperatures at higher elevations compared to the windward side (Luckman et al., 2014). This process can be responsible for increased surface air temperatures and increased surface melt at higher elevations (Parizek et al., 2004).

2.3 Supraglacial Lake Evolution

During the ablation season, SGLs will develop in one of two ways: either the snow/ice that covers a perennial lake will begin to melt to reveal a SGL from the previous year (Morriss et al., 2013), or a depression will be filled from catchment melting and routing of water to the undulation (Sundal et al., 2009). SGLs will initiate at the lower altitudes and latitudes first before becoming increasingly prevalent at higher altitudes and latitudes as the melt season progresses (Figure 2.2) (Sundal et al., 2009; Bartholomew et

al., 2011). However, once SGLs have formed, their demise can involve three principle mechanisms: refreezing, draining through ice, and drainage via surface channels (Selmes et al., 2011). Which pathway a SGL takes depends on external factors such as their elevation, volume, and proximity to surface fractures and crevasses (Zwally et al., 2002). These three principle mechanisms are summarised below.

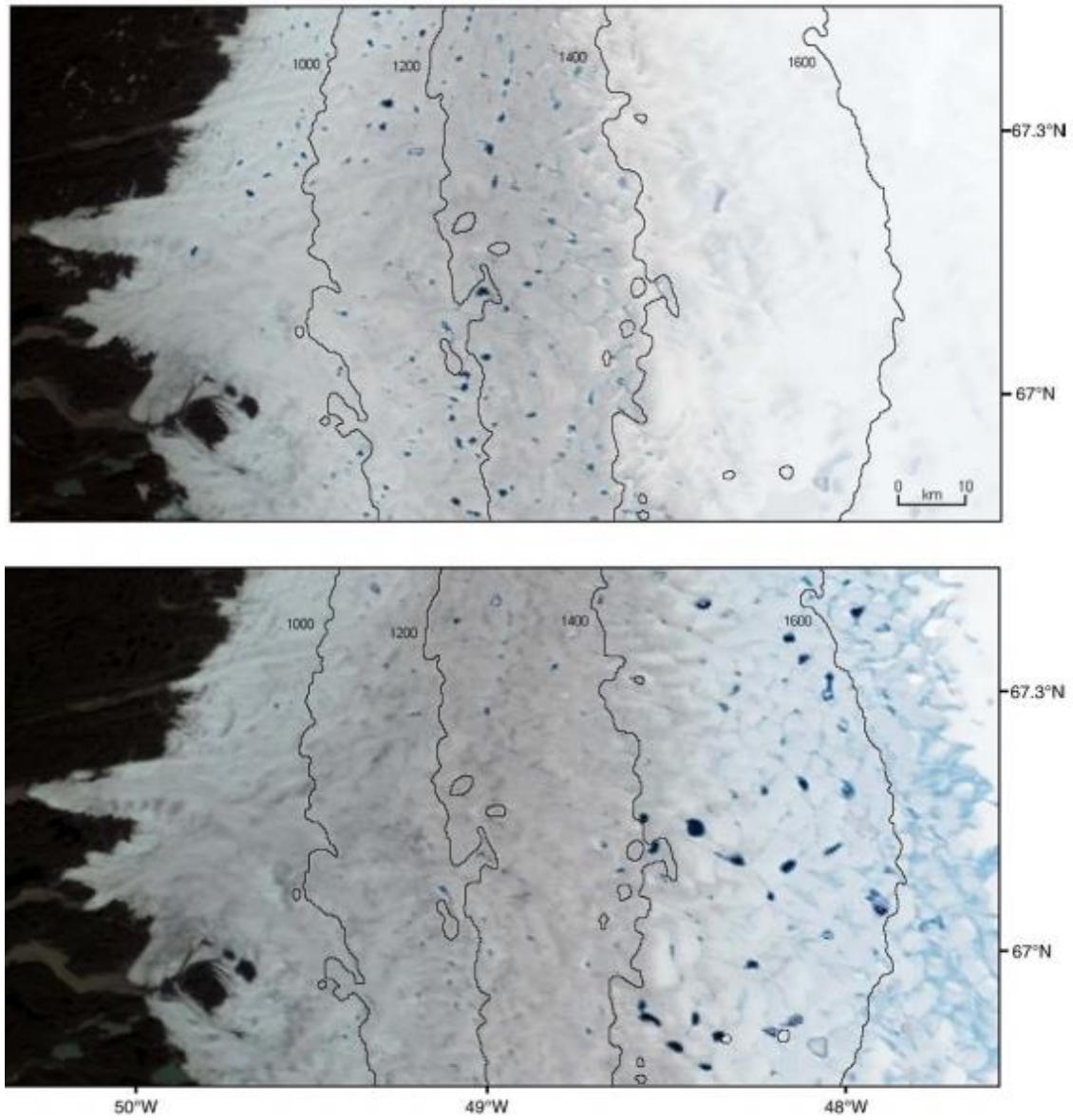

Figure 2.2: MODIS true-colour image of SGLs on the south-west part of the GrIS in 2003, taken from Sundal et al. (2009). The images are 37 days apart (11th June 2003 – 18th July 2003) and show lake growth (and drainage) at lower elevations before lakes develop at higher elevations.

2.3.1 Refreezing

Refreezing occurs at the end of the ablation season, when surface air temperatures decrease below a threshold for liquid water to exist on the ice surface (Figure 2.1d).

This process is often detected in satellite imagery by the ice that encroaches the centre of the lake (Figure 2.3) (Selmes et al., 2011). It is also characterised by an increase in the albedo of the surrounding ice, further marking the end of the ablation season (Luthje et al., 2006). In Greenland it is possible for water to be retained and buried under this surface ice and snow layer, forming perennial lakes (Koenig et al., 2015; Liang, 2012).

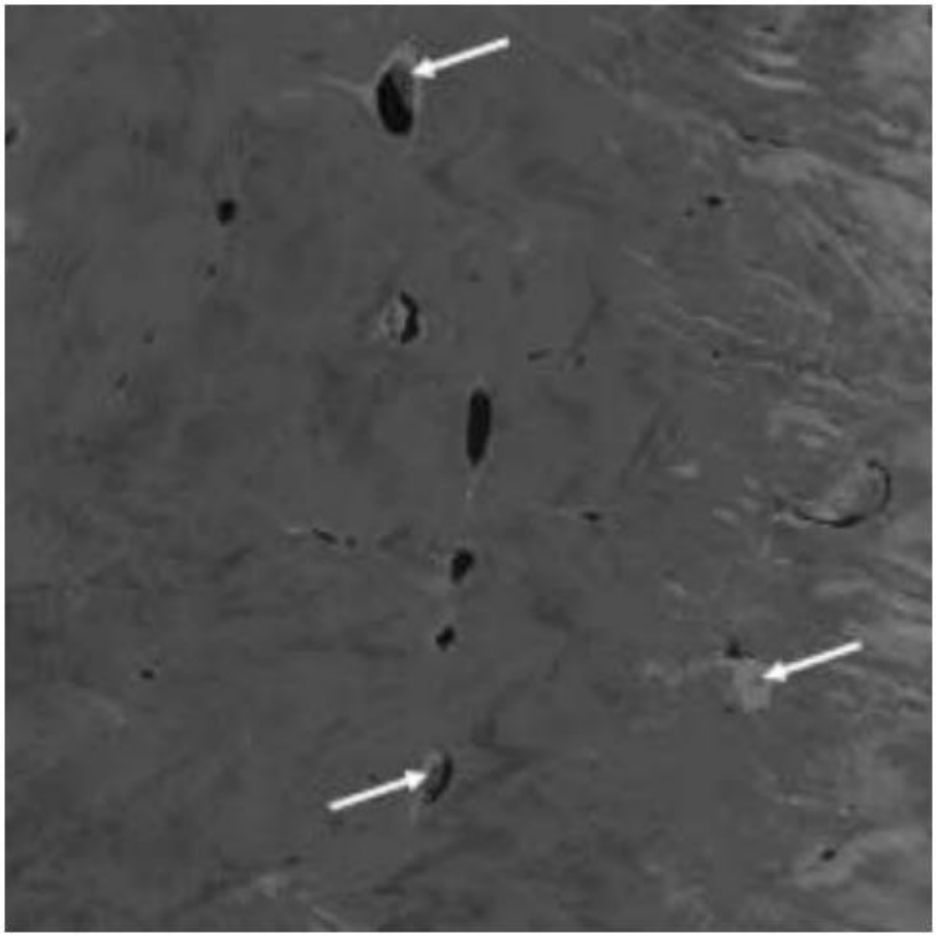

Figure 2.3: Landsat-7 satellite image showing supraglacial lakes refreezing (characterised by ice encroaching the lake surface) on the west Greenland ice sheet margin on 23rd August 2000, from Luthje et al. (2006).

2.3.2 Drainage Through-Ice

The propagation of meltwater through ice is observed both on ice sheets (e.g. Das et al., 2008) and on ice shelves (e.g. Banwell et al., 2012). Although the theory of water-filled crevasses reaching the base of glaciers has been discussed since the 1970s (Weertman, 1973), investigations into SGLs and this mechanism did not arise until 1990

(Echelmeyer and Harrison, 1990). Localised upwelling of highly turbid water on Jakobshavn Isbræ glacier, West Greenland, first correlated SGLs with subglacial meltwater (Echelmeyer and Harrison, 1990). Although Echelmeyer and Harrison (1990) rejected the idea of SGL drainage, based on insignificant variation in surface velocity readings during their observations, subsequent researchers did observe a speed-up of ice in the equilibrium zone following summer melting (Zwally et al., 2002). Consequently, the mechanism by which surface water could penetrate through thick (> 1 km) ice was theorised and modelled as 'water-driven fracture propagation' (Figure 2.4) (Alley et al., 2005; Van der Veen, 2007). For surface water to propagate the full ice thickness, abundant ponding of water at the surface and an initial water-filled crevasse are required (Alley et al., 2005; Van der Veen, 2007). The penetration of the crevasse is powered by the inflow of water, with the speed of penetration proportional to the rate of water inflow (Van der Veen, 2007). To maintain fracture propagation, and to offset refreezing, a large injection of water at a constant rate is required (Krawczynski et al., 2009). Once a full ice thickness fracture is developed, further melting and energy dissipation from the turbulent flow of water can widen and maintain a moulin that offers a more effective means of transporting meltwater to the bed throughout the ablation season (Boon and Sharp, 2003). Model predictions for fracture propagation have been confirmed by field investigations in west Greenland (Das et al., 2008). The rapid (< 2 hours) drainage of a SGL, with observable km-scale fractures (Figure 2.5), and synchronous ice-sheet uplift and transient acceleration, strongly suggest hydraulic connectivity to the bed is possible (Das et al., 2008).

On ice shelves, this process can be enhanced by the viscoelastic properties of the ice (MacAyeal and Sergienko, 2013) and the presence of basal crevasses (McGrath et al., 2012). Unlike an ice sheet, floating ice will flex in response to the loading and unloading of mass, in order to achieve hydrostatic balance (i.e. equilibrium). Consequently, the gravitational load of SGLs can induce a fracture network that will aid in the delivery of meltwater through the ice (MayAyeal and Sergienko, 2013). For example, as a SGL creates a depression on the ice surface, it will often create a forebulge in a ring surrounding the lake (Figure 2.6a). Within this ring, tensile stresses can promote a circular fracture, as well as basal radial fractures on the underneath of the ice shelf. Water within the SGL, in addition to water flowing nearby on the bare ice, can fill the ring-shaped fracture and allow it to penetrate deeper (van der Veen, 1998). The ice shelf will be viscoelastically relaxed with SGL loads on top (i.e. maintaining hydrostatic equilibrium). However, once a lake drains, it will induce complementary

fractures (similar to those described above) on the underneath of the ice shelf (Figure 2.6b), and can cause a ripple effect on the stress regime of surrounding ice, promoting further SGLs in the area to drain (Banwell et al., 2013). These empty, often uplifted lake basins are termed 'ice dolines' (Bindschadler et al., 2002). The presence of basal crevasses can aid in water-driven fracture propagation on ice shelves also (McGrath et al., 2012). Basal crevasses will greatly reduce the thickness of ice, and thus propagation distance, for meltwater to travel through. As basal crevasses often induce surface crevasses and surface depressions for meltwater to accumulate in, it is likely that SGLs on floating ice shelves are perfectly aligned with a basal crevasse (McGrath et al., 2012).

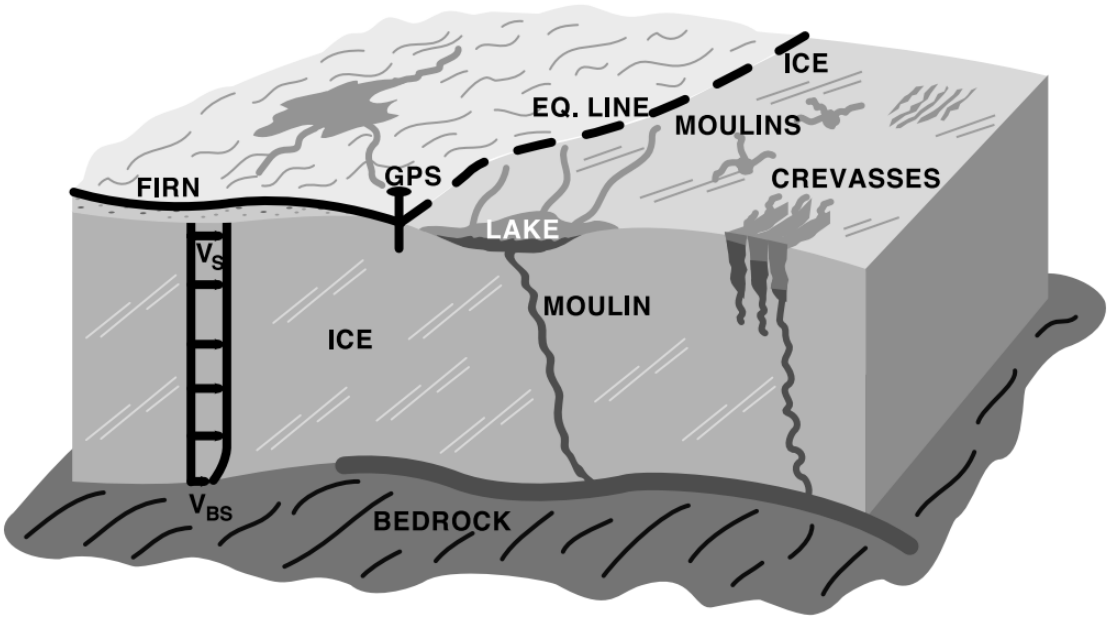

Figure 2.4: Glaciological features within the equilibrium zone, including SGLs that are able to penetrate to the ice-bed interface (taken from Zwally et al., 2002).

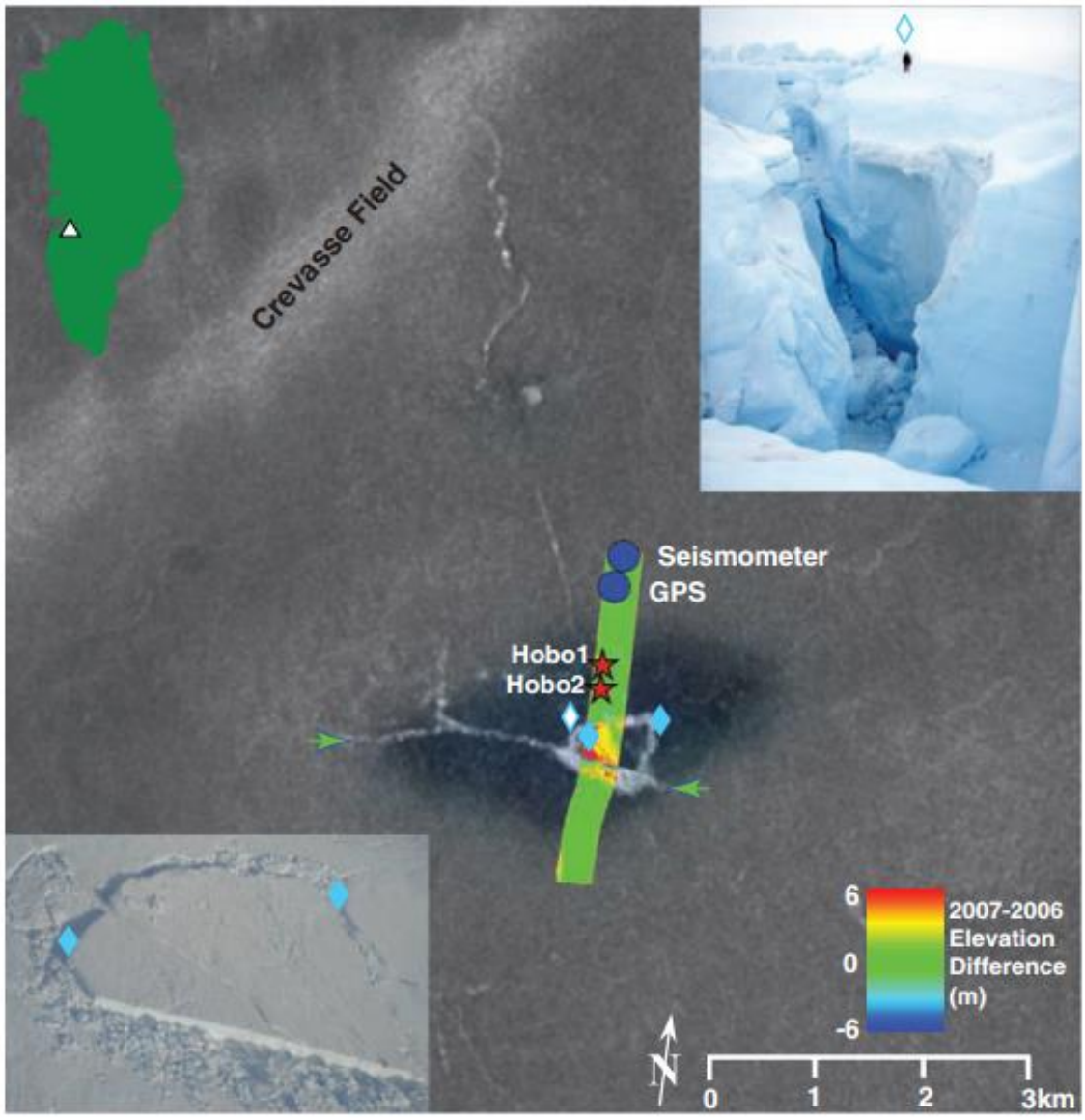

Figure 2.5: Synthetic aperture radar (SAR) image (gray-scale background) from October 2006, taken from Das et al. (2008). Image shows a large fracture (long, bright linear feature) marked by green arrows. Blue diamonds indicate locations where the sonar and ATM measurements detected large 'holes' in the lake bed before drainage in 2006. Upper-right photograph shows a 1.8 m-tall person standing close to a similar hole. Overlaid Moderate Resolution Imaging Spectroradiometer (MODIS) shows lake extent (shaded darker around the fracture) on 29th July 2006.

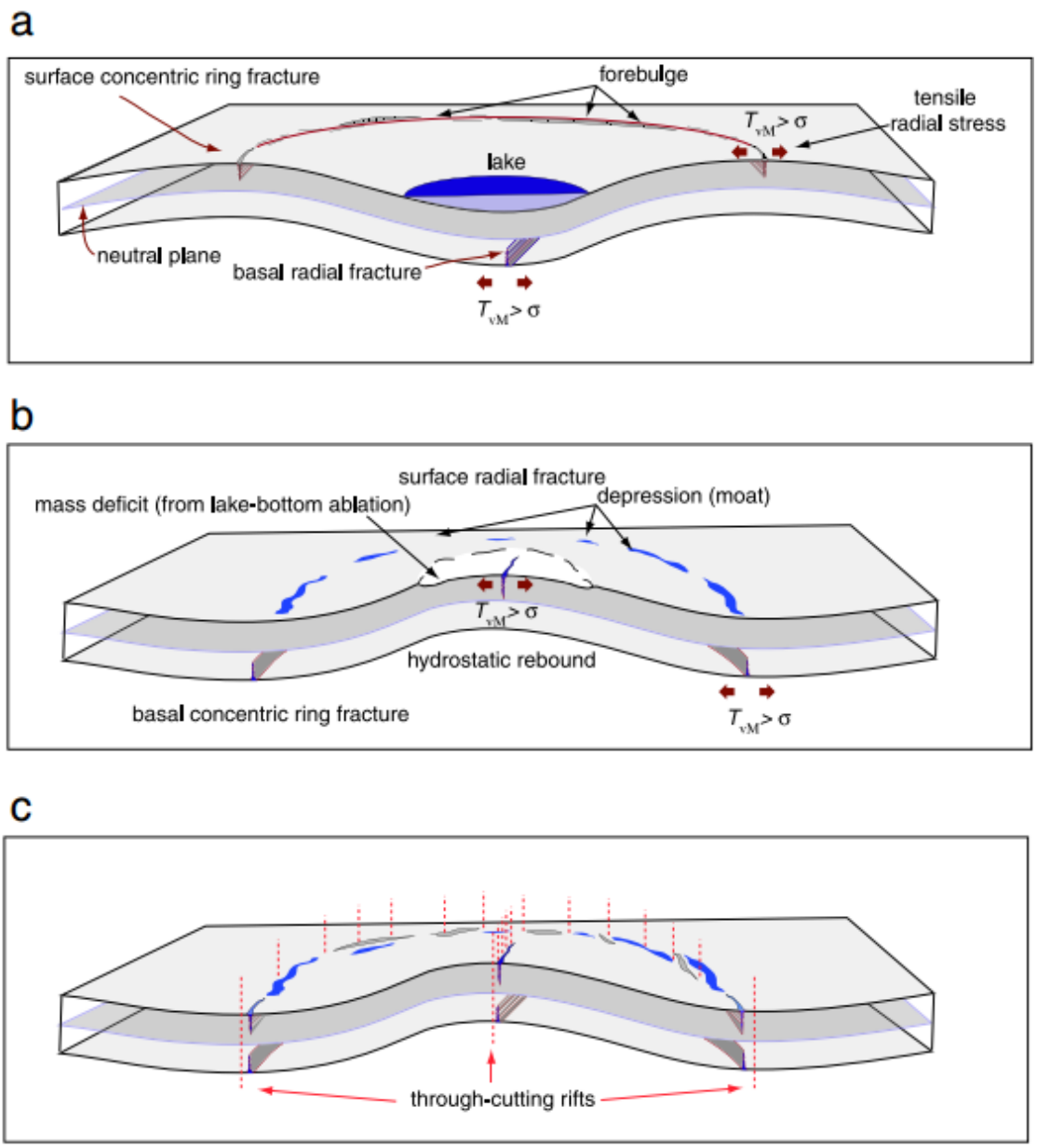

Figure 2.6: Schematic of fracture patterns and stress regimes associated with the filling and draining of SGLs on ice shelves, taken from Banwell et al. (2013). (a) As water fills an undulation and depresses the surface, it generates an upward radial forebulge. In the forebulge, downward propagating, ring fractures form at the ice shelf surface. Conversely, at the ice shelf base, tension and upward propagating fractures form directly opposite of the lake. (b) When a SGL drains, hydrostatic rebound generates tensile stress, created in an inverted forebulge, likely to produce upward propagating ring fractures. (c) The repeated filling and draining of SGLs over the years can potentially create a network of ring fractures surrounding each lake, and radial fractures below each depression.

2.3.3 Drainage via Surface Channels

The overspilling of SGLs (Figure 2.1b) into surface channels is also documented on both ice sheets (e.g. Tedesco et al., 2013) and ice shelves (e.g. Kingslake et al., 2015). The mechanism initiates when an SGL reaches its critical limit and is able to flow downslope (Raymond and Nolan, 2000). A supraglacial channel may continue to form from melting due to the turbulent dissipation of frictional heat as the water flows (Tedesco et al., 2013). The channel will incise deeper and wider depending on the magnitude of water supplied by the SGL (Tedesco et al., 2013). If moulins are present downslope of an SGL, water can be directly funnelled to the ice-bed interface (Figure 2.7). There are two modelled evolutions of SGLs considered on the EAIS: stable and unstable (Kingslake et al., 2015). Stable lake drainage occurs when lake-level drawdown is greater than channel incision, resulting in less and less meltwater being fed to the channel (and the lake does not drain completely) (Kingslake et al., 2015). Unstable lake drainage refers to when channel incision exceeds lake-level drawdown (the lake drains completely). The latter mechanism favours large lake areas (and thus greater water input) and steep channel slopes (Kingslake et al., 2015).

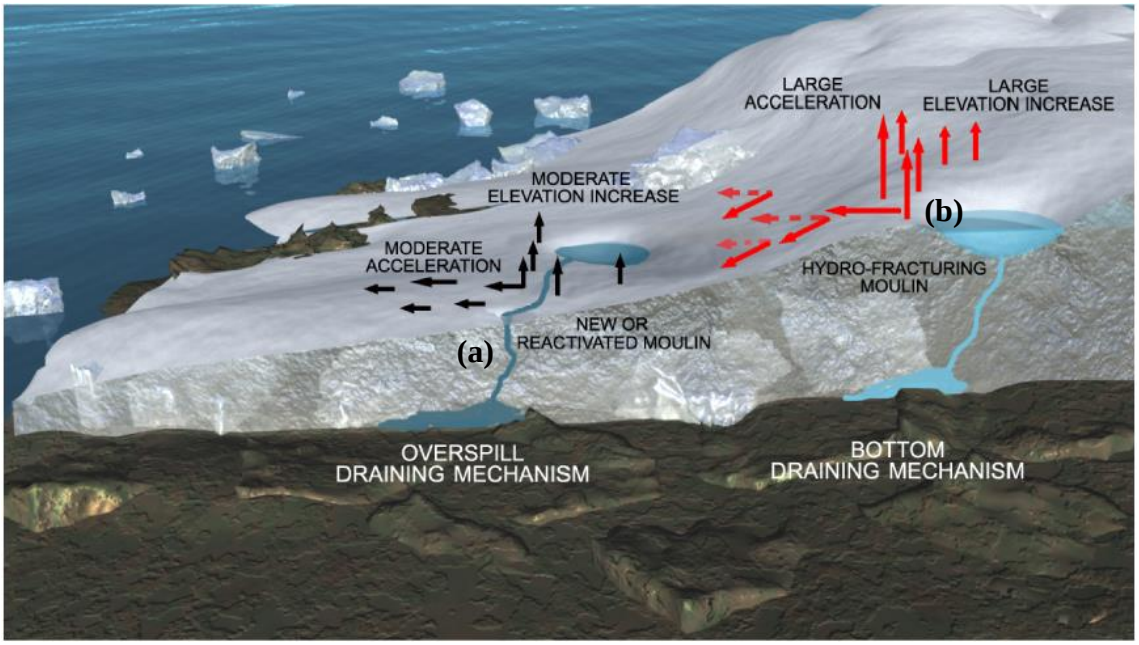

Figure 2.7: Schematic of SGL activity in the ablation zone, from Tedesco et al. (2013). (a) SGL drainage via a surface channel, which is able to navigate to a moulin on the glacier surface and feed meltwater to the ice-bed interface. (b) Fracture propagation of a SGL (Section 2.3.2).

2.4 Significance for Ice Sheet Dynamics

Although there are a number of ways SGLs develop over the course of a melt season, their ability to impact on ice sheet/shelf dynamics requires further insight. There are comparatively few studies on the impact of refreezing lakes in glaciated environments. The immobility of meltwater indicates that limited/no connections to the en- or sub-glacial systems have been made. However, the thawing and refreezing of surface melt can still impact on the surface composition, altering thermodynamics of the upper layers of glacier ice (e.g. Phillips et al., 2010; Tedesco and Steiner, 2011). Research has shown that refreezing surface melt can in fact modify the snowpack energy budget, morphology, density, and isotopic signature of the ice (Cuffey and Paterson, 2010). The following sections, however, look at drainage through-ice (on ice sheets and ice shelves) and across the surface.

2.4.1 Fracture Propagation through Ice Sheets

The supply of meltwater to the subglacial system can alter the effective pressure (defined as ice overburden minus subglacial water pressure) at the ice-bed interface. Therefore, higher water pressure (lower effective pressure) can reduce drag between the ice and the bed and result in faster sliding (Iken and Bindschadler, 1986). In addition, moulins and the flow of relatively warmer water can generate a localised warming effect on surrounding ice (termed cryo-hydrologic warming) (Phillips et al., 2010). By warming the ice, and providing more fluid, this can possibly enable further ice-sheet flow due to internal deformation (Phillips et al., 2010). The causal relationship between increased meltwater influx to the subglacial environment and increased speed-up of ice, followed by deceleration after melting ceases, initially dominated this area of research in Greenland (Zwally et al., 2002). The magnitude of interannual variations in ice acceleration was thought to be controlled by the intensity of surface melting during the ablation season (Zwally et al., 2002). However, this cause and effect is not clear, with a major control on subglacial water pressure being the structure of the drainage system (Rothlisberger, 1972; Schoof, 2010). More recent investigations (Schoof et al., 2010) have highlighted the dramatic temporary acceleration of ice in response to SGL drainage, but with no real subsequent change, and perhaps even a subsequent slow-down of ice.

The magnitude and duration of meltwater reaching the ice-bed interface is considered a key control of ice speed. Where water flux through a subglacial system is low, a spatially distributed system with low capacity predominates (Figure 2.8) (Schoof, 2010). This system is 'inefficient', and would transmit water at relatively slow speeds, typically through interlinked cavities or drainage through sediments (e.g. Hubbard and Nienow, 1997). Consequently, such systems would raise water pressure and therefore increase basal sliding.

Conversely, as more meltwater flows through the subglacial system, the interface starts to adapt. Drainage conduits become enlarged as the meltwater provides a warming mechanism, and efficient 'R-channels' develop (Rothlisberger, 1972). In this way, the drainage system can develop over the course of a melt system, from a spatially distributed inefficient system to a discrete network of efficient channels (Nienow et al., 1998). The transition to an efficient channelized system is essential in reducing the impact of lake drainage on ice velocity, and installing a drainage system that actually slows down ice velocity over the subsequent winter. However, it is important to note that the temporary imbalance between the volume of water delivered to a subglacial system and its ability to evacuate that water are accommodated by temporary spikes in subglacial water pressure even once the drainage system has become more efficient (Schoof, 2010).

Considering this, there has been growing concern over the migration of SGLs to higher elevations during warmer ablation seasons, and the initial response to meltwater flux considering that a poorly channelized subglacial system is likely (Howat et al., 2013). In southwest Greenland, the maximum elevation at which SGLs are observed has shifted 53 km inland over the past 40 years, following the inland migration of the ice-sheet equilibrium line (Howat et al., 2013). This migration has been particularly fast in the past 20 years, due to rapid regional temperature change as a result of global warming (Hanna et al., 2012). Model simulations using moderate (RCP 4.5) and extreme (RCP 8.5) climate change scenarios, have suggested an expansion of SGLs 103-110 km further inland by the year 2060, with up to half of these lakes showing potential to drain and contribute water and heat to the ice-bed interface in regions where the subglacial evacuation system is poor (Figure 2.9) (Leeson et al., 2015).

As researchers have moved away from diurnal studies of SGL drainage (Zwally et al., 2002) and onto seasonal studies (Bartholomew et al., 2012), in order to gain a more holistic understanding of the role of SGLs on interannual velocity change, a more recent

report has focused on the decadal timescale (Tedstone et al., 2015). Based on our understanding that the subglacial system is able to channelize and accommodate meltwater, it is thought that this hydrodynamic coupling has resulted in a decadal slowdown of land-terminating margins of the GrIS (Tedstone et al., 2015). Despite a 50% increase in surface meltwater production, an 8000 km^2 sector of the west GrIS margin was 12% slower in 2007-14 compared with 1985-94 (Tedstone et al., 2015). Such research suggests that these melt-influenced subglacial environments may be more resilient to projected climate warming than previously thought.

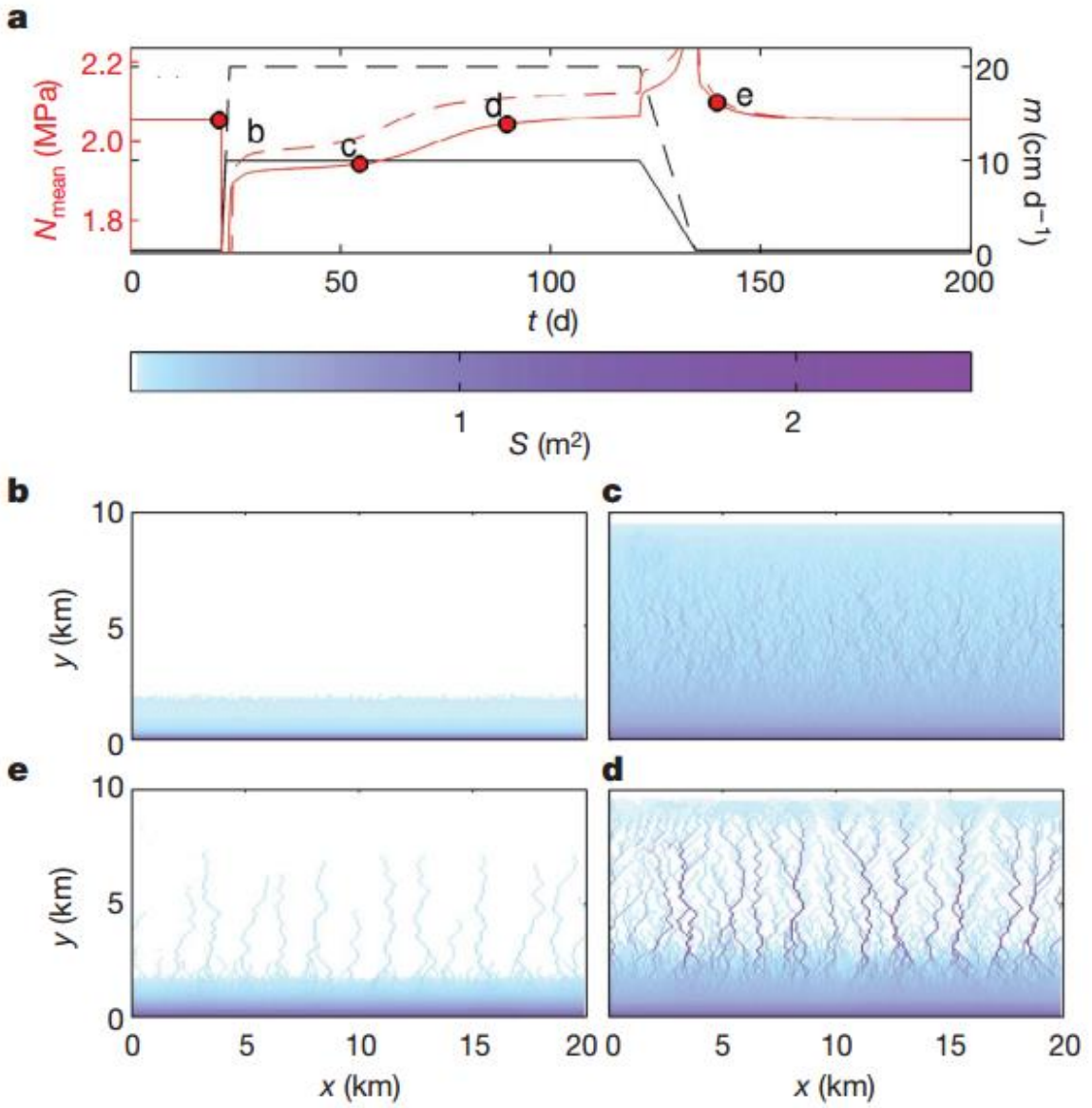

Figure 2.8: Modelling the channelization of the subglacial drainage system based on meltwater supply over the ablation season (taken from Schoof, 2010). **(a)** The spatial mean of effective pressure, *N* (overburden minus basal water pressure: a lower effective pressure reduces the ice-bed contact and allows faster sliding and vice versa) is marked as red lines, and plotted against time. *m* (black line) demarcates the water supply, which is forced by a sharp increase in water supply from a wintertime value of 0.33cmd^{-1} to a summertime value of 10cmd^{-1} (solid lines) and 20cmd^{-1} (dashed lines). This is followed by a steady water supply for 100 days and a gradual return to 0.33cmd^{-1}. Red dots marked **b-e** relate to the spatial drainage configurations displayed in panels **b-e**. **(b-e)** The spatial drainage system begins close to an unchannelized steady state with small conduits. **(b)** An abrupt increase in *m* causes a sharp drop in effective pressure, which opens up drainage conduits to accommodate this discharge but does not initially channelize the system. **(c)** After some time, efficient channelization starts, causing the effective pressure to increase (i.e. reduces sliding). **(d)** The efficiency of the drainage system continues to develop, so despite the same input of water (*m*) the effective pressure is now greater than wintertime (i.e. sliding is reduced to less than wintertime). **(e)** Both simulations in **(a)** (larger and smaller water supply) show qualitatively the same response. However, the large input of water supply (dashed line in **a**) causes a shorter and less pronounced period of low effective pressure than the smaller jump (solid line in **a**).

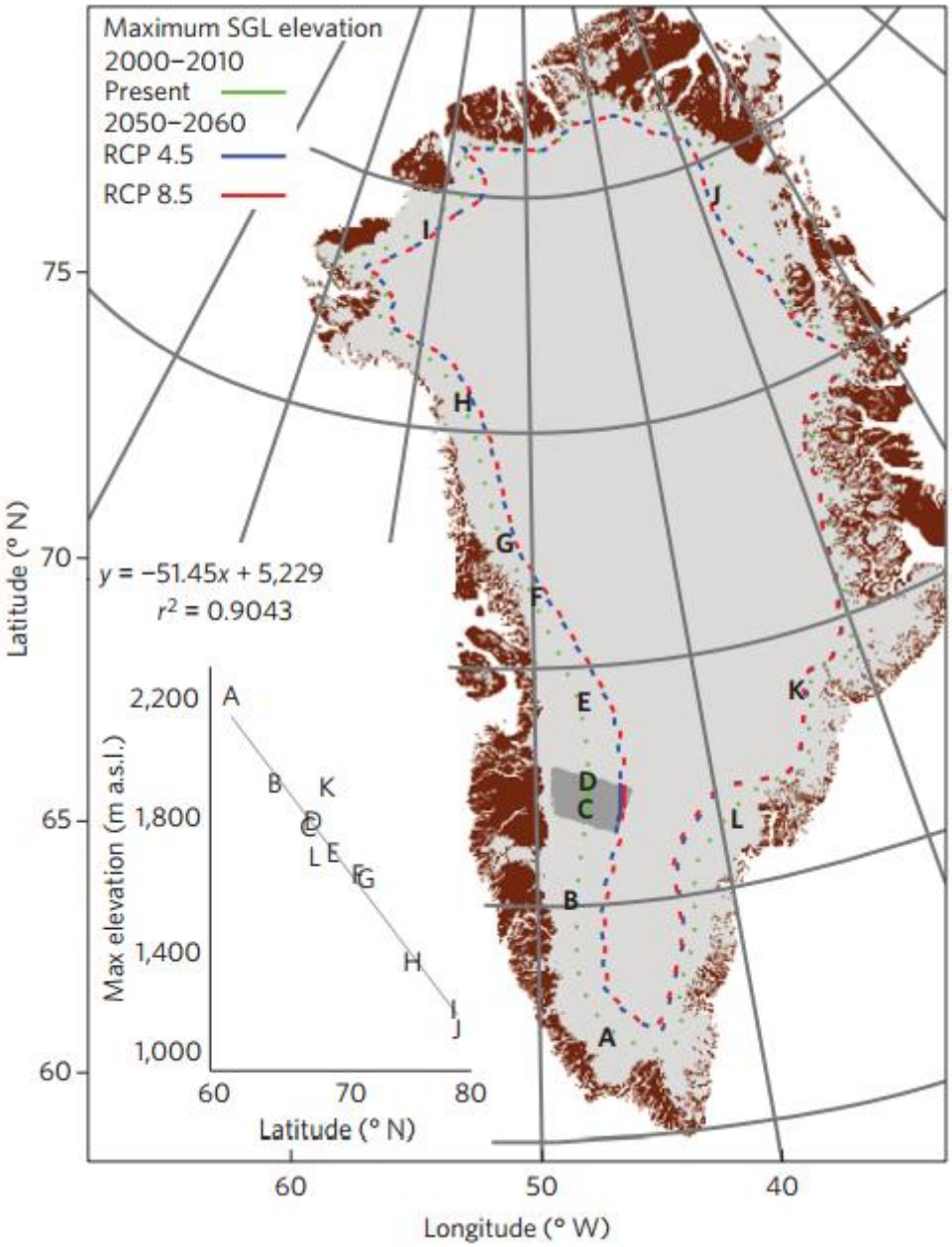

Figure 2.9: Maximum elevation of SGLs in 2000-2010 (green dashed line) and in 2050-2060 (blue dashed line for RCP 4.5 and red dashed line for RCP 8.5), taken from Leeson et al. (2015).

2.4.2 Fracture Propagation through Ice Shelves

A relatively large quantity of research on SGLs on ice shelves has taken place on the AP, with its lower latitude (~ 69.5ºS, 65ºW) favouring a comparatively warmer climate, and thus greater melting, compared to elsewhere on the Antarctic ice sheet (Trusel et al., 2012). The ice shelves that fringe the AP have shown unprecedented mass loss over the past two decades (Domack et al., 2005). The Larsen ice shelf (which is subdivided into A, B, C and D) has presented a series of collapse events (Vaughan and Doake, 1996;

Glasser and Scambos, 2008). The first of these occurred in January 1995, when the Larsen A disintegrated and released 1600 km^2 of ice (Rott et al., 1996). This was shortly followed in 2002 with the partial loss of Larsen B and 3200 km^2 of ice (Scambos et al., 2003; Rack and Rott, 2004). The two collapse events generated an influx of media and scientific attention, with great concern over future repercussions and conserving the largest remaining ice shelf on the AP: Larsen C (e.g. Scambos et al., 2004).

Although ice shelf disintegration and regrowth has been recorded for the Holocene, with sedimentary records indicating that some AP ice shelves (such as Prince Gustav Channel ice shelf) retreated mid-Holocene (Pudsey and Evans, 2001), the Larsen B collapse is unprecedented in the recent geological past (Domack et al., 2005). Research has pointed to a change in oceanic and atmospheric temperatures as a plausible mechanism (Shepherd et al., 2003). The threshold for ice shelf viability corresponds with the -1.5^{o}C January isotherm and the -5^{o}C mean annual isotherm, which have both shifted south over the past 50 years (Vaughan and Doake, 1996; Morris and Vaughan, 2003). Consequently, over the past two decades the ablation season has doubled, with the mean summer temperatures at near-melting (van den Broeke, 2005). This has generated widespread surface ablation and SGL growth on AP ice shelves, which have become the centre of debate surrounding ice shelf collapse (e.g. MacAyeal et al., 2003; Van der Veen, 2007).

Investigations have focused on studying SGLs in satellite imagery prior to the Larsen B ice shelf collapse. In particular, studies showed the dramatic increase in the number of SGLs on the ice shelf, from near zero to ~ 3000, in the decades preceding its collapse (Glasser and Scambos, 2008). Imagery indicates that within days of final disintegration most of the ~ 3000 SGLs drained, suggesting a trigger between the coordinated movement of water and ice shelf deterioration (Scambos et al., 2003; Banwell et al., 2013). A plausible mechanism is via the chain-reaction of SGL drainage (Banwell et al., 2013), described in Section 2.3.2. It is possible that the stress regime of an ice shelf that is populous with SGLs can cause dramatic, synchronous drainage. As the shelf is viscoelastically relaxed in response to the SGL loads, a single lake drainage event (known as a starter lake), can possibly create a ripple effect on the fracture network, resulting in SGLs draining in chain-reaction (Figure 2.10) (Banwell et al., 2013). Alongside the obvious holes in the ice shelf created by this mechanism, the physical removal of surface mass will also create strong flexure-induced tensile stresses (as the ice shelf tries to achieve hydrostatic balance) that will also aid in its disintegration

(MacAyeal and Sergienko, 2013). For example, for every metre of ice removed from the upper surface of the ice sheet, the underlying ice must move (via flexure) ~ 90 cm upwards to retain equilibrium (Archimedes principle). Consequently, the response of the ice shelf to a reduced surface load will itself generate stress fractures that will further aid in its deterioration (MacAyeal and Sergienko, 2013).

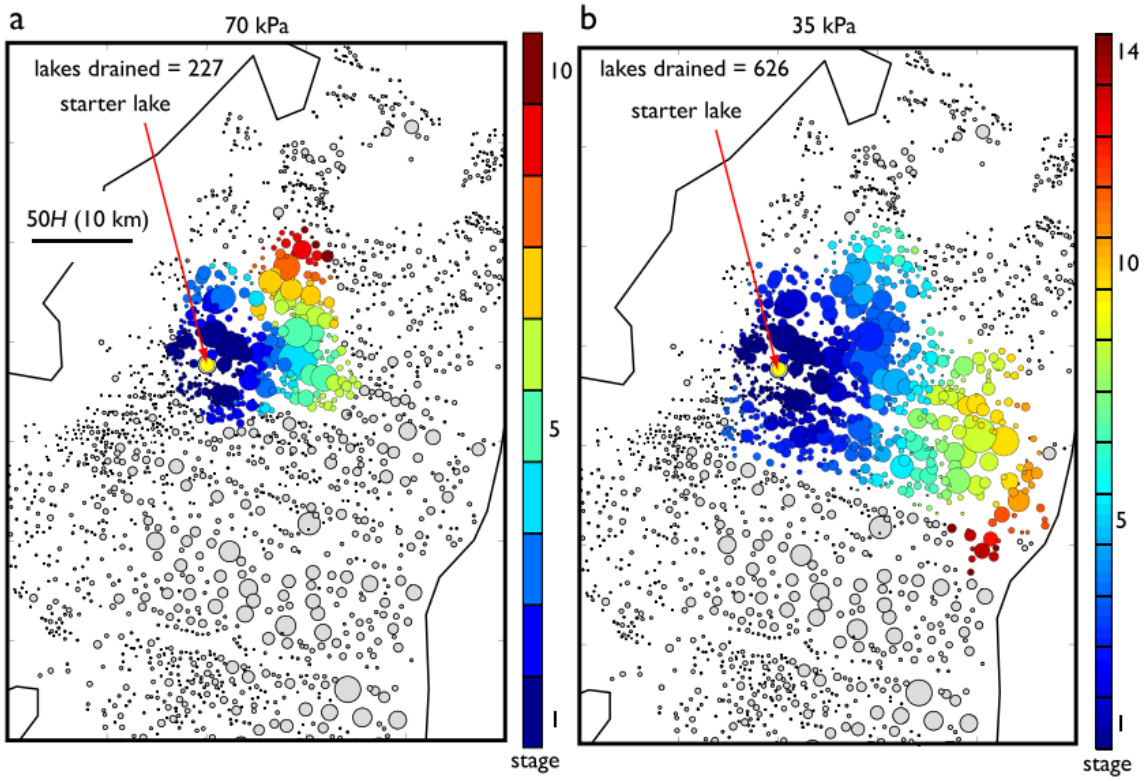

Figure 2.10: Drainage of SGLs in chain reaction on the Larsen B Ice Shelf, taken from Banwell et al. (2013). The lake considered to trigger the drainage of neighbouring lakes is labelled 'starter lake'. If an SGL is triggered by the flexure stresses of the 'starter lake' (see figure 2.10 for information on stress regimes of individual SGLs) it corresponds to stage 1 on the colour bar. If it is indirectly triggered by the 'starter lake' it's colour will correspond to a later stage (2,...,10). (a) Fracture criterion is 70 kPa. (b) Fracture criterion is 35 kPa.

2.4.3 Overspill Drainage

The drainage of lakes via surface channels introduces a number of concerns regarding ice stability. Firstly, supraglacial channels can redistribute SGL water from a basin which cannot form fracture connections to an SGL that already has (or will now be able to due to the influx of meltwater) (Kingslake et al., 2015). In this way, lakes that are unable to form connections themselves are able to contribute their meltwater to the surrounding hydrological network. Similarly, supraglacial channels can funnel water

directly to moulins across the ice sheet surface (Das et al., 2008). As moulins are often able to stay open for the entire ablation season on Greenland, this provides a constant means for surface water to reach the ice-bed interface (Tedesco et al., 2013). In addition, supraglacial channels are a direct means of removing snow and ice from the ice surface. Aside from the contribution to the basal environment, even surface channels that traverse the ice surface can influence surface energy balance (Rippin et al., 2015) and contribute to meltwater runoff at the ice shelf edge (Rignot et al., 2011). Using a combination of gravimetry and/or climatological and glaciological modelling, research has estimated that the freshwater runoff from the GrIS accounts for at least half of the mass loss (van den Broeke et al., 2009; Zwally et al., 2011; Anderson et al., 2015).

2.5 Lake Identification Methods

SGLs have been studied for the past 25 years, and data collection methods have been continuously improving. Research on SGLs has been both observational (e.g. Das et al., 2008; McMillan et al., 2007) and model-based (e.g. Banwell et al., 2012; Luthje et al., 2006). The majority of studies use satellite remote sensing products or *in situ* fieldwork (Leeson et al., 2013). *In situ* investigations provide data at a resolution to inform and verify processes that are consistent with satellite data. They also allow detailed surface energy balance measurements and real-time observations of drainage events, difficult to obtain via satellite imagery. Researches can use technology such as water-level sensors, seismic sensors, and local Global Positioning Systems (GPS) to confirm lake drainage events (e.g. Das et al., 2008). In addition, field research allows observations of smaller features such as fractures and moulins which are often difficult to detect in a satellite image. However, *in situ* field research is not always feasible, nor necessary with a growing inventory of high-resolution optical remote-sensing instruments. Although lakes can be studied in more detail on the ground, satellite imagery allows observations over a wide spatial extent and over longer periods of time. The use of Moderate Resolution Imaging Spectroradiometer (MODIS) (Sundal et al., 2009); Landsat-7 Enhanced Thematic Mapper Plus (ETM+) (Lampkin and Vanderberg, 2011); and Advanced Spaceborne Thermal Emission and Reflection Radiometer (ASTER) (Banwell et al., 2012) have allowed researches to study SGL properties over multiple ablation seasons.

The most common parameters measured from satellite imagery are (total) lake area (Sundal et al., 2009; Johannson and Brown, 2003), number of lakes (Selmes et al., 2011; Fitzpatrick et al., 2014), lake depth (Box and Ski, 2007; Banwell et al., 2014), and lake volume (Georgiou et al., 2009). Studies which focus on constraining the quantity of meltwater available to propagate to the bed find 'lake depth' and 'volume' significant indicators (e.g. Clason et al., 2014). Whereas studies which look at the spatial and temporal distributions of SGLs over a large area tend to use 'lake area' and 'number of lakes' (e.g. Leeson et al., 2012).

There are multiple techniques for measuring each of these parameters outlined in the literature. These can be manual (e.g. McMillan et al., 2007) or automated/semi-automated (e.g. Sundal et al., 2009). Manual delineation involves digitizing around lakes on a satellite image (Georgiou et al., 2009). This technique relies on the operator distinguishing the spectral properties of a thawed lake, and accurately tracing its perimeter (e.g. Glasser and Scambos, 2008). Although operator error will exist, this method is still considered the most accurate means of gaining lake area data (e.g. Leeson et al., 2013). However, it is also time-consuming and, as such, many researchers opt for automated techniques to gain more data over a shorter period of time. A study by Leeson et al. (2012) demonstrated that it takes ~ 4 hours to manually digitize lakes in a single MODIS image (~10 x ~10 km) of West Greenland, whereas an automated approach reduces the processing time to minutes. Two particular automated techniques for quantifying lake area involve 'pixel' or 'object' based classifications. The historical technique for classifying multispectral images is pixel-based image analysis (PBA), which utilises the information stored in each pixel. Selmes et al., (2011) uses PBA on MODIS imagery to calculate the total lake area. Their automated technique assigns pixels 'lake' or 'non-lake' status depending on whether its reflectance exceeds 65% of the average within a standard referencing window (Selmes et al., 2011). However, PBA often fails to map the entire lake (Johansson et al., 2013), and post-processing is limited in efficiency (Rastner et al., 2014).

Conversely, object-based image analysis (OBA) has offered a new means of calculating lake areas over the last decade. For example, Sundal et al. (2009) determine an object as a 'lake' or 'non-lake' based on their exceedance of a reflectance threshold. This technique runs by grouping pixels (an object) based on three broad factors: shape, scale and compactness (Rastner et al., 2014). This allows a more precise understanding of the entire lake, incorporating contextual factors into the model that determines 'lake' or

‘non-lake’ status (Rastner et al., 2014). Coupled with better post-processing abilities, a comparative study shows that OBA produces ~ 3% higher quality classifications than PBA (Rastner et al., 2014). However, in practise it is not as simple, as documented by Leeson et al., (2012). The OBA method (Sundal et al., 2009) was best able to report the number of lakes more accurately. However, the PBA method (Selmes et al., 2011) yielded more accurate total lake area estimates on a MODIS image compared to OBA. Being able to consider each pixel in turn at a known lake location proved more reliable.

In summary, automated techniques can offer an effective means of gaining lots of data in a short amount of time. However, this is often at the expense of accuracy. Although time-consuming, manual delineation of a high-resolution image (such as ASTER) does remain the most accurate means of identifying and mapping lakes (Leeson et al., 2012; McMillan et al., 2007). Specifically, it offers greater accuracy in determining ice-covered/non-covered lakes, calculating areal extent, and identifying smaller lakes, with fewer false positives (Leeson et al., 2012).

Study Area

Compared to both the GrIS and the AP, East Antarctica has been the focus of few SGL studies. This chapter will first review our understanding of regional climate and surface melt on the EAIS. This is followed by an overview of Langhovde Glacier, detailing the previous research that has taken place at this study site.

3.1 East Antarctica

East Antarctica is remote and believed to be less vulnerable due to its relative isolation from climatic perturbations (Alley and Whillans, 1984). However, recent thinning (2003-2007) has been detected by researches, showing a negative imbalance in some catchments of East Antarctica (King et al., 2012). Similarly, a study by Miles et al. (2013) highlights a dynamic and synchronous response of outlet glaciers on the South Pacific Coast to decadal-scale air temperature fluctuations. The overall trend has been retreating glacier terminus positions in 1974-1990, advancing in 1990-2000, and retreating in 2000-2010 (Miles et al., 2013). This cyclical variability has been considered synchronous with the Southern Annual Mode (SAM), with research indicating that a combination of increased surface air temperatures, increased melting, warming ocean temperatures and thus reduced buttressing from sea ice, are forcing mechanisms for the variability observed.

Although there is a growing body of literature into the sensitivity of outlet glaciers to oceanic and atmospheric variability, there are limited studies on the role of SGLs. Thus far, research has focused on Antarctic-wide datasets of surface melt extent and duration (e.g. Trusel et al., 2012). Although this provides limited means of understanding the behaviour of lakes, it is a useful tool in understanding the ice sheet's mass balance and locations where meltwater accumulation is greatest, conducive to SGL prevalence. More recent studies have utilised higher precision radar scatterometers (e.g. Trusel et al., 2012) documenting a greater amount of melting over a greater length of time, compared to previous reports (e.g. Tedesco et al. 2007; Torinesi et al. 2003; Picard and Fily, 2006).

Figure 3.1 documents the strong inter-annual variability in the melt intensity (liquid water production) across the entire Antarctic ice sheet. The results indicate that melting is generally confined to the low altitude regions along the coast, with nearly all ice shelves subject to some degree of melting each year (Trusel et al., 2012; Tedesco et al., 2007; Liu et al., 2006). Figure 3.2 displays the inter-annual variability in melt extent,

index, and intensity across individual regions. Dronning Maud Land (the region which encompasses Langhovde Glacier) covers a vast proportion of the coast, and is situated at similar latitude to the Antarctic Peninsula. Radar backscatter documents strong inter-annual variation in the melt extent, index, and intensity, with 2004 and 2005 presenting the highest melt seasons (Trusel et al., 2012).

A recent study by Kingslake et al. (2015) has focused on surface meltwater on a small-scale, assessing and modelling how lakes and channels interact near the grounding line of the Nivlisen ice shelf, Dronning Maud Land. The research modelled the thresholds required for channels to breach, and discussed the difference between 'stable' and 'unstable' drainage (see 2.3.3). However, a detailed multi-year study of the evolution of SGLs in East Antarctica, similar to studies on the GrIS, is still lacking. We do not currently know the spatiotemporal characteristics of SGLs around the ice sheet, their geometry, or behaviour.

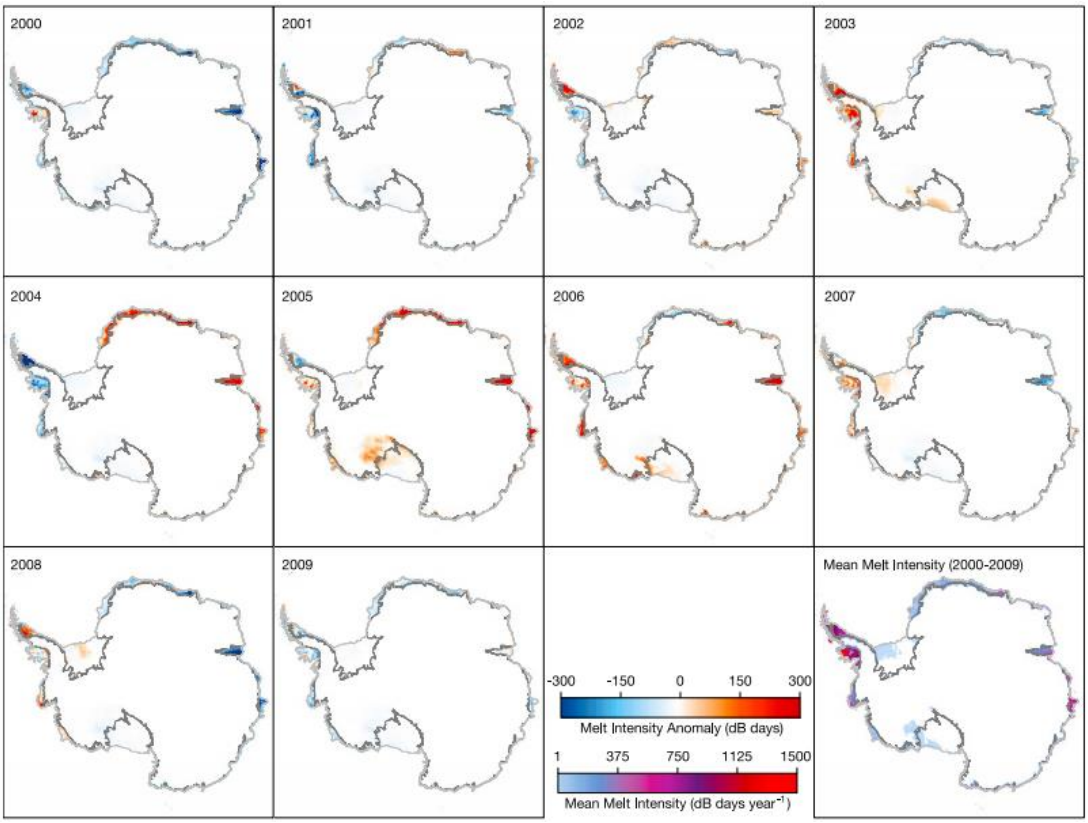

Figure 3.1: Inter-annual variability (2000-2009) of melt intensity anomalies (+ or – the average over the entire 10 year period), taken from Trusel et al. (2012).

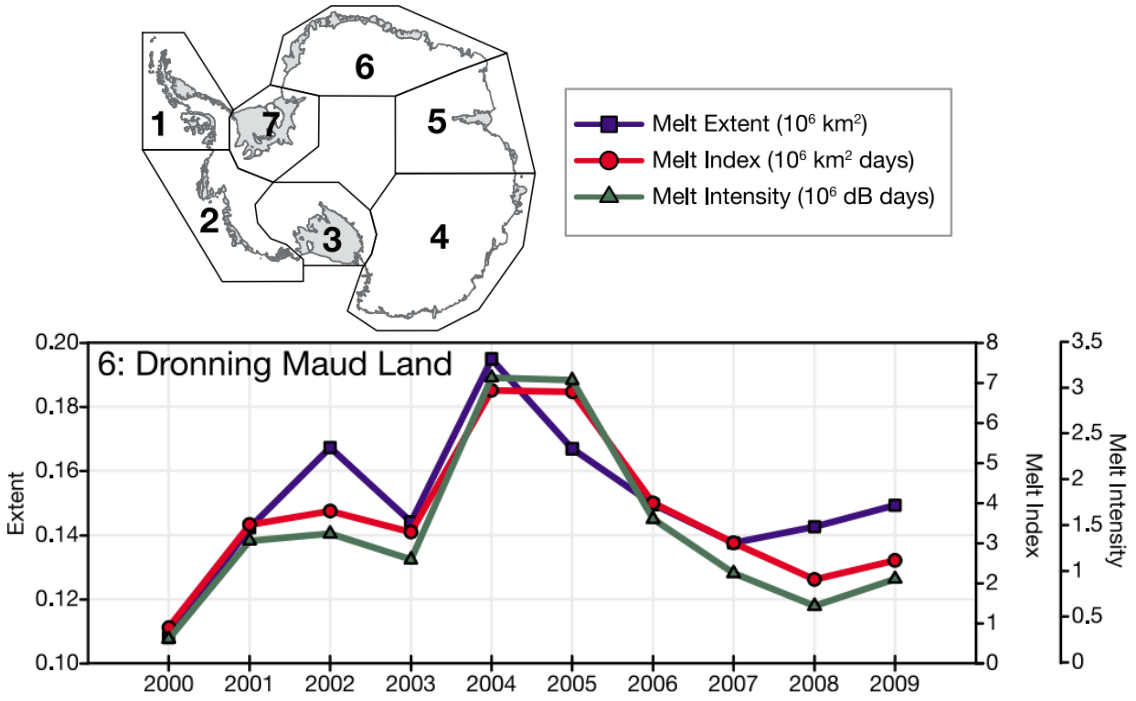

Figure 3.2: Inter-annual variability in melt extent, index, and intensity at Dronning Maud Land (number 6 on Antarctic map), taken from Trusel et al. (2012).

3.2 Langhovde Glacier, Dronning Maud Land

Langhovde Glacier flows into Lützow-Holm Bay on the Soya Coast, Dronning Maud Land (Figure 1.2). The region is at similar latitude to the Antarctic Peninsula, and has been documented to display surface meltwater on a yearly basis (Trusel et al., 2012). However, glaciological studies across the Soya Coast are sparse, primarily due to its limited accessibility (Fukuda et al., 2014). The *in situ* research that has taken place has been focused on Langhovde Glacier, due to its accessibility by helicopter from East Ongul Island (Figure 1.2). Studies by the Japanese Antarctic Research Expedition (JARE) scientists have focused on the behaviours of the glacier terminus and the microbial life in the sub-shelf cavity (Fukuda et al., 2014; Sugiyama et al., 2014). The research provides a useful indication of the stability and evolution of the glacier over a 12 year period (2000-2012). In particular, the surface elevation, terminus position, and ice flow velocity have been studied over this time frame (Fukuda et al., 2012). The terminus position of Langhovde Glacier was manually delineated from Landsat-7 and ASTER imagery over the 12 years, to produce a yearly mean displacement of the calving front (Fukuda et al., 2014). The results are displayed in Figure 3.3, and indicate that although the glacier has overall advanced by 180 m from 2000-2012 (potentially a

result of the positive SAM during this time period), there have been sudden retreats (Fukuda et al., 2014). Most notable, were those in 2000-01 (170 m), 2003 (180 m) and 2011 (200 m), due to large calving events (icebergs 400-500 m long) (Fukuda et al., 2014). Velocity readings of the glacier from 2003-2012 were obtained through feature tracking of ASTER images and COSI-Corr (Leprince et al., 2007), and field GPS measurements (Fukuda et al., 2014). The results show two tributaries (one from the south and one from the east) which merge ~4.5 km from the terminus. The velocity along the central grounding-line is > 100 m a^{-1}, reaching as high as 128 m a^{-1} (between 5th January 2011 and 25th January 2012). The inter-annual variability in the velocity at different sites along the terminus (GPS1-4) is displayed in Figure 3.4. Velocity changes are usually synchronous across all GPS locations. However, in 2008-2009, there was an acceleration of the glacier that was initiated at GPS1 (close to the terminus) before the upper reaches of GPS2-4 (Fukuda et al., 2014).

The aforementioned research on the glacier terminus position and velocity, has led to conclusions that Langhovde Glacier was relatively stable during this time period (Fukuda et al., 2014). However, the terminus is primarily controlled by these sporadic calving events rather than ice velocity (Fukuda et al., 2014). A weak correlation was found between the calving rate and both surface air temperature (correlation coefficient = 0.15; p = 0.63) and sea ice concentration (correlation coefficient = 0.39; p = 0.21). Although Fukuda et al. (2014) suggest that the likely mechanism is sea ice concentration, their study suggests potential for an alternative forcing mechanism such as supraglacial melt. Prior studies that have taken place on Langhovde Glacier have documented the presence of supraglacial meltwater (Figure 3.5). However, there has been no prior research on their distribution, sensitivity, and potential influence on the glacier.

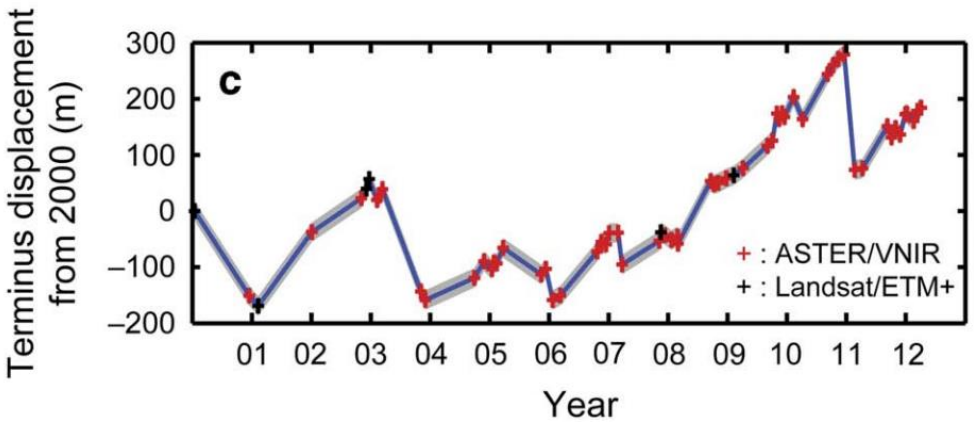

Figure 3.3: Displacement of glacier front relative to position on 15 January 2000, taken from Fukuda et al. (2014). ASTER and Landsat-7 imagery is indicated by red or black crosses, and the measurement error is defined by the width of the blue connecting lines.

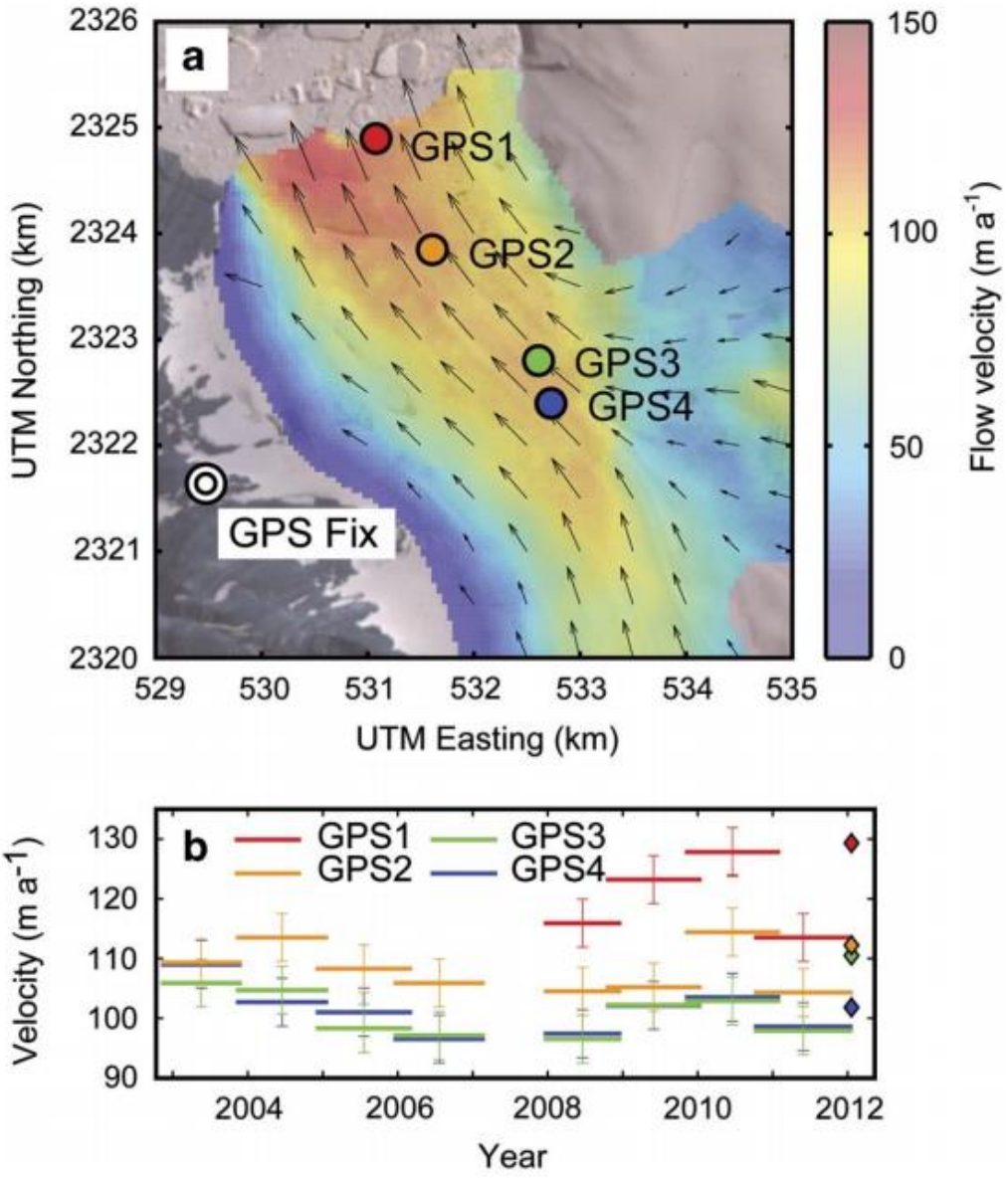

Figure 3.4: Langhove Glacier velocity readings, taken from Fukuda et al. (2014). (a) Horizontal velocity (colour scale) from feature tracking analysis between 5th January 2011 and 24th January 2012. The GPS positions (1-4) and the GPS reference station (GPS Fix) are also shown. (b) Ice flow velocity (GPS 1-4) from 2003-2012. The width of each data point highlights the period of COSI-Corr analysis.

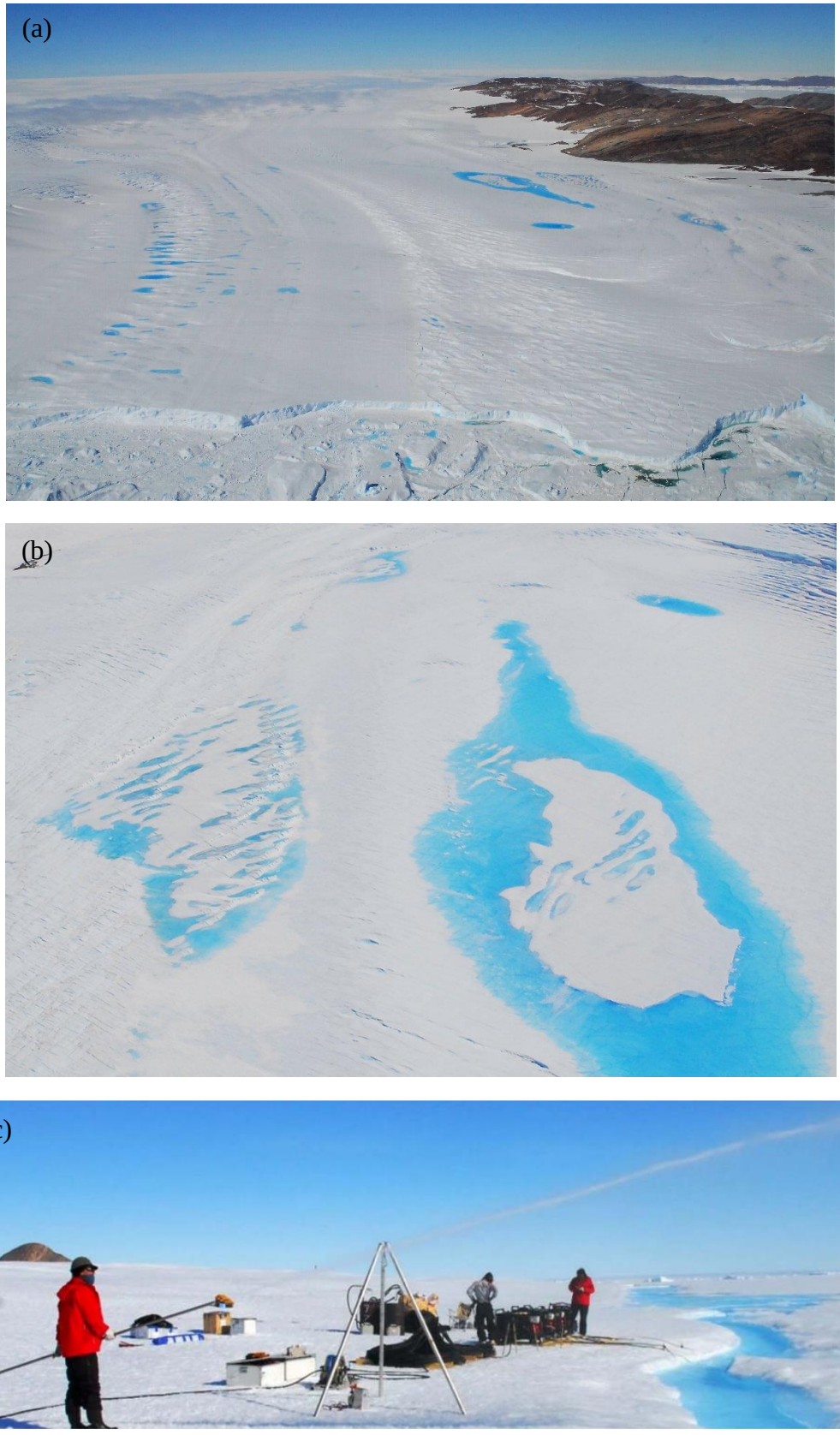

Figure 3.5: Photographs of supraglacial melt features on Langhovde Glacier, from Fukuda et al. (2012/13) field season. (a) Facing up-glacier with the bedrock outcrop on right and a series of SGLs aligned on the ice shelf. (b) Two SGLs refreezing. (c) A supraglacial stream.

Methods

4.1 Introduction

This study combines satellite optical remote sensing with output from regional climate modelling and meteorological data to classify and map SGLs, distinguish their position in relation to the grounding line, and to examine their links to surface air temperature records. This chapter describes the types of imagery and processing methods used to meet the research aims.

4.2 Remote Sensing of Lakes

In supraglacial lake investigations it is often necessary to use satellite imagery to gain both a spatial and temporal perspective on lake behaviour (see Section 2.5). Previous studies of SGL activity on the GrIS and AP have used a range of satellite instruments, including MODIS (Box and Ski, 2007; Sundal et al., 2009; Selmes et al., 2011), Landsat (McMillan et al., 2007; Luckman et al., 2014), and ASTER (Wessels et al., 2002; Georgiou et al., 2009). However, each satellite offers differing spatial, radiometric and temporal resolutions known to optimize different tasks. Differences in aerial coverage often correspond to the ground resolution, with high aerial coverage often equalling low ground resolution. Thus, it is important to assess the size of lakes within the study area, the temporal resolution needed, and the required aerial coverage before satellite images are chosen.

4.2.1 Overview of Satellite Imagery Data Sources

Table 4.1 outlines the properties of three optical sensors used in SGL studies. MODIS (Moderate-resolution Imaging Spectroradiometer) has the coarsest resolution out of the three aforementioned satellites (250 m), but has a far higher temporal sampling with imagery captured at least once every two days. Therefore, it is more accurate in resolving the evolution of lakes, capturing initiation, growth, shrinkage and disappearance. Despite this, an initial test using MODIS imagery to study lakes at Langhovde Glacier proved difficult due to its 250 m spatial resolution. The lakes on this glacier are smaller in comparison to those observed on Greenland and, therefore, it is

more difficult to accurately delineate lake boundaries on MODIS imagery. Therefore, a satellite instrument with greater spatial resolution is necessary for this study.

Table 4.1: Spatial, temporal and spectral resolution of optical sensors used in previous SGL research. Revisit time (nadir) refers to a full orbital cycle with a revisit directly above the same target. Revisit time (off nadir) refers to steerable sensors which can view an area surrounding its target to provide a shorter revisit time compared to the orbit cycle time.

	MODIS	**Landsat-7 ETM+**	**ASTER**
Satellite	Terra and Aqua	Landsat-7	Terra
Number of bands	36	8	15
Resolution	Bands 1-2 (250 m) Bands 3-7 (500 m) Bands 8-36 (1000 m)	Bands 1-7 (30 m) Band 8 (15 m)	Bands 1-3 (15 m) Bands 4-9 (30 m) Bands 10-14 (90 m)
Swath width	2330 km	180 km	60 km
Revisit time (nadir)	16 days	16 days	16 days
Revisit time (off nadir)	1-2 days	16 days	1-2 days

Landsat-7 Enhanced Thematic Mapper (ETM+), launched in 1999, has much higher spatial resolutions (30 m with 15 m panchromatic band) compared to MODIS imagery (Table 4.1). Unfortunately, Landsat-7 scenes have been compromised since May 2003 when the Scan Line Corrector (SLC), which accounts for the forward motion of the satellite, failed. Consequently, the ETM+ line of sight now traces a zig-zag pattern along the satellite ground track. As a result, an estimated 22% of any given scene is lost due to this failure, with duplication of the imaged area increasing towards the scene edge (Moon and Joughin, 2008). Fortunately, a strip of undistorted imagery with very little duplication or data loss centres each scene at 22 km wide. As Langhovde Glacier is just 3 km wide, with an 18 km length area of interest, it is possible to find enough imagery of the glacier (Figure 4.1). The temporal resolution of Landsat-7 is comparably low to MODIS, with a given point imaged with the same geometry every 16 days.

ASTER (Advanced Spacebourne Thermal Emission and Reflection Radiometer), a Japanese sensor on board the Terra satellite launched in 1999 offers an effective addition to Landsat-7 imagery. With revisit times of 1-2 days, ASTER provides a means of capturing finer changes in lake character (Table 4.1). Its high spatial resolution (15 m) favours the accurate delineation of lakes, making lake observations more reliable

and more precise. The resolution of ASTER imagery can be used to calibrate low-resolution imagery and verify automated results (e.g. Selmes et al., 2011; Sundal et al., 2009). Therefore, this study required the use of both Landsat-7 and ASTER imagery in order to reliably and accurately study SGL evolution.

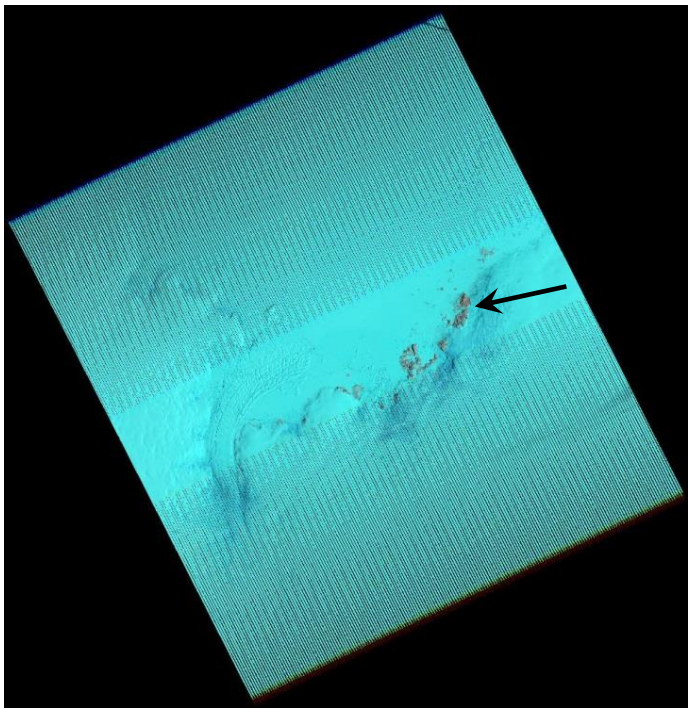

Figure 4.1: Landsat-7 ETM+ image from 2012 (SLC-off) highlighting zig-zag pattern with 22 km wide strip of undistorted imagery in the centre. Black arrow points to location of Langhovde Glacier, unaffected by the distorted area in this image.

4.2.2 ASTER Imagery

ASTER L1A imagery, which has geometric, radiometric, and band-to-band registration already applied, was used. All cloud-free imagery from 2000-2013 were downloaded from Land Processes Distributed Active Archive Centre (DAAC). Images were imported into the image processing software ERDAS, and multispectral bands 1 (0.52–0.60 μm), 2 (0.63-0.69 μm), and 3N (0.76-0.86 μm) were stacked to produce a 15 m resolution true-colour composite image. After trialling a number of false-colour composites, it was clear that natural colour allowed easier interpretation of lake boundaries (Figure 4.2a). As ASTER imagery has a lower swath width (60 km) compared to Landsat-7 ETM+ (180 km), it was often necessary to create raster image mosaics, to ensure full area coverage of Langhovde Glacier in each scene. This process was completed in ArcGIS geoprocessing tools.

4.2.3 Landsat 7 Imagery

Landsat-7 was obtained free of charge from the US Geological Survey Earth Resources Observation Science Centre (USGS). All cloud-free imagery were downloaded for the period 2000-2013, and reprojected from Polar Stereographic to WGS84 to be compatible with ASTER imagery. In ERDAS, 30 m multispectral bands 1 (0.45-0.515 μm), 2 (0.525-0.605 μm), and 3 (0.63-0.69 μm) of each scene were stacked to generate true-colour composite images. The subsequent stacked image had a resolution of 30 m, 15 m greater than ASTER. Consequently, to ensure consistency between sensors, Landsat-7 imagery was pan-sharpened using panchromatic band 8 (0.52-0.9 μm). This produced a 15 m resampled image that was comparable to the ASTER product (Figure 4.2).

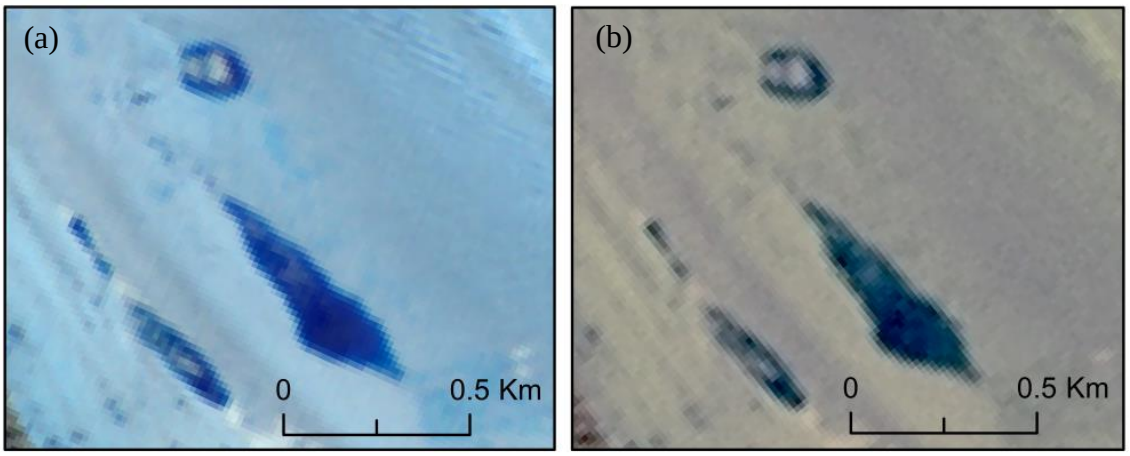

Figure 4.2: (a) ASTER and (b) pan-sharpened Landsat-7 image from the same location and on the same day (20th December 2007).

4.2.4 Co-registration

Combined there were 153 cloud-free images of ASTER L1B and Landsat-7 ETM+ from 2000-2013. However, due to the frequent revisit times of the ASTER satellite, and the malfunction of the Landsat-7 ETM+ sensor, there was a vast difference in the temporal resolution of each (Figure 4.3). Conversely, ASTER was the most prevalent source of imagery for our study region over the 13 years.

In general, there is little or no shift in images taken from the same sensor. However, there is a shift in pixels between ASTER and Landsat-7 imagery, making it difficult to distinguish whether SGLs had shifted down-glacier or whether they were stationary.

Therefore, registration to a base scene was needed. A base scene was taken from an ASTER image (12th November 2014). This satellite and image was chosen as it is not affected by SLC failure and that date displayed no cloud interference, allowing for accurate co-registration.

Firstly, images were cropped in ArcGIS to a smaller area. By having a greater area of nunatak/coastal bedrock outcrop to ice, co-registration was more accurate (Scambos et al., 1992). To register all images to the base scene, Ground Control Points (GCPs) were placed on an immovable feature in both images (Kääb, 2002). For this study area, the bedrock outcrop to the east of Langhovde glacier snout was chosen as well as the Ongul Islands (Figure 4.4). Between 15 and 30 GCPs were used, as recommended by previous researchers (e.g. Paul and Andreassen, 2009). Prior to image transformation, GCPs which generated the highest root mean square error (RMSE) were deleted. Post transformation, the link table was analysed to ensure the error was below 7 m (considering each pixel is ~ 15 m, an error of less than half a pixel is very accurate). Registration accuracy was also verified by laying each image over the base image and using the 'swipe' tool in ArcGIS. This allowed us to check that pixels matched up and that there was no image warping.

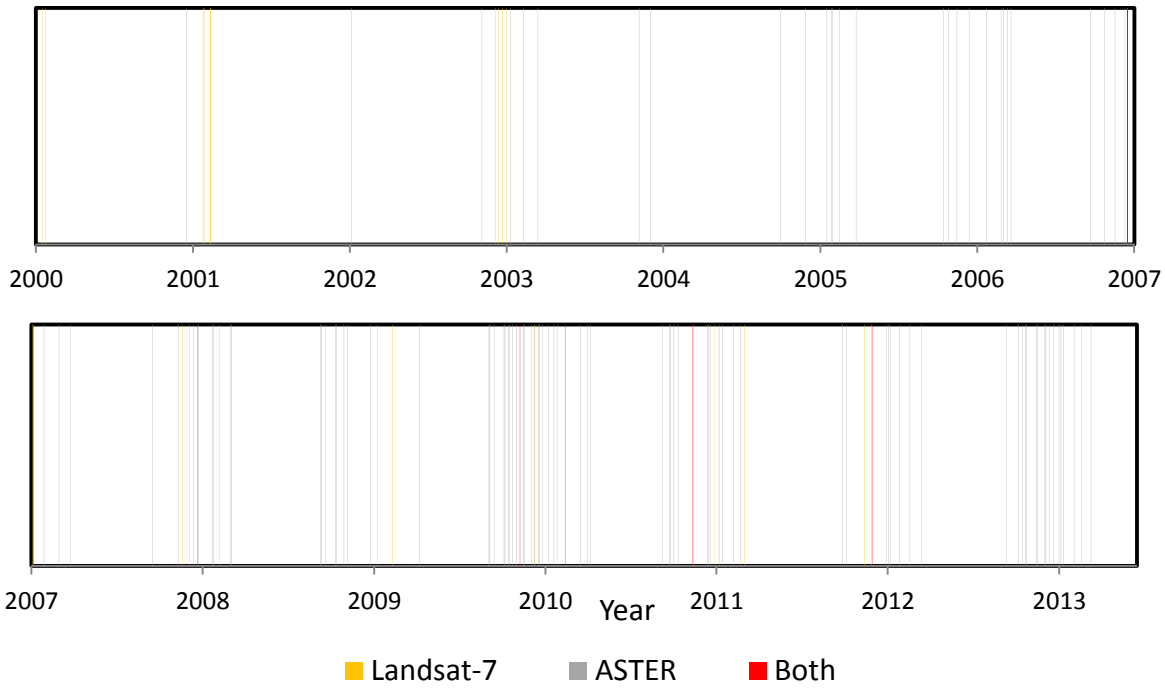

Figure 4.3: Inter-annual variability in the availability of imagery from Landsat-7 and ASTER. Vertical lines represent an observation date from either Landsat-7 (yellow), ASTER (grey), or both (red). Each year on the x-axis demarcates the 1st January.

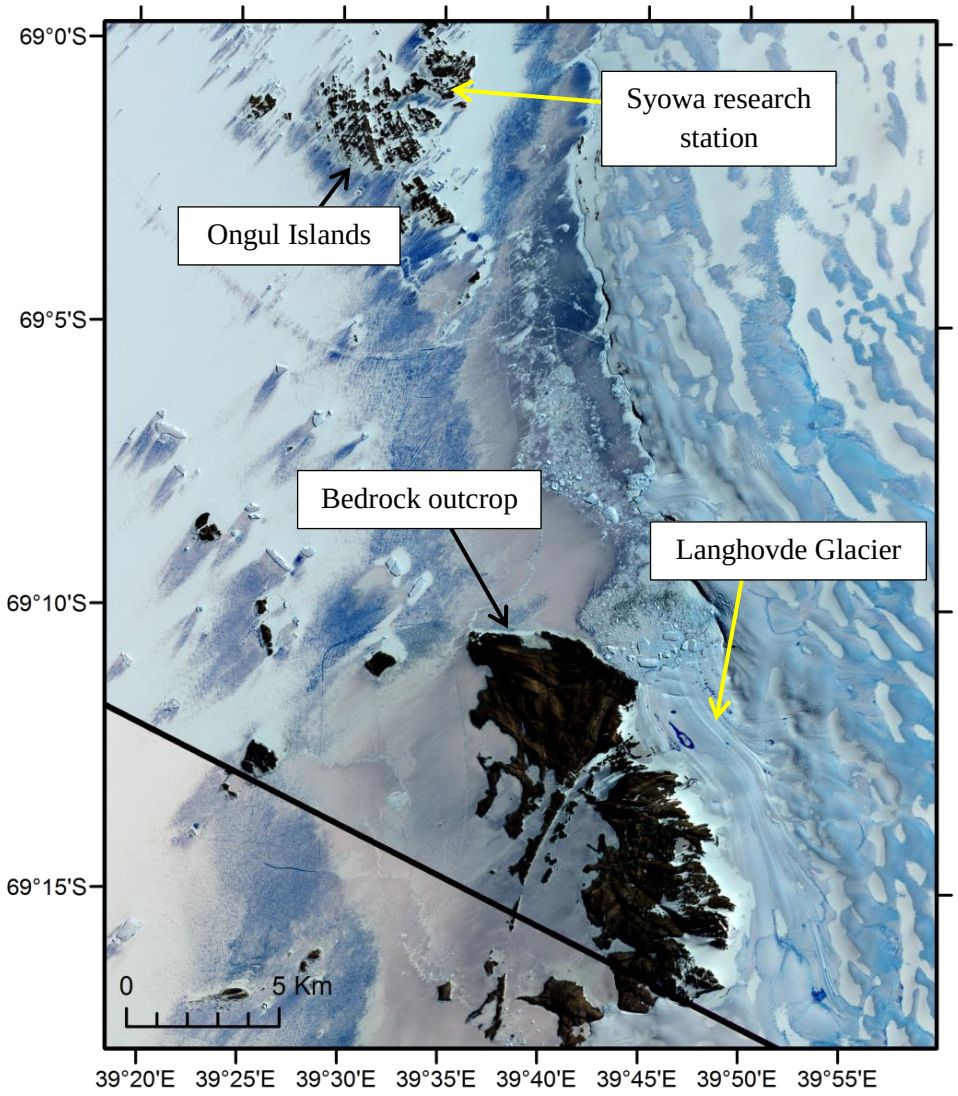

Figure 4.4: Location map of Langhovde Glacier, with immovable features used for GCPs in co-registration (Ongul Islands and the bedrock outcrop).

4.3 Supraglacial Lake Identification

Considering that the research aims are to study the spatiotemporal characteristics and behaviour of lakes, it was decided that 'number of lakes', 'total lake area', and 'mean lake area' were the most valuable lake qualities to quantify. This is in line with previous studies (see section 2.5) that have similar research aims (e.g. Selmes et al., 2011; Sundal et al., 2009). SGLs in this region are previously unreported, so these parameters allow us to build an inventory of lake size and prevalence. From hereafter 'total number of lakes' will be abbreviated to N_{total}, 'total lake area' will be abbreviated to A_{total}, and 'mean lake area' will be abbreviated to A_{mean}.

4.3.1 Manual Delineation vs Pixel-based Classifications

To quantify the N_{total} in each image, it was most reliable to count manually (cf. McMillan et al., 2007). However, to quantify the $A_{total,}$ there were a number of approaches we could use (section 2.2). On the GrIS, automated techniques have been favoured for their quick processing time compared to manual digitization; however their accuracy can vary (e.g. Leeson et al., 2012). To constrain the most reliable and efficient technique to use on the SGLs on Langhovde Glacier, we trialled a pixel-based automated classification based on spectral properties. We then compared these with results from manually digitized lakes from the same image.

The digital numbers (DN) of a lake pixel in a multi-spectral image should be very different to the surrounding bare ice (Box and Ski, 2007), i.e. the distinct blue should be highly distinguishable from glacier ice. Therefore, by utilising the difference in DNs between pixels, one should in theory be able to use an automated algorithm to separate pixels into different classes (i.e. lake, glacier ice, snow). This was trialled using a pan-sharped Landsat-7 image taken on the 21st January 2008. Firstly, the bedrock and ocean were removed from the image, as they can often display similar spectral qualities to lakes (particularly where the bedrock has meltwater pools). This was done by digitizing the bedrock outcrop and around the glacier terminus to produce a land/ice mask, and a simple binary image. Training samples were created, which allow the operator to visually distinguish and program the difference between a lake and bare ice (Paul et al., 2004). 30 training samples were used for each element (i.e. lake, bare ice, blue ice). The image was then classified to reveal where pixels with a similar DN to the lake training sites were (Figure 4.5). However, the success of this supervised classification was varying. In this case, and subsequent re-trials, there was not enough separation between classes. This issue arose due to the monochrome nature of SGLs, which display different shades of the same colour depending on their area, depth, and time in the season. This meant that lake water could have a DN of between 3.5 and 6.5. However, if this threshold was used, there were greater false positives, with blue ice areas and shaded topography often classified as SGLs. If this threshold was reduced then lakes were not identified and missed in the classification (Figure 4.5). Post-processing which involved carefully studying the image to find false positives/unreported lakes, as well as

masking out areas, was time consuming. Therefore, this method was not considered an efficient technique for this study area.

Thus, manual delineation was chosen as the most accurate way of discerning A_{total}, in line with previous investigations (Leeson et al., 2012; McMillan et al., 2007). Lakes were mapped by visual interpretation, utilising the relative spectral contrast between dark, water-filled lakes and bare ice (Lampkin and Vanderberg, 2011). Lake boundaries were manually-digitized using multiple band combinations and standard image enhancement procedures (histogram equalization and contrast stretching) (Glasser and Scambos, 2008). In order to ensure consistency in digitization of lake features, only lakes large enough to discern lake boundaries were mapped. This meant that lakes smaller than 450 m^2 (2 pixels in area) were not mapped because their identification was more uncertain. Due to the high spatial resolution of imagery used, it was easy to distinguish between an ice covered and non-covered lake, allowing detailed observations as the melt seasons progressed.

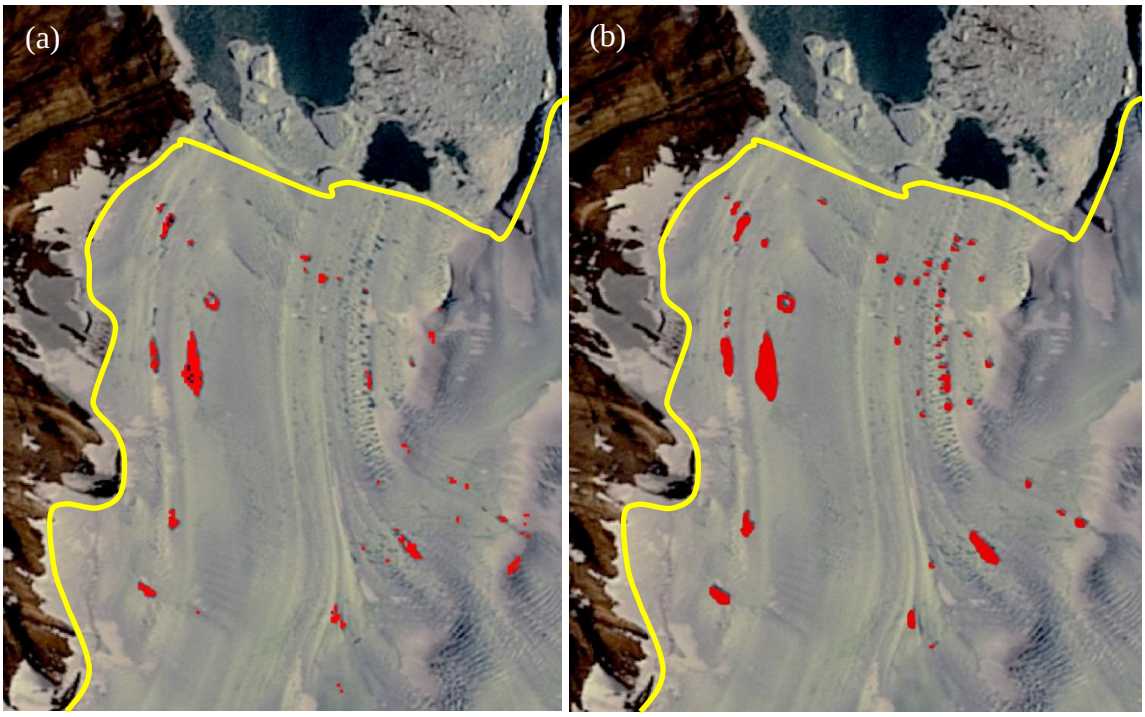

Figure 4.5: Comparison between (a) pixel-based classification and (b) manual digitization. Landsat-7 image is from 21st January 2008. Outside of the yellow line is the area of the image masked out prior to analysis. Note that compared to manual methods there are a far greater number of unreported lakes in the automated classification, and those that are reported have much smaller areas.

4.3.2 Error Analysis

To calculate the error from manually digitizing lake boundaries, a set of 10 SGLs (of varying sizes) from the 20th December 2007 were re-digitized (Figure 4.6). This date was chosen as there was an ASTER and Landsat-7 image available, so SGLs could be re-digitized in both. The set of SGLs were digitized 5 times in ASTER and 5 times in Landsat-7, the results of which are shown in Table 4.2. The largest difference in extracted area was converted to percentage error. The maximum error is likely to be +/- 10%.

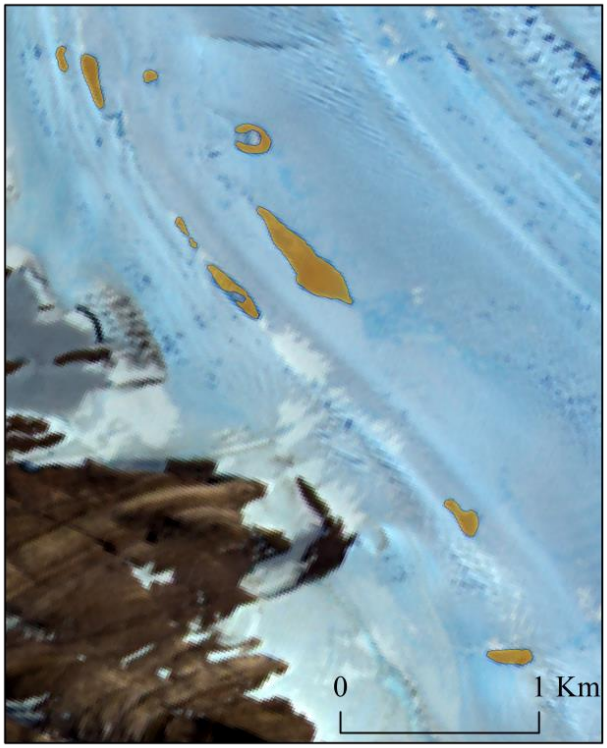

Figure 4.6: ASTER image from 20th December 2007, displaying the 10 chosen SGLs that were manually re-digitized to extract a maximum likely error.

Table 4.2: The total area of 10 SGLs calculated in each image, and the maximum and minimum value extracted to calculate the maximum error from manual digitization.

Satellite	Total Area of 10 SGLs (m^2)	Minimum	Maximum
ASTER	162343.8		
ASTER	160402.8		
ASTER	153095.3		
ASTER	160640.9		
ASTER	156710.3		
Landsat-7	152652.4		
Landsat-7	147065.0	✓	

Landsat-7	147180.4		
Landsat-7	162142.4		
Landsat-7	174048.5		✓
		Maximum error: 10%	

4.4. Supraglacial Channel Identification

Rectilinear features that indicated surface streams were observed on Langhovde Glacier, and manually digitized in a separate class to SGLs. Due to their narrow width, yet variable lengths, we mapped these features as polylines in order to gain information on their spatial extent. To ensure that these channels were actively flowing and not frozen, these features were only mapped when thawed SGLs were present in the surrounding area. If SGLs had not formed yet, or were frozen at the end of the season, it would be unlikely that such a thin supraglacial feature would be melted. We utilised the relative contrast in colour, to distinguish between supraglacial streams and crevasses/fractures. From hereinafter, the total number of linear melt features, indicative of surface streams, is abbreviated to $C_{total.}$

4.4.1 Supraglacial Channels and Meltwater Routing

To understand the nature of supraglacial streams observed on Langhovde's glacier surface, and their relation to surface topography, flow pathways were modelled to understand their preferential flow (Arnold, 2010). A supraglacial hydrological network was modelled using a 30 m ASTER digital elevation model (DEM), taken from the 16th December 2009 (Leeson et al., 2013). Spatial analysis tools in ArcGIS were used to calculate the preferential (i.e. steepest) flow direction of each cell in the DEM and the corresponding potential accumulation for each cell. Cells with higher than average accumulations were classified as flow pathways. This produced an idea of the hydrological catchment, major water pathways, and minor water pathways. The model output does not translate into actual streams, it simply shows how the water would flow if enough were available, and can be compared with the digitized channels (Section 4.4).

4.5 Grounding Lines

To constrain where SGLs are in relation to grounded and floating ice, an estimation of the grounding line position was required. Within grounding line studies, researchers often exploit the surface features of a glacier in order to determine where the grounding line will be, a method termed 'break-of-slope analysis' (Haran et al., 2014; Fricker et al., 2009). This technique is used to find the elevation minimum which is a visual feature that is close to the actual grounding line ('I_m', Figure 4.7). This feature is between the landward limit of ice flexure (where there is no tidal movement) and the landward limit of free-floating ice (where the ice is free-floating). Although not directly on the grounding line, this feature gives a reasonable estimate of its location.

Previous research on Langhovde Glacier has utilised this technique to determine the grounding line position (Fukuda et al., 2014). Fukuda et al. (2014) obtained satellite imagery from Moderate Resolution Imaging Spectroradiometer Mosaic of Antarctica (MOA) (Scambos et al., 2007) and Landsat Image Mosaic of Antarctica (LIMA) (Bindschadler et al., 2008) to calculate their break-of-slope on Langhovde Glacier between 1999 and 2003. However, in order to verify the location (particularly as the grounding line of glaciers can fluctuate, Rignot and Jacobs (2002)), and because it is important to know whether lakes might drain to the grounded portion of the ice sheet, a few other tests were undertaken.

Firstly, Antarctic-wide grounding line datasets such as MOA2009 (MODIS Mosaic of Antarctica) and ASAID 1999-2003 (Antarctic Surface Accumulation and Ice Discharge project), were analysed and compared to Fukuda et al. (2014) grounding line. The MOA grounding line (resolution: 150 – 200 m) is constructed from MODIS satellite imagery between 2008 and 2009, and is generated from break-of-slope analysis (Scambos et al., 2007). ASAID is developed from Landsat-7 imagery and ICESat (Ice, Cloud and land Elevation Satellite) laser altimetry, with data collected between 1999 and 2003 (Bindschadler et al., 2011). Both MOA2009 and ASAID are draped onto an image of Langhovde Glacier (see Figure 4.8). However, in both cases, the grounding line is estimated from these dataset to be very close to the ice shelf edge, which is unlikely based on the fact that Fukuda et al. (2014) carried out borehole measurements that reached the sub-shelf cavity ~ 3 km from the calving front. This discrepancy in MOA2009 and ASAID is possibly due to the small terminus width of Langhovde Glacier and the fact that the topographic detail may have been lost in these Antarctic-wide datasets.

Consequently, break-of-slope analysis on a 30 m ASTER DEM (representing the ice surface on 16th December 2009) was undertaken in this study to compare with the grounding line produced by Fukuda et al. (2014). In ArcGIS, a series of profile transects were created across the glacier terminus (e.g. Rignot et al., 2011) (Figure 4.9a). Each transect was visually analysed to locate the elevation minimum (I_b) (Figure 4.9b), until the entire width was mapped.

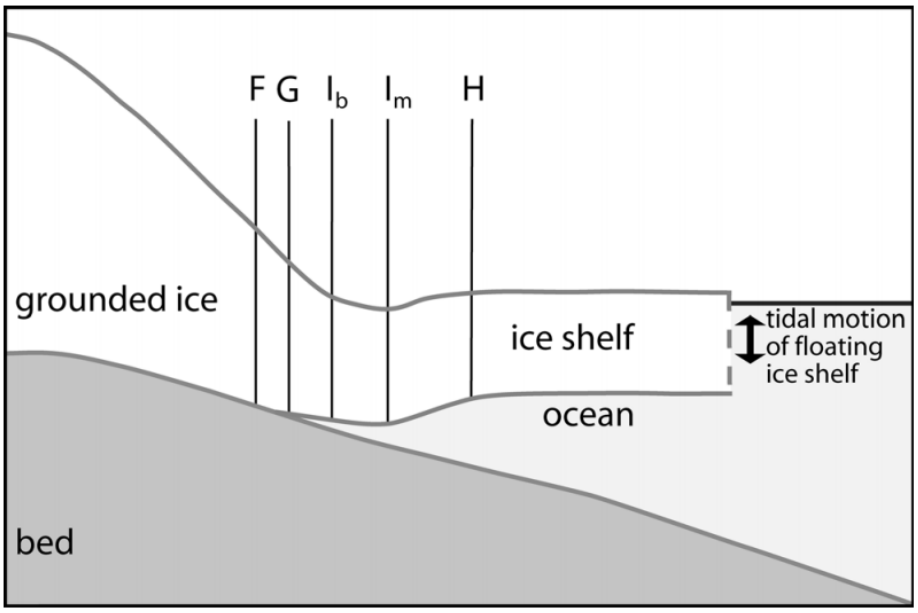

Figure 4.7: Schematic diagram of the grounding zone (F-H) of a marine-terminating glacier, from Fricker et al. (2009). (F) is the landward limit of ice flexure from tidal movement. (G) is the exact grounding line (limit of ice flotation). (I_b) is the break-in-slope. (I_m) is the local elevation minimum. (H) is the seaward limit of ice flexure. The schematic is based on a glacier which is several kilometres wide, but the exact distance between F, G, I_b, I_m, and H will depend on the local bedrock topography and ice thickness.

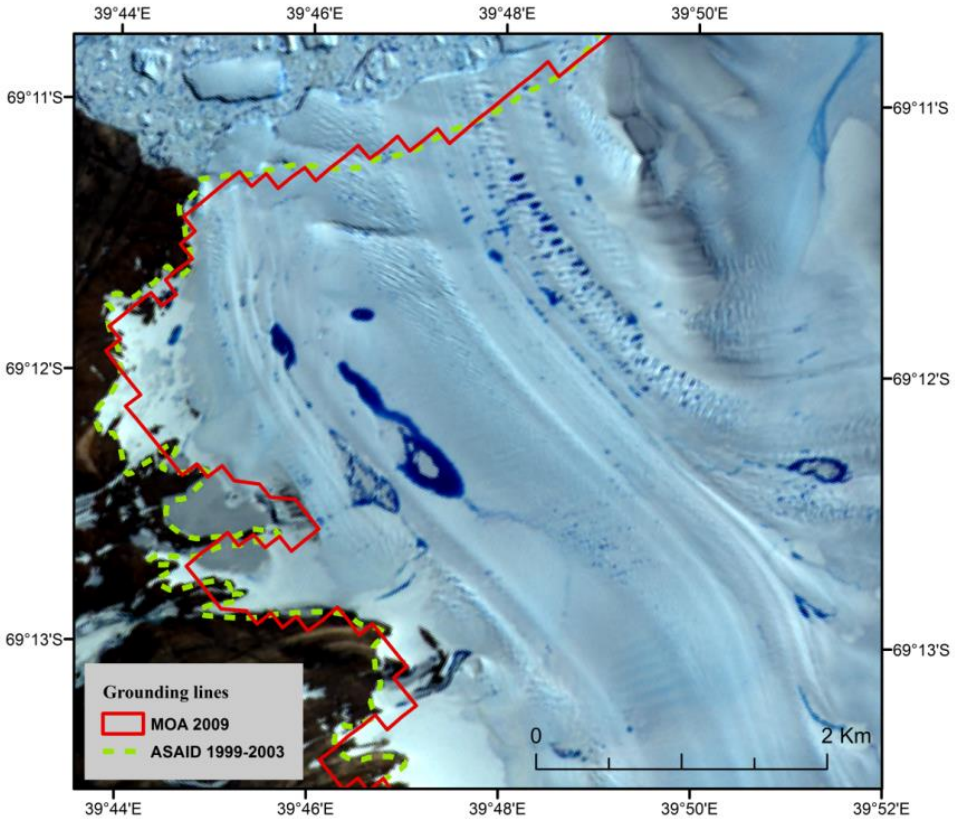

Figure 4.8: Antarctic-wide grounding line datasets projected onto Langhovde Glacier. Red line is MOA2009 (Haran et al., 2014) and yellow dashed line is ASAID 1999-2003 (Bindschlader et al., 2011). Underlying is an ASTER image of Langhovde Glacier terminus taken on 31st December 2012.

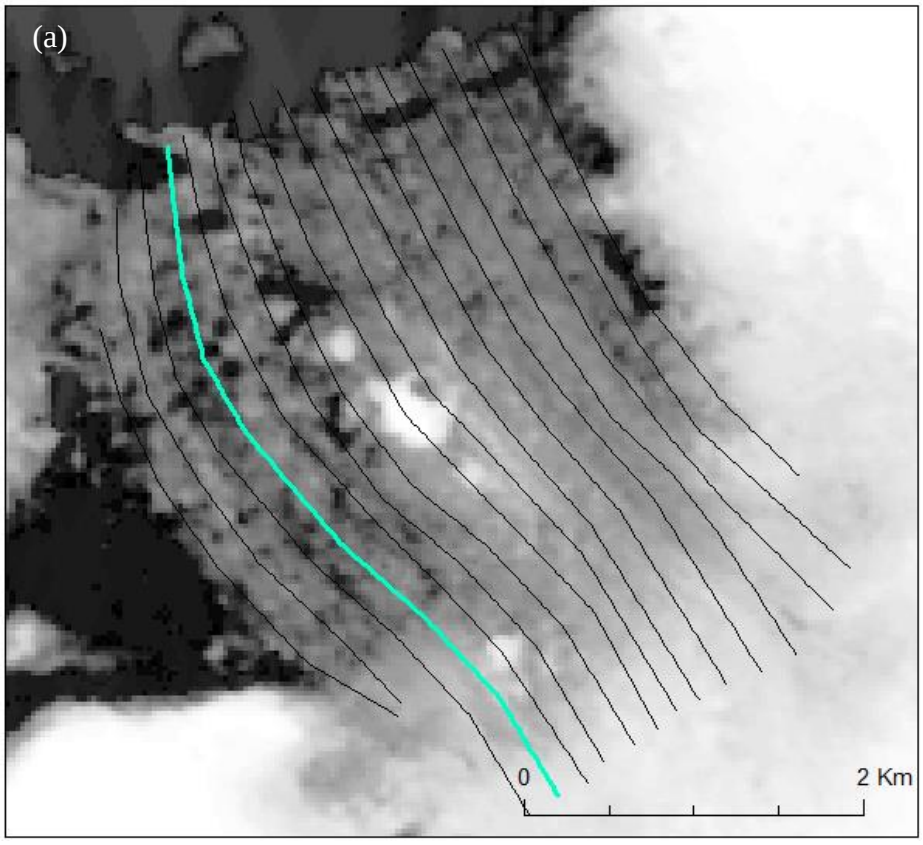

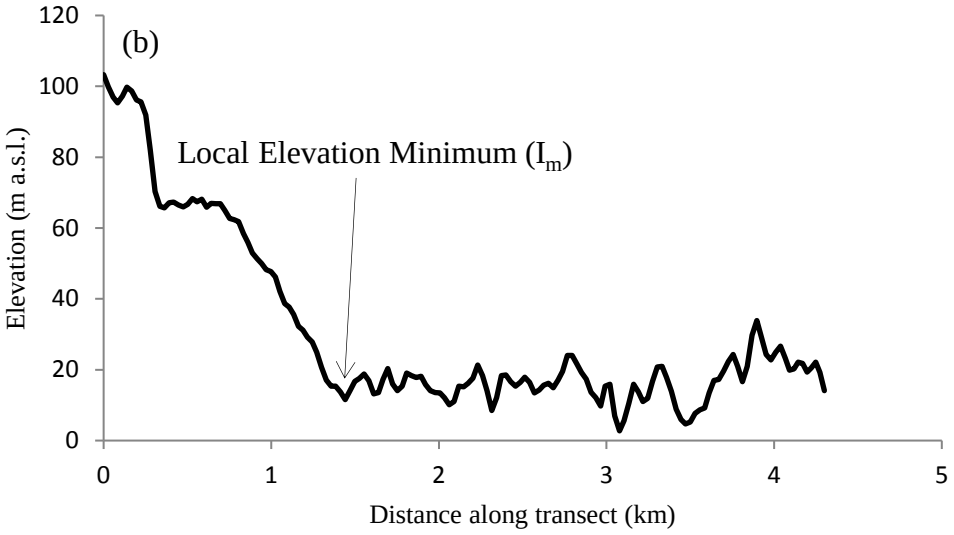

Figure 4.9: (a) ASTER DEM (16th December 2009) of Langhovde Glacier terminus with transects used to identify the elevation minimum. (b) Example elevation profile from transect 4 (blue line on DEM) showing a clear transition from grounded (steep) to floating (level) ice.

4.6 Temperature Data

4.6.1 Meteorological Records

Daily mean surface air temperature data is measured at the Syowa research station (Japanese Antarctic Research Expedition base), and accessible from www.data.jma.go.jp/antarctic/datareport/index-e.html. The station is located 20 km south of Langhovde Glacier on East Ongul Island at an elevation of 18 m (Figure 4.4). Considering its proximity and altitude, it is reasonable to expect that surface air temperature at Syowa research station is similar to the lower reaches of Langhovde Glacier. Moreover, Mellor (1960) calculated the lapse rates in surface air temperature applicable to the Dronning Maud Land region. According to the modelled estimates, a 100 m increase in elevation equates to a 1.05°C decrease in surface air temperature (Mellor, 1960). This lapse rate was used when studying external forcings on the lakes at elevations higher than 18 m a.s.l.

4.6.2 RACMO2.3 Regional Climate Model

RACMO2.3 has been used in other Antarctic melt studies to model regional climate and daily ice sheet runoff (Moon et al., 2014; Van Wessem et al., 2014). Modelled runoff is defined as the liquid water flux (meltwater) that is not retained at the ice sheet surface (e.g. refreezing in firn), and therefore may be available to form SGLs, supraglacial channels, or drain through the ice. Although this study benefited from daily mean surface air temperature readings from Syowa research station, and regular satellite observations, RACMO2.3 modelled melt and temperature readings were compared with observations to assess its diagnostic and prognostic viability on this outlet glacier.

Daily surface temperatures and surface runoff were simulated by RACMO2.3 for 2000-2013, forced at the boundaries by the ERA-Interim re-analysis. The data are from the nearest RACMO2.3 grid cell to Langhovde, which is centred at 39.86, -69.13 and is 27 km wide (Figure 4.10). RACMO2.3 merges the elevation of its grid cells, meaning that a single elevation value (per 27 km) is used to generate temperature and melt readings. In Langhovde's grid cell, the elevation was merged to 240 m a.s.l. (despite highly variable elevations, from 7 to 630 m a.s.l.). Consequently, the temperature and melt output is modelled for 240 m a.s.l.; not representative of the lower elevations of Langhovde Glacier. When using RACMO2.3 it is therefore necessary to apply lapse rates to modelled temperature and melt readings (Van Wessem et al., 2014). The surface temperature lapse rates of Mellor (1960) for the Dronning Maud Land region were utilised, which means a 1.05°C increase for every 100 metres regressed. By interrogating the wider RACMO2.3 dataset, we found this temperature lapse rate was in almost perfect agreement (r^2 = -0.98).

Considering what lapse rate to apply to the modelled melt readings (so that we could gain information on meltwater runoff at lower elevations of the glacier), was more challenging. Melting in RACMO2.3 is calculated using a surface energy balance model, with some parameters (such as sensible and latent heat fluxes) being temperature dependent (Van Wessem et al., 2014). Temperature varies with elevation and so, in theory, we would expect melt to vary with elevation. However, when calculating mean daily melt in each grid cell and regressing with elevation, the correlation was not strong (r^2 = -0.32), indicating that the model does not recognise a strong relationship between melting and elevation change. This meant that there was a poor case to make such corrections, and, unlike temperature, melt was left as simulated by the model.

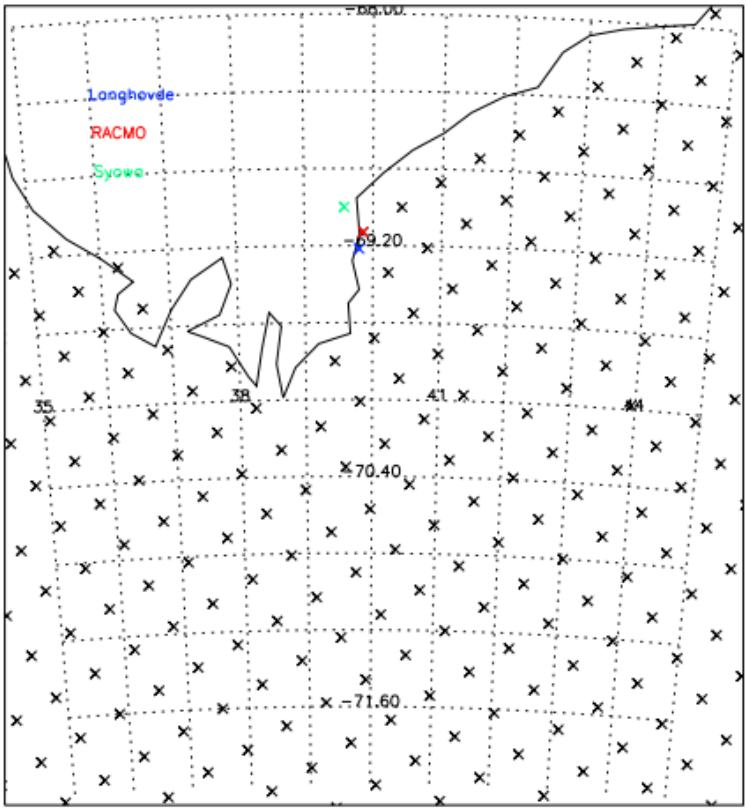

Figure 4.10: Location of Landhovde Glacier (blue cross) and Syowa research station (green cross) on RACMO2.3 grid cell. Note the large cell size in comparison to the glacier, which has resulted in a generalised elevation of 240 m a.s.l. for the glacier.

Results

5.1 Annual and Inter-annual Trends

In 153 satellite images over the 13 year period, a total of 7,990 SGLs and 855 supraglacial channels were digitized. Figure 5.1 documents the inter-annual variability in N_{total}, A_{total}, A_{mean}, and C_{total} over the 13 years. There is significant inter-annual variation in the temporal resolution of imagery between years, ranging from 1 to 19 observations over each austral summer. The first seven years were particularly sparse in imagery, averaging 4.7 images over a melt season (duration = ~77 days). In line with previous work (Leeson et al., 2012), lake evolution is difficult to study in less than 10 images over an austral summer. Therefore, summers with 10 or greater cloud-free observations, that were at regular intervals, enabled a robust evaluation of lake evolution during these years. Thus, the ablation seasons of 07/08 (11 images), 09/10 (19 images), 10/11 (14 images), 11/12 (11 images), and 12/13 (16 images) were chosen to study in further detail. These years offered a cloud-free image on average every 13 days. The analysis of annual and inter-annual trends is primarily based on these five complete seasons of imagery (Figure 5.2).

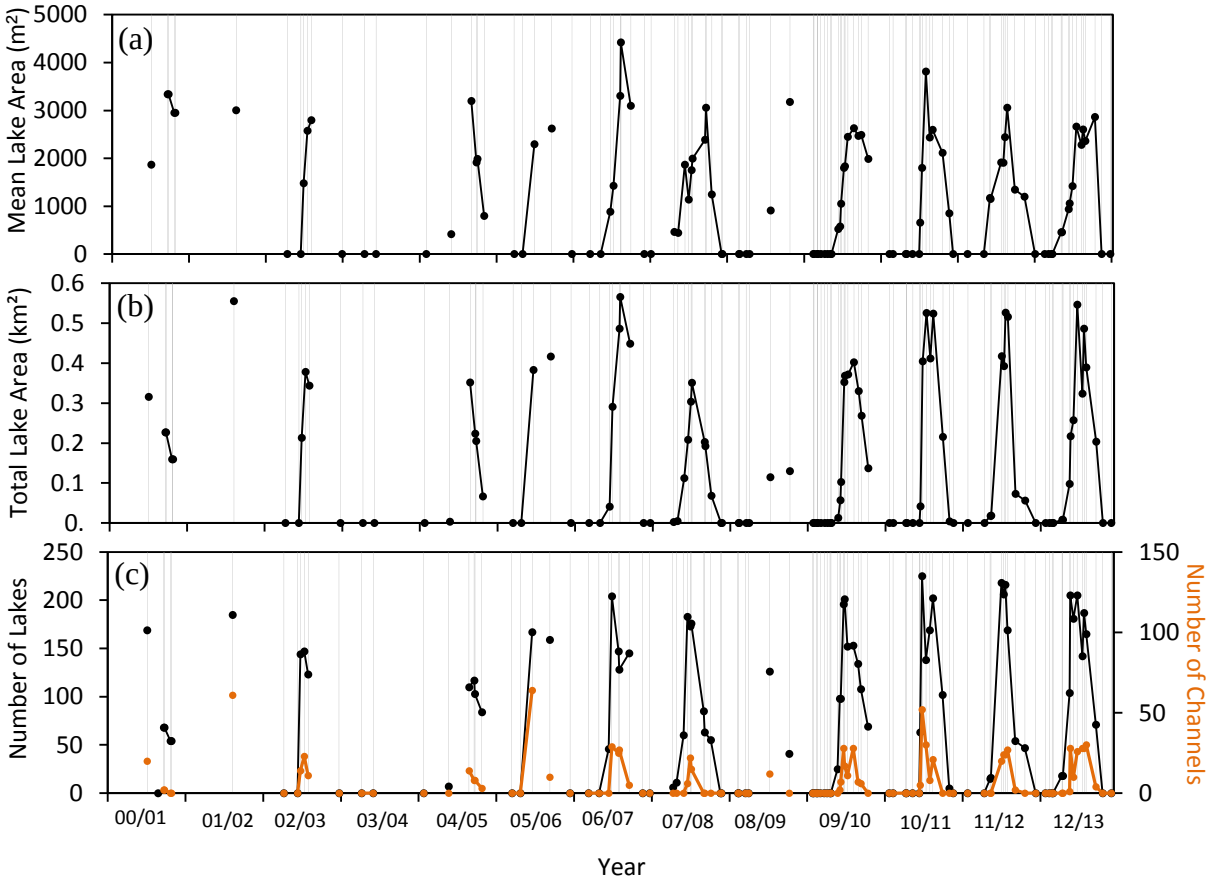

Figure 5.1: Inter-annual variability in N_{total}, A_{total}, A_{mean}, and C_{total} from 2000-2013. Lines join dots (observations) that are less than 30 days apart. Grey vertical lines represent cloud-free observations.

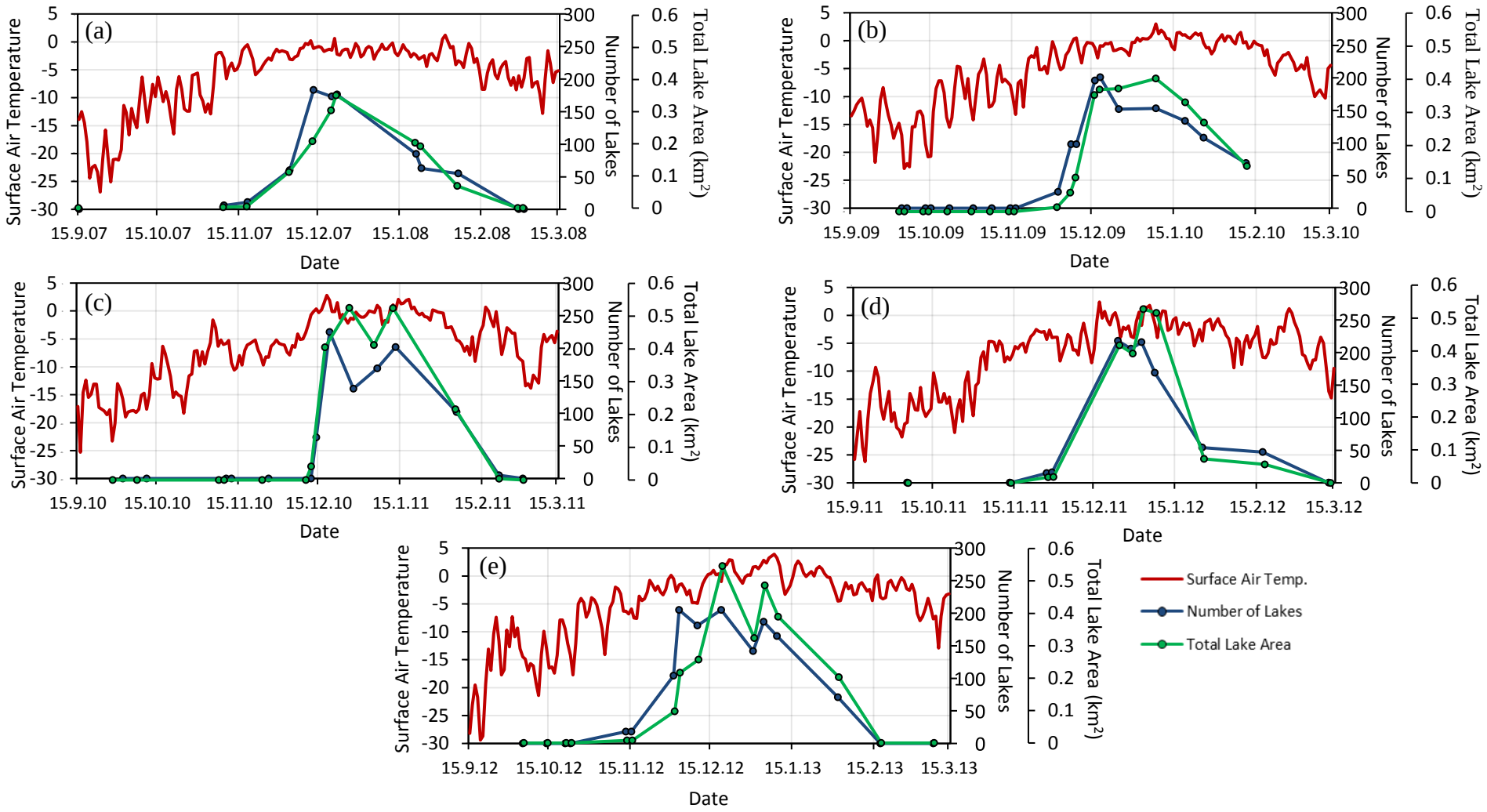

Figure 5.2: Annual variations in N_{total}, A_{total} and daily mean air surface temperatures (°C) (reviewed in Section 5.2). Years 07/08, 09/10, 10/11, 11/12, and 12/13 are displayed from the 13 year series due to their high temporal resolution. Note the strong coupling between total lake area and number of lakes.

5.1.1 Annual Variability of Supraglacial Lakes

A lake season is typically three months, with lakes forming in late November and disappearing by mid-February (maximum observed in 2011/2012 with 82 days) (Figure 5.2). However, there are often periods during the season where temperatures fluctuate above and below freezing. Therefore, it is not unusual to see a reduction in the N_{total} and A_{total} mid-season. For example, in mid-December of 2010/11, temperatures declined below 0°C, resulting in a reduction in A_{total} and N_{total} for approximately 20 days before temperatures increased again (Figure 5.2c). The overall trend in lake evolution observed each year consists of lakes forming rapidly, reaching a maximum and maintain this maximum for a relatively short period of time, before disappearing at a slower rate compared to lake onset. The peak in N_{total}, A_{total}, and $A_{mean}$is observed between late December and mid-January. During this peak, an average of 206 lakes, 0.47 km^2 total lake surface area, and a mean lake area of 3082 m^2 are measured.

5.1.2 Inter-annual Variability of Supraglacial Lakes

Although the pattern of lake evolution is the same for each austral summer, the absolute values differ between years. The maximum observed A_{total} A_{mean}, and N_{total} can differ on an annual basis (Figure 5.2). For example, within the five summers of detailed observations, the A_{total} varied from 0.35 and 0.5 km^2. The highest peak in A_{total} was observed on the 4th January 2007, with a total surface meltwater area of 0.56 km^2 present (Figure 5.1b). Similarly, there is an observed difference in the N_{total} documented at one time on Langhovde Glacier during peak melt. The maximum number of SGLs observed each year varied between 160 and 220 (Figure 5.2). The average lake size during peak melt also varied from 2627 m^2 and 4419 m^2 depending on the year.

Alongside inter-annual variability in these measured variables, we observed inter-annual variance in the date of melt onset and disappearance. Despite lakes on average forming in late November, there were occasions where this was not the case. For example, 2010/11 saw the longest delay in lake formation, with lakes appearing between the 12th and 14th December (no lakes observed on the 12th, 63 lakes observed on the 14th). There are cloud-free observations from the 10th, 12th, and 16th November 2010 which also signify no lakes. In comparison, lakes in 2012/13 developed at least four weeks earlier

in the season (no lakes observed on the 23rd October, but 18 lakes observed on the 13th November).

5.1.3 Annual and Inter-annual Variability of Supraglacial Channels

The inter-annual variability in C_{total} is displayed in Figure 5.1c. Over the five year series, there is a delay between the formation of SGLs and the formation of channels. Unlike SGLs, supraglacial channels are not observed in November imagery, with their formation documented between early December and mid-December. In addition, surface channels refreeze earlier in the season compared to SGLs. Supraglacial channels are not observed in February imagery, with these features disappearing by late-January. This gives surface channels a much shorter lifespan (~ 47-60 days) on Langhovde Glacier, compared to SGLs. Conversely, the peak in the C_{total} coincides with the peak in the N_{total} (late December to mid-January). The maximum C_{total} observed each year during peak melt can range from 22 to 52.

5.1.4 Statistical analysis

From observation alone, it is clear that a link exists between the four variables measured (N_{total}, A_{total}, A_{mean}, and C_{total}). However, to determine the significance and strength of these relationships, statistical significance tests were carried out. As the data are normally distributed, a *t*-test was used to determine the probability (p-value) and likelihood that our observations are significantly correlated ($p = 0.05$). Because we are interested in the possibility of a relationship in either direction (for example, an increase in the N_{total}, may relate to significantly more or less A_{total}), a two-tailed distribution is required. Unpaired *t*-tests were more appropriate as the study focusses on sets of independent, but identically distributed, samples. In these unpaired tests, heteroscedasticity (unequal variance) was assumed, based on initial investigations into the variability of values across the range. It is clear that there is dispersion and variation around the mean, particularly during maximum observed lake areas where a number of feedbacks interfere with direct correlations.

The results of our significance tests are shown in Table 5.1 and Figure 5.3. We calculate an overall highly significant relationship between the A_{total} and N_{total} ($p < 0.01$). On an annual scale, the significance slightly varies, with years 2010/11 and 2011/12 demonstrating a significant relationship ($p < 0.01$). Whereas, 2007/08, 2009/10, and

2012/13 demonstrate a highly significant relationship ($p < 0.05$). Similarly, as expected, there is a highly significant relationship between the N_{total} and the C_{total} over the five melt seasons ($p < 0.01$). However, there are also annual variations in this trend. For example, 2010/11 and 2011/12 document a significant relationship ($p < 0.05$) between N_{total} and C_{total}. Whereas, 2007/08, 2009/10, and 2012/13 document a highly significant relationship ($p < 0.01$).

Table 5.1: Results of two-tailed *t*-tests that highlight the significance between N_{total} and A_{total}, and N_{total} and C_{total}. **n** is the number of images available for that year.

Sample	Year	n	P-value
A_{total} **Vs.** N_{total}	2007/08	11	0.0028
	2009/10	19	0.0016
	2010/11	14	0.0143
	2011/12	11	0.0141
	2012/13	16	0.0024
	All	71	< 0.0001
N_{total} **Vs.** C_{total}	2007/08	11	0.0047
	2009/10	19	0.0014
	2010/11	14	0.0227
	2011/12	11	0.0151
	2012/13	16	0.0026
	All	71	< 0.0001

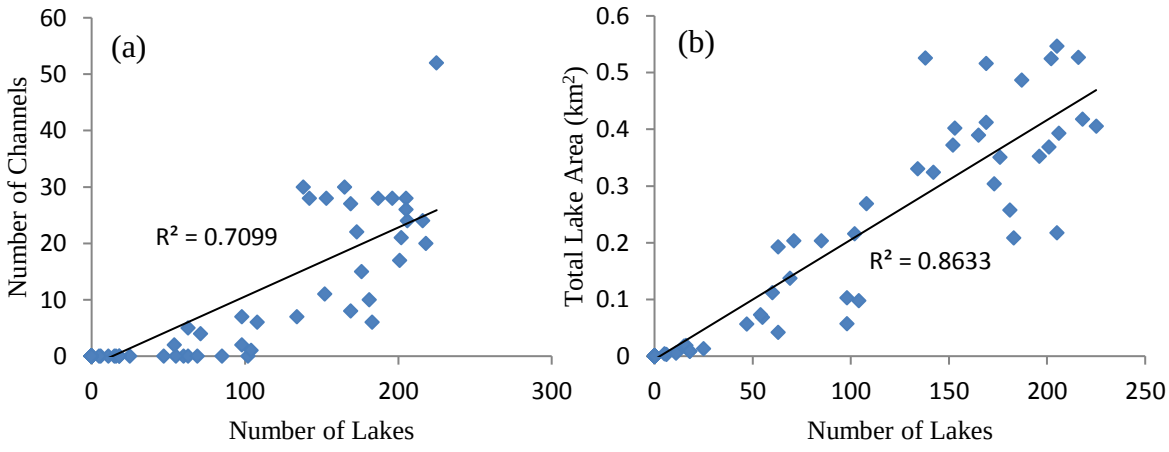

Figure 5.3: Statistically significant positive correlation between (a) number of lakes and number of channels ($p < 0.01$) and (b) number of lakes and total lake area ($p < 0.01$).

5.2 Climate Data

5.2.1 Daily Surface Air Temperature

Thus far, we have observed inter-annual variability in four correlated variables: N_{total}, A_{total}, A_{mean}, and C_{total}. Based on previous research (e.g. Trusel et al., 2012), the most likely cause for such variation is air temperature, which affects the amount of energy available for melt. To consider this relationship, the same *t*-test (as described above) was carried out using daily surface air temperatures from Syowa research station (Figure 4.4). Table 5.2 documents the results of this *t*-test, and Figure 5.4 plots each variable against daily surface air temperature. Overall, there is a highly significant relationship between all four variables and daily mean surface air temperature. On an annual scale, the variables N_{total} and C_{total} all show a highly significant relationship ($p < 0.01$). For A_{total}, there are only two years (2010/11 and 2011/12) which display a significant relationship ($p < 0.05$) rather than highly significant. In Figure 5.4, note the obvious thresholds between no melt and the appearance of lakes and channels. Once this threshold is reached, SGLs and supraglacial channels are highly responsive to small temperature fluctuations. Melt onset is rapid, with maximum observed N_{total}, A_{total}, A_{mean}, and C_{total} documented soon after temperatures reach a threshold. Also note the appearance of lakes and channels before temperatures reach 0º C at Syowa (Discussed in Section 6.1).

Surface air temperatures fluctuate on an inter-annual basis, with some years experiencing more days that are on average above 0ºC (Figure 5.2). Due to the strong coupling and significance between meltwater evolution and surface air temperatures, there are fluctuations in the N_{total}, A_{total}, A_{mean}, and C_{total} documented each year. Inter-annual temperature fluctuations help to explain the inter-annual variability in SGLs shown in Figure 5.2. For example, the warmest summer over the 13 year period was 2012/13, with 37 positive degree days and an average daily surface air temperature of -0.7˚ C (December-February). In comparison, 2007/08 had 5 positive degree days and an average daily surface air temperature of -2.5˚ C. As is expected, 2012/13 produced significantly greater A_{total} (55.7%) and N_{total} (12%). In addition, Langhovde's glacier surface in 2012/13 was characterized by 36% more surface channels, six overspilling lakes, and a calving event. Such widespread ablation was not observed in 2007/08.

Table 5.2: Results of two-tailed *t*-test to constrain the significance between N_{total}, A_{total}, A_{mean}, and C_{total} and daily mean surface air temperature. **n** is the number of images available for that year.

Sample	Year	n	P-value
A_{total} **Vs.** Surface air temperature	2007/08	11	0.0028
	2009/10	19	0.0016
	2010/11	14	0.0143
	2011/12	11	0.0140
	2012/13	16	0.0025
	All	71	< 0.0001
N_{total} **Vs.** Surface air temperature	2007/08	11	0.0022
	2009/10	19	0.0002
	2010/11	14	0.0053
	2011/12	11	0.0045
	2012/13	16	0.0004
	All	71	< 0.0001
A_{mean} **Vs.** Surface air temperature	2007/08	11	0.0063
	2009/10	19	< 0.0001
	2010/11	14	0.0006
	2011/12	11	< 0.0001
	2012/13	16	< 0.0001
	All	71	< 0.0001
C_{total} **Vs.** Surface air temperature	2007/08	11	0.0085
	2009/10	19	< 0.0001
	2010/11	14	0.0057
	2011/12	11	0.0011
	2012/13	16	0.0003
	All	71	< 0.0001

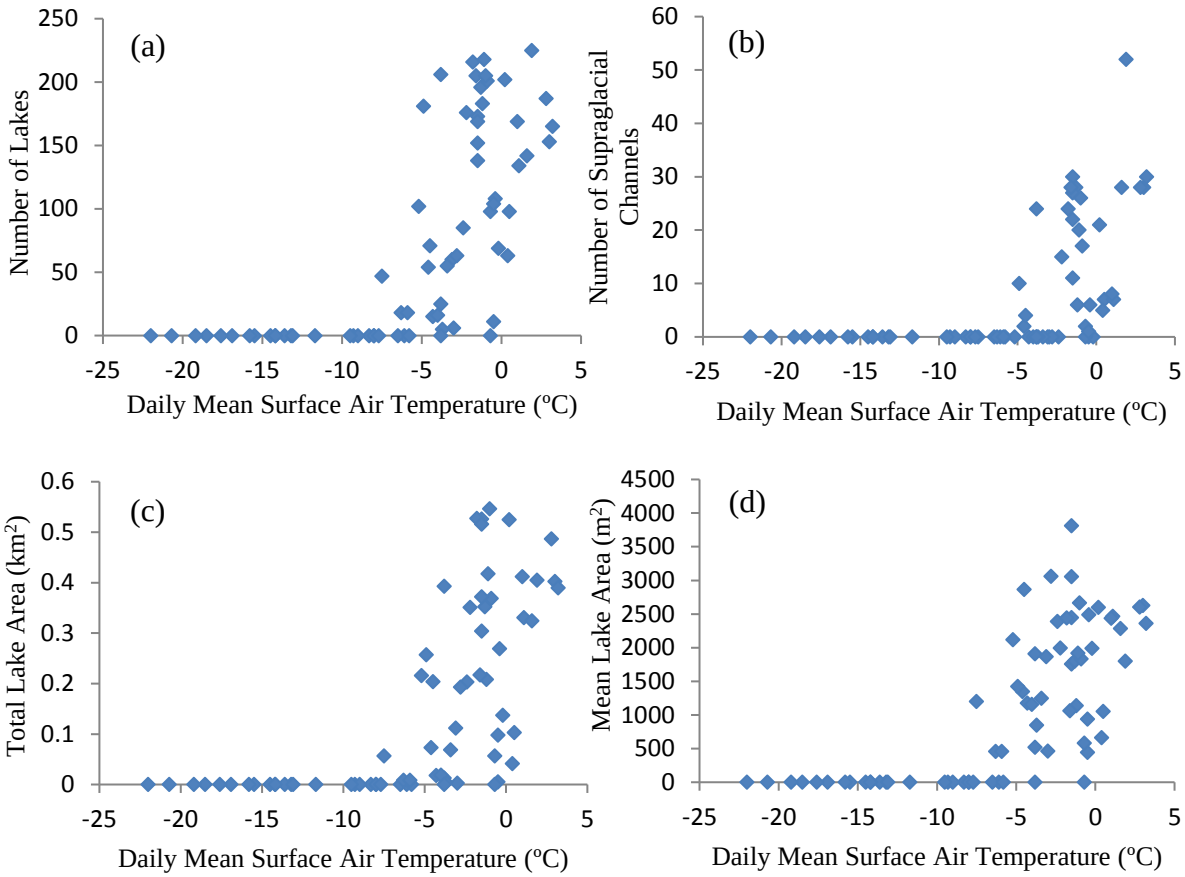

Figure 5.4: Statistically significant positive correlation between daily mean surface air temperatures and (a) number of lakes ($p < 0.01$), (b) number of surface channels ($p < 0.01$), (c) total lake area ($p < 0.01$) and (d) mean lake area ($p < 0.01$).

5.2.2 RACMO2.3 Analysis

Daily surface temperatures and melt rates, simulated by the RACMO2.3 regional climate model for 2000-2015, are displayed in Figure 5.5. RACMO2.3 melt rates also show strong inter-annual trends, with maximum melt rates varying between 4.1 mm/week and 15.1 mm/week on an annual basis. When comparing manually derived A_{total} from 07/08, 09/10, 10/11, 11/12, and 12/13 with RACMO2.3s modelled years, we can see a reasonably good correlation (Figure 5.2 and Figure 5.5). RACMO2.3 also shows a particularly high melt year in 2012/13 (with a maximum modelled melt rate of 12.8 mm/week). In addition, RACMO2.3 recognises a particularly low melt year in 2007/08 (with a maximum melt rate of 4.1 mm/week).

These results highlight the promise of using RACMO2.3 in predicting inter-annual melt rates. However, the correlation is weaker on an annual scale. Figure 5.6 compares the

RACMO2.3 cumulative melt with our calculated A_{total} for 2007/08 and 2012/13. Cumulative melt was plotted against A_{total} as it is a closer variable. As RACMO2.3 is simulating total melt production (whether it accumulates in a lake or not), and we calculated total lake area, the quantitative figures cannot be directly compared. However, the timing of events (such as melt onset, maximum observed melt, and melt decline) are comparable. For both years, but particularly for 2012/13, there is a delay between observed lake growth and modelled seasonal melt. In 2012/13, significant melting continues to be simulated by RACMO2.3 after the peak in observed lake area. We observe peak total lake area between the 19th December and 4th January. However, RACMO2.3 predicts a peak in seasonal melt on the 26th January. This suggests that either: (1) lakes had filled to their maximum capacity and any excess water was routed away from the lakes via supraglacial streams (RACMO2.3 incorporates the lateral transport of water), (2) conduits may have formed and remained open during this period, with moulins draining any additional meltwater englacially before it could pond, or (3) RACMO2.3 simulates a melt peak that did not occur in reality. There were 30 surface channels observed in 2012/13, so explanation (1) is physically plausible. *In situ* observations of moulins or conduits were not possible, so explanation (2) is not possible to analyse. The initial delay in the melt season between RACMO2.3 and the observations, alongside a similar pattern in 2007/08, suggests a modelling error. Therefore, explanation (3) was explored in greater depth.

Surface temperatures simulated by RACMO2.3 (with and without applied lapse rate, see section 4.6.2) are compared with daily mean surface air temperature readings from Syowa research station (Figure 5.7). As is expected, the RACMO2.3 modelled surface air temperatures (elevation of 240 m a.s.l. without lapse rate) produces much cooler temperatures in 2007/08 and 2012/13, which explains the delay in seasonal melt onset compared to observed lakes. However, there are occasions where the temperatures RACMO2.3 produce exceed those measured at the research station. For example, on the 15th January 2013, RACMO2.3 predicts a surface temperature of 0.9ºC, whereas Syowa research station documented a temperature of -1.4ºC. This explains why RACMO2.3 continued to model high melt rates into the end of January (whereas we observed peak melt between 19th December and 4th January as mentioned above). With applied lapse rates, we can see a bridge in the gap between modelled and station data. However, the lapse rate does not correct the times where RACMO2.3 predicts a negative trend in air

temperature, and Syowa recorded a positive trend (e.g. between the 8th January 2013 and 15th January 2013).

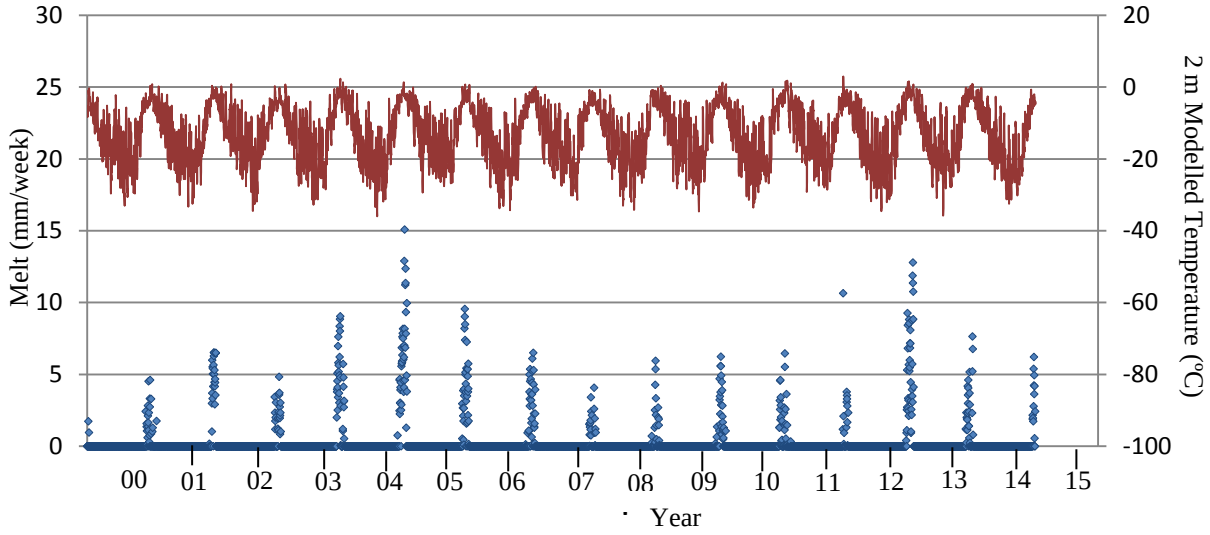

Figure 5.5: Inter-annual variability in modelled melt (mm/week) and modelled 2 m surface air temperature, simulated by the RACMO2.3 regional climate model for 2000-2015. Each year is labelled on the 1st January.

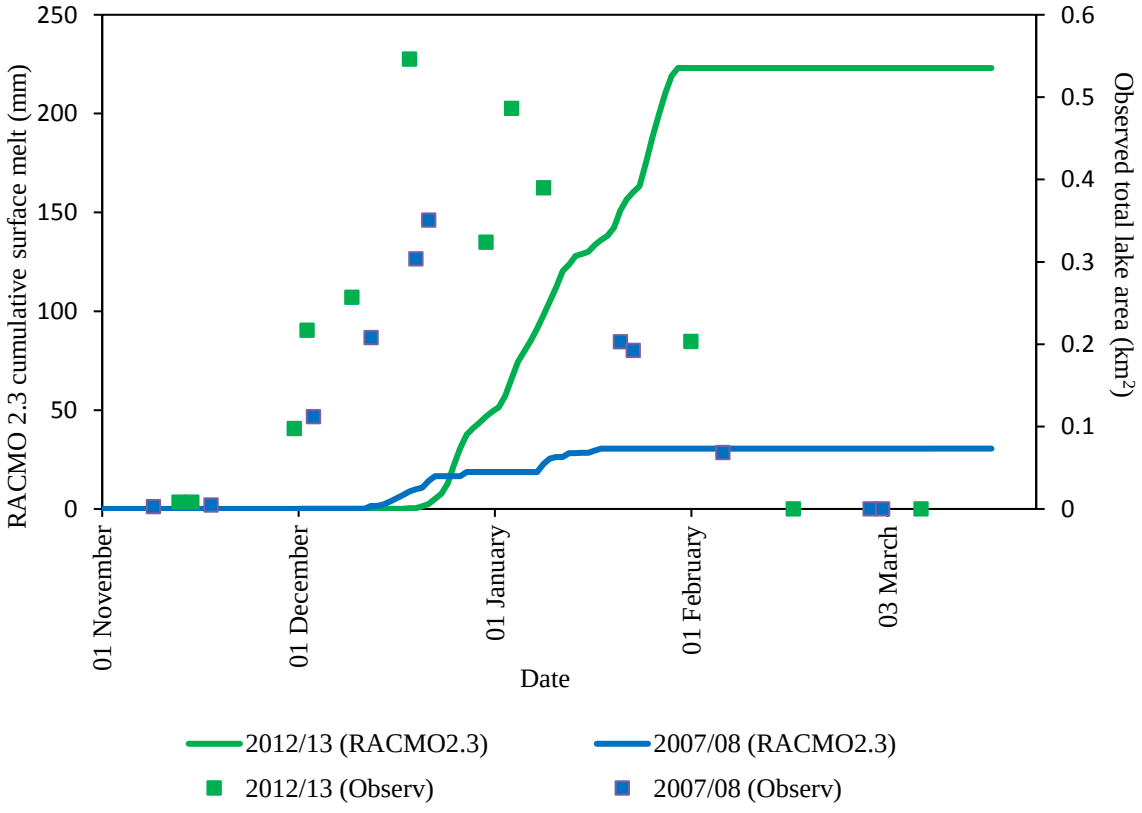

Figure 5.6: Cumulative melt simulated by RACMO2.3 compared with observed A_{total} for 2007/08 (blue) and 2012/13 (green). Note the delay in model estimates of melt onset and peak melt.

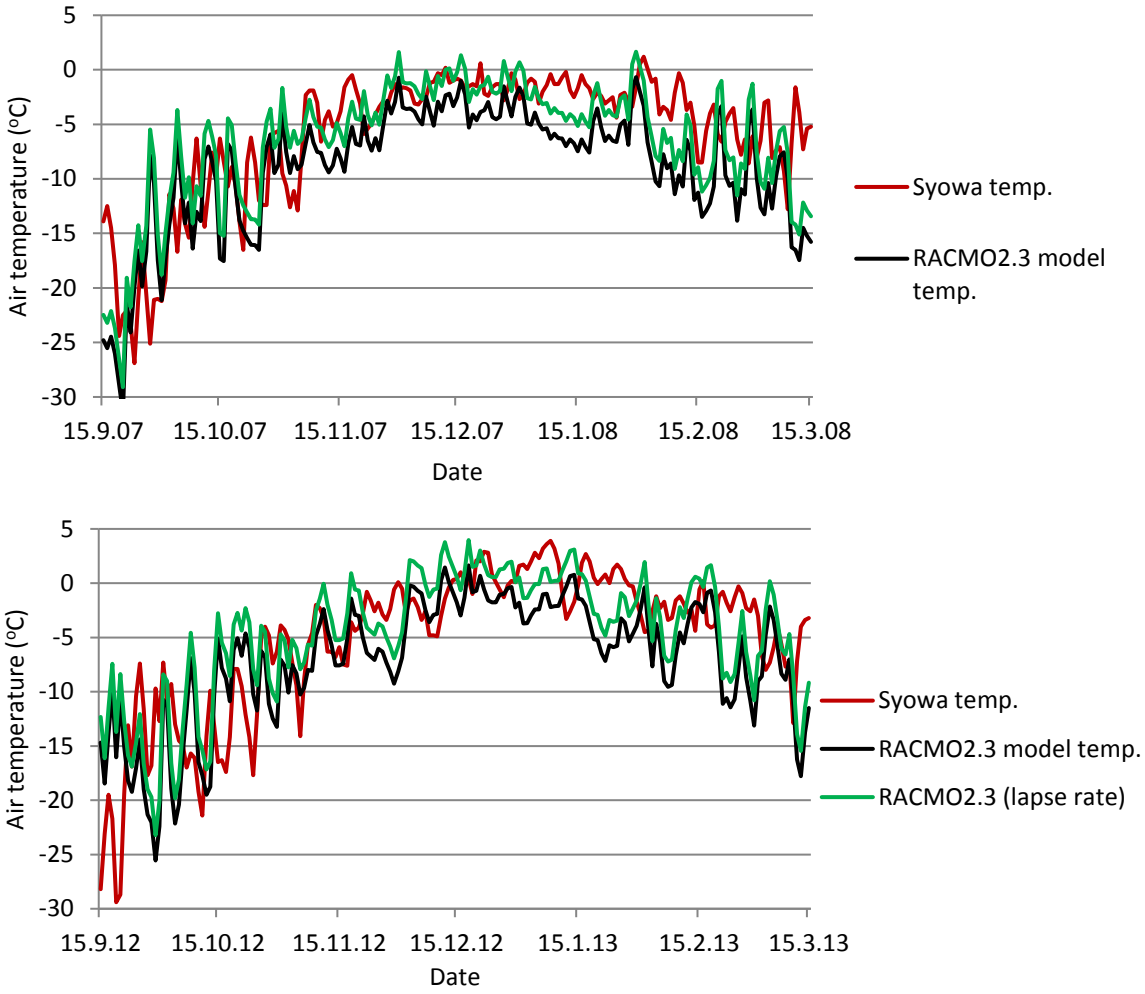

Figure 5.7: A comparison between recorded temperatures from Syowa research station (18 m a.s.l.), RACMO2.3 modelled temperatures (240 m a.s.l.) and RACMO2.3 modelled temperatures with applied lapse rate (18 m a.s.l.). (a) 2007-2008. (b) 2012-2013.

5.3 Supraglacial Lake/Channel Geometric and Spatial Properties

5.3.1 Summary of Grounding line position

The results of this study's break-of-slope analysis are shown in Figure 5.8. The elevation minimum across the glacier terminus depicted a non-uniform pattern, with the centre of the glacier terminus being grounded much further down-glacier than at the peripheries. These results closely resembled the grounding line position proposed by Fukuda et al., (2014) (Figure 5.8).

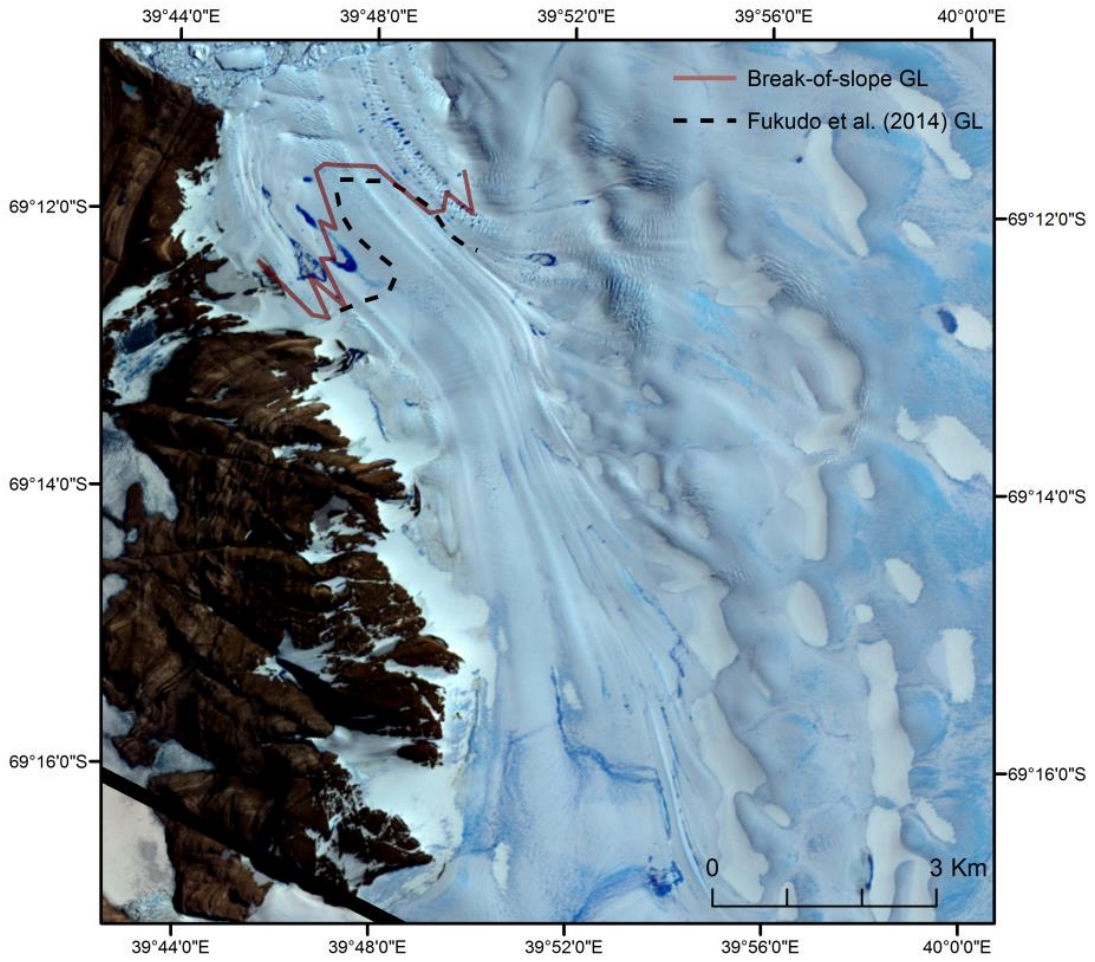

Figure 5.8: Results from break-of-slope analysis which provides an estimated location of the grounding line (brown line). Black dashed line is the grounding line from Fukuda et al. (2014).

5.3.2 Geometry and Distribution of Supraglacial Lakes

Figure 5.9 maps SGL distribution across Langhovde Glacier between 2000 and 2013. Lakes were found across the lower 18.1 km of the glacier, and range in elevation from 7 m a.s.l at the ice shelf edge to 670 m a.s.l. up-glacier. Each year, approximately 85% of lakes are present below 100 m a.s.l, and 10% above 380 m a.s.l., with an area in between that is almost devoid of SGLs.

Lake dimensions range from 30 m to 1,200 m in diameter during the warmest time in the ablation season, depending on their topographic location. There are two distinct populations of lakes: SGLs that persistently occupy the same depressions each year, and those that are transient. SGLs that reoccur in the same basins are found on the grounded part of Langhovde Glacier. They are the largest lakes observed here, reaching 1,200 metres in diameter and 450 to 166,852 m^2 in area. In comparison, transient SGLs are

observed on the floating ice shelf, and appear in different basins each year. They are much smaller than those observed at higher elevations, rarely exceeding 130 metres in length (450 to 16,900 m^2 in area). They often form in depressions that lie between the flow-stripes of the glacier surface, as well as accumulating in major crevasses. They are observed overspilling and coalescing into larger networks of water during high-melt years (i.e. 11/12). There are a few lakes which are identified as being a combination of the above. They initiate from the same location each year, but have gradually advected and elongated with ice flow over the 13 years (Figure 5.9 inset). They are located on the potential grounding line, and suggest that they are therefore forming on ice that is part-grounded and part-floating.

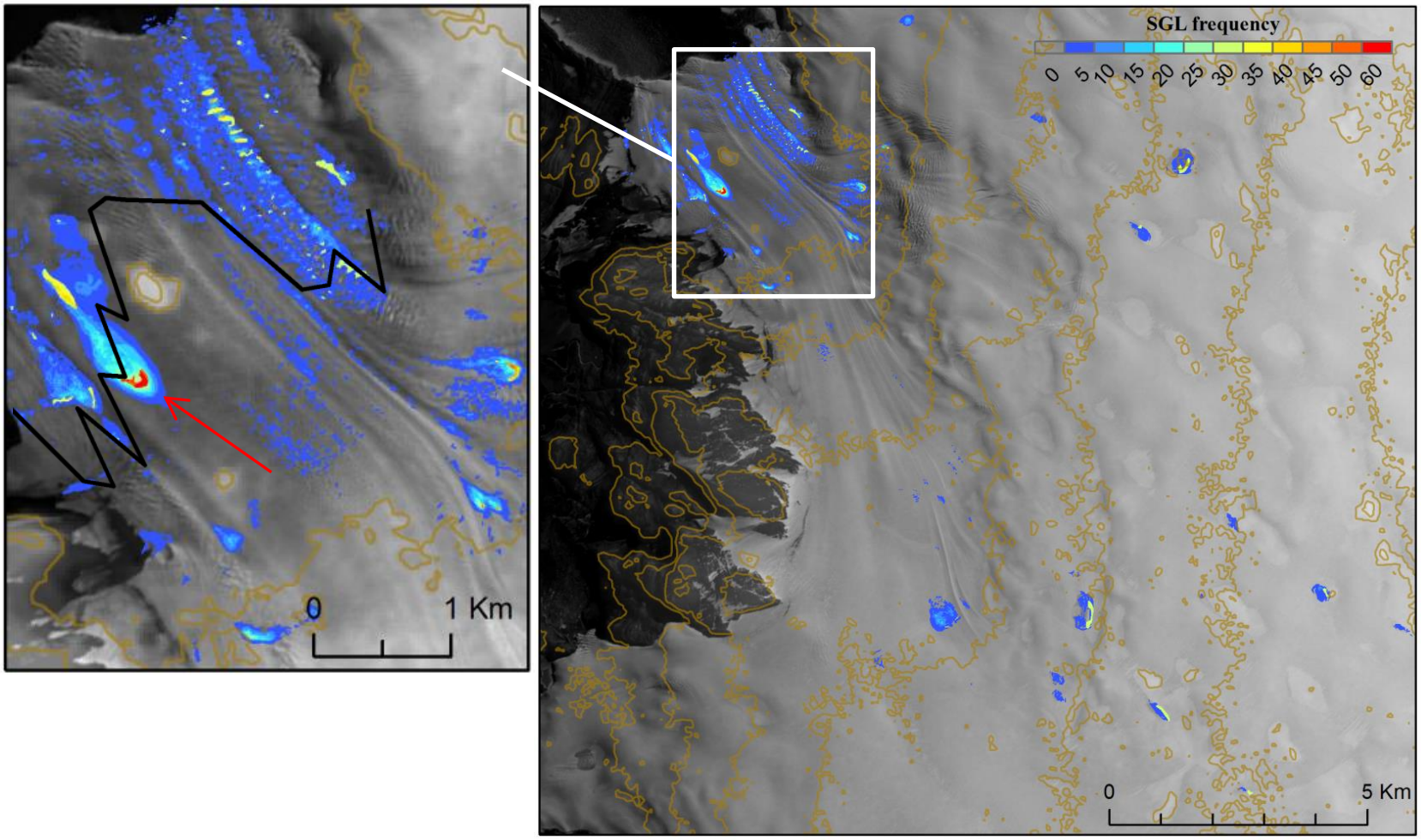

Figure 5.9: The spatial distribution of lakes from 2000-2013 (n = 7,990). Lakes are observed up to 18.1 km inland and reach elevations of 670 m a.s.l. (surface elevation is contoured at 100 m intervals in yellow). Two different configurations are observed: (1) lakes that occupy the same depressions each year, and (2) lakes that occupy different lake basins each year. Inset is a close-up of the lower reaches where SGLs both initiate from the same position and elongate with ice flow (red arrow). Black line is the grounding line.

5.3.3 Geometry and Distribution of Supraglacial Channels

The spatial distribution of supraglacial channels from 2000-2013 is mapped in Figure 5.10. These features follow the same paths each year, commonly initiating from the same point and terminating at the same point. They are present up to 630 m a.s.l. (15 km inland), and can reach lengths of 3.5 km. Their behaviour is dependent on their location, with some being a key mechanism in rerouting surface meltwater, whereas others appear static and motionless. The more dynamic linear features often initiate from SGLs and play a role in connecting SGLs to one another, and even to crevasses on the floating ice shelf. These channels appear and disappear over the course of a melt season, and are observed draining SGLs across the surface. The more static features often do not initiate from an SGL and simply form alone. These thin bodies of water are immobile during the summer months, and do not appear to have a role in the routing of water across the glacier surface.

To understand how linear meltwater features interact with the topography, results from hydro-routing on an ASTER DEM are presented in Figure 5.11. The image shows where surface channels would form and flow if there were sufficient amounts of water supplied to the system. It also demarcates the hydrological catchment area, highlighting the watershed whereby any water which forms will be directed towards Langhovde Glacier (in reality it is highly unlikely that meltwater would be available at this divide due to the altitude and temperature change). The surface channels mapped from the satellite imagery closely follow the same pathways as the modelled predictions. In addition, mapped SGLs are aligned along this network (Figure 5.11b), with channel features routing water to the lower elevations. The model reinforces the correlation between the location/behaviour of meltwater and the topography of the glacier surface.

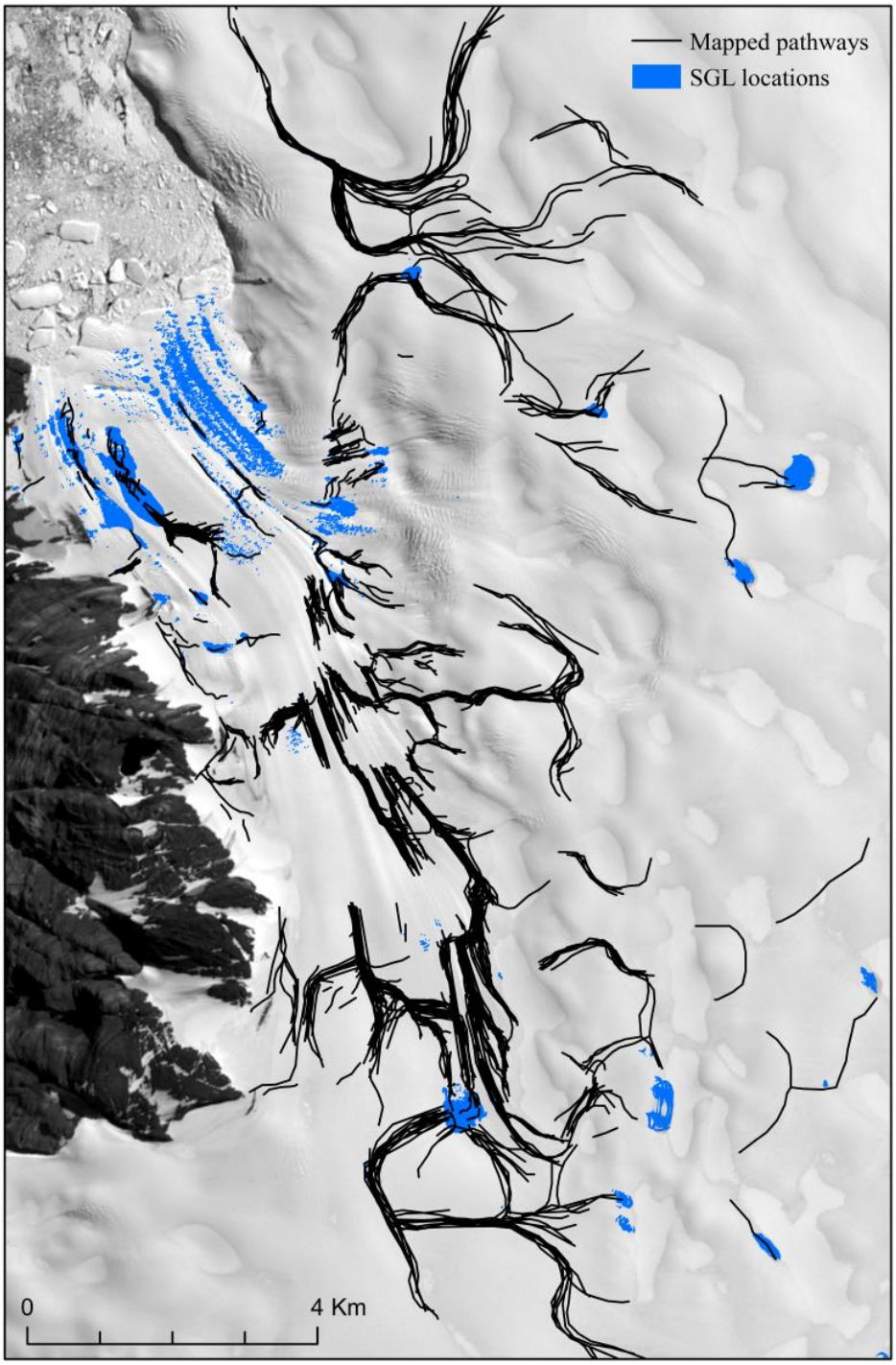

Figure 5.10: Spatial distribution of supraglacial channels (black lines) on Langhovde Glacier between 2000 and 2013. These features were mapped, and their transparency reduced, to allow observations of the key meltwater pathways. SGL polygons (blue) are underneath to show how they align and interact with surface channels.

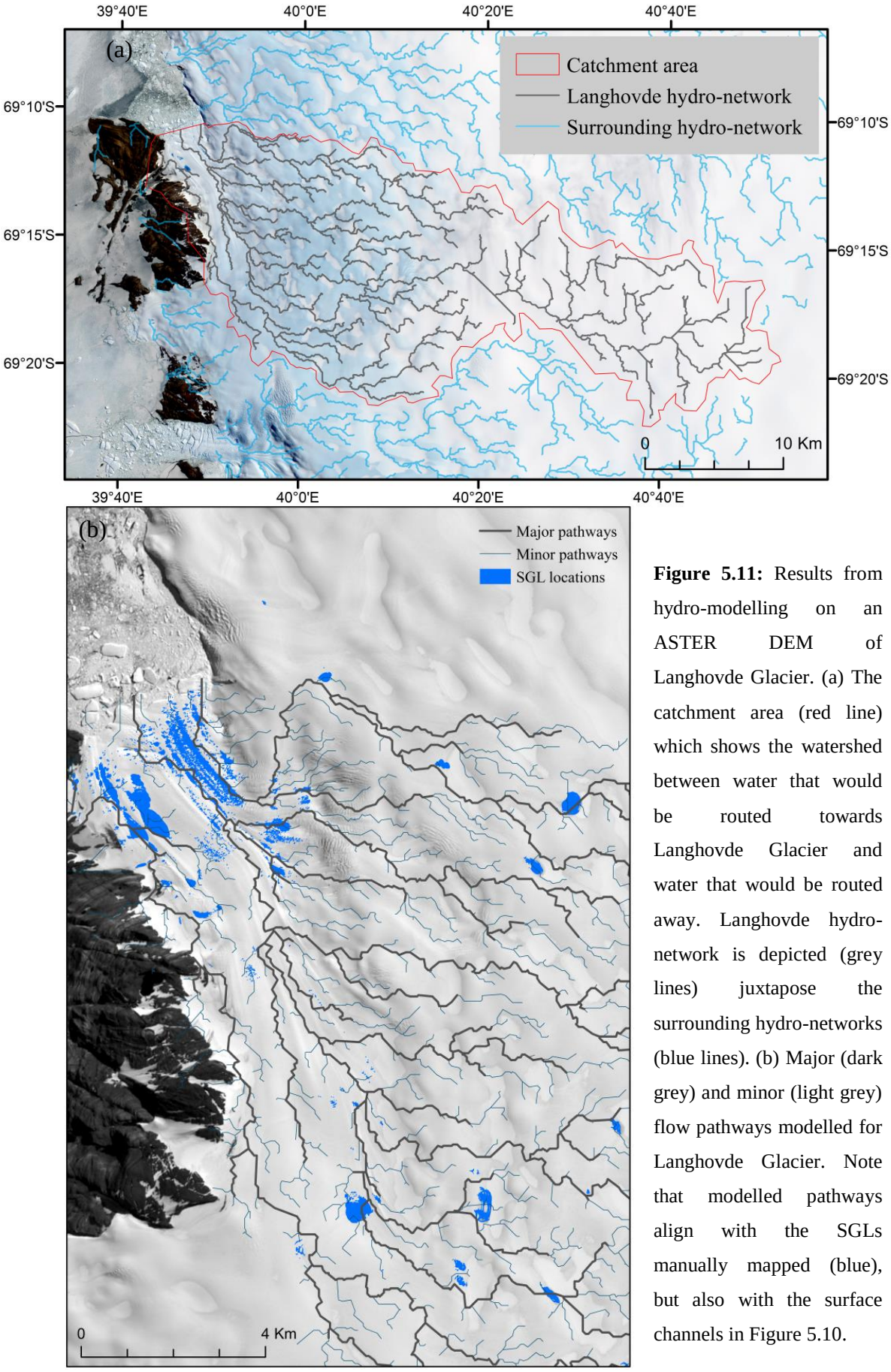

Figure 5.11: Results from hydro-modelling on an ASTER DEM of Langhovde Glacier. (a) The catchment area (red line) which shows the watershed between water that would be routed towards Langhovde Glacier and water that would be routed away. Langhovde hydro-network is depicted (grey lines) juxtapose the surrounding hydro-networks (blue lines). (b) Major (dark grey) and minor (light grey) flow pathways modelled for Langhovde Glacier. Note that modelled pathways align with the SGLs manually mapped (blue), but also with the surface channels in Figure 5.10.

5.4 Lake and Channel Demise

In this section, the typical behavioural properties of lakes over the ablation season at Langhovde Glacier are described. These evolutionary characteristics were observed over the 13 year study period. Evidence is based on visual observations from ASTER, Landsat-7 and Google Earth imagery.

5.4.1 Refreezing Lakes

As temperatures fall below 0° C and melt energy declines at the end of the austral summer, lakes are observed refreezing. This process is easily discernible on ASTER and Landsat-7 imagery. Ice is observed encroaching on the surface of lakes, often from the centre outwards (Figure 5.12). It is not unusual for a thin layer of ice to form on the surface in early February, insulating the liquid water beneath for a longer period of time (Figure 5.13). A completely thawed SGL appears dark blue on a high-resolution image. However, once freezing begins, SGLs appear lighter in colour. Refreezing occurs at higher altitudes first, before lower elevations experience the cooler surface air temperatures. As these SGLs also melt later at the start of the season, it gives SGLs at higher elevations a shorter overall ablation season. Refreezing appears to be the most common cause for SGL disappearance on Langhovde Glacier.

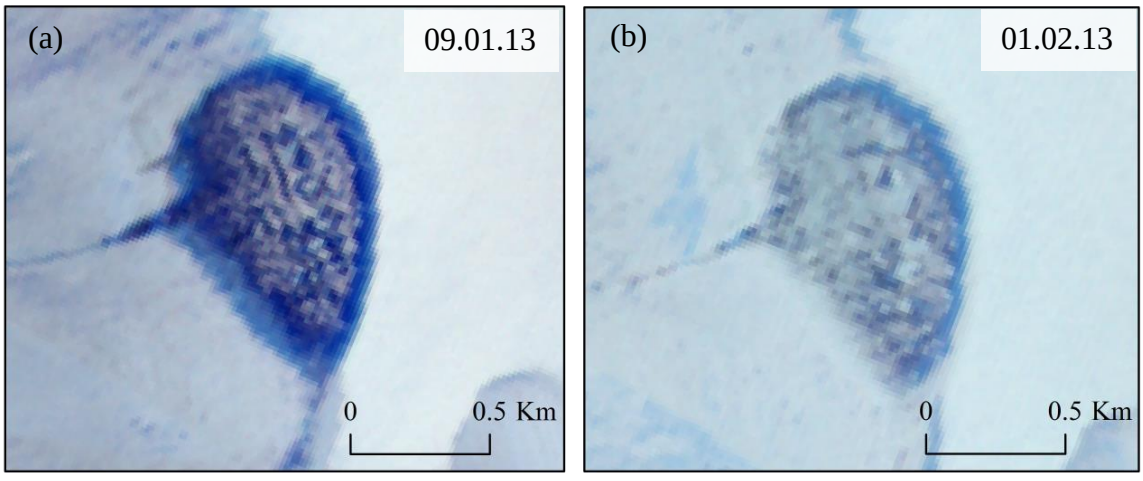

Figure 5.12: ASTER images of a refreezing lake at the end of the austral summer in February 2013. It is characterised by ice in the centre that encroaches to the peripheries, as a result of cooling surface air temperatures.

Figure 5.13: A DigitalGlobe image (Google Earth) of two SGLs on Langhovde Glacier on the 11th February 2010, located on the grounding line boundary. Despite below freezing temperatures and surface ice, underneath still appears melted at this present time.

5.4.2 Shrinking Lakes

There were a number of occasions where SGLs on the floating ice shelf reduced in size mid-season. Their visual characteristics were very different to the refreezing of SGLs observed elsewhere. Instead of a gradual refreezing process whereby ice encroaches the lake surface, here surface ice was not observed, with lakes shrinking from the outside in (Figure 5.15). This shrinking behaviour occurs over a short period of time, when surface air temperatures are well above 0° C, indicating an alternative mechanism to refreezing. For example, between 04-01-2013 and 09-01-2013 the mean air temperature was 3.2° C in the lower reaches of the glacier, 3.8° C higher than the January average for 2000-2013. During this 6-day period, 21 lakes shrunk (11% of total number of lakes) (Figure 5.14b-c). Ice was not observed on the surface of these lakes, and instead lakes shrunk from their peripheries. Within the same 6-day period lakes were observed appearing and growing elsewhere, due to the relatively warm temperatures. A mechanism to explain these observations is lake drainage through the ice shelf.

Observations of the floating ice shelf from a high-resolution (~ 0.5 m) DigitalGlobe image sourced from Google Earth provide further support for the notion of lakes draining. A 230 x 170 m feature left by a former lake was displayed in this imagery (Figure 5.16). It appears as an empty basin, which is circled by a fracture filled with

meltwater (being fed by a channel). Within the basin there are four holes, also appearing to contain meltwater. The lake that occupies this basin during the ablation seasons has been observed shrinking in other years (e.g. Figure 5.17a-b).

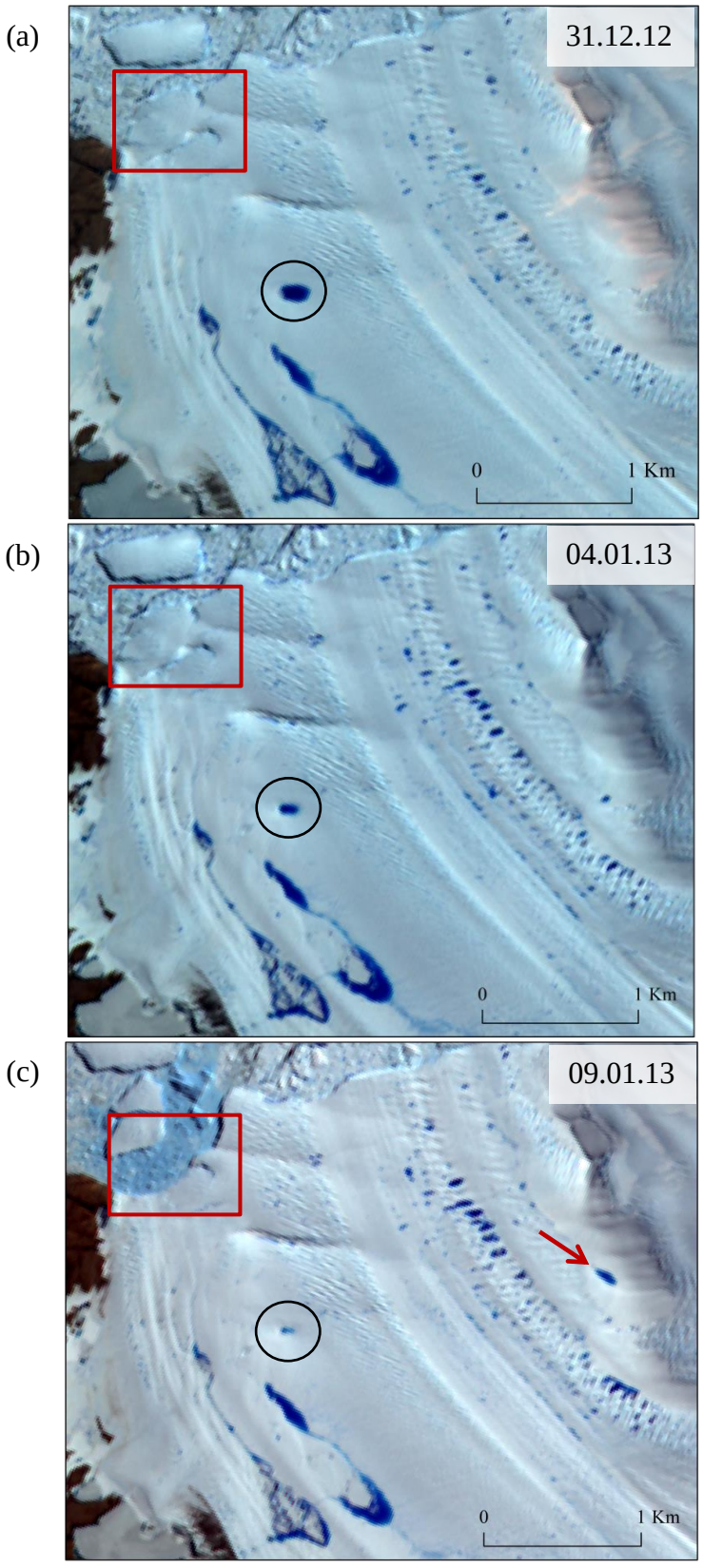

Figure 5.14: Despite above freezing temperatures and lakes growing in the area (red arrow), 21 lakes shrink/disappear in 2012/13. Red box identifies a calving event during this time period.

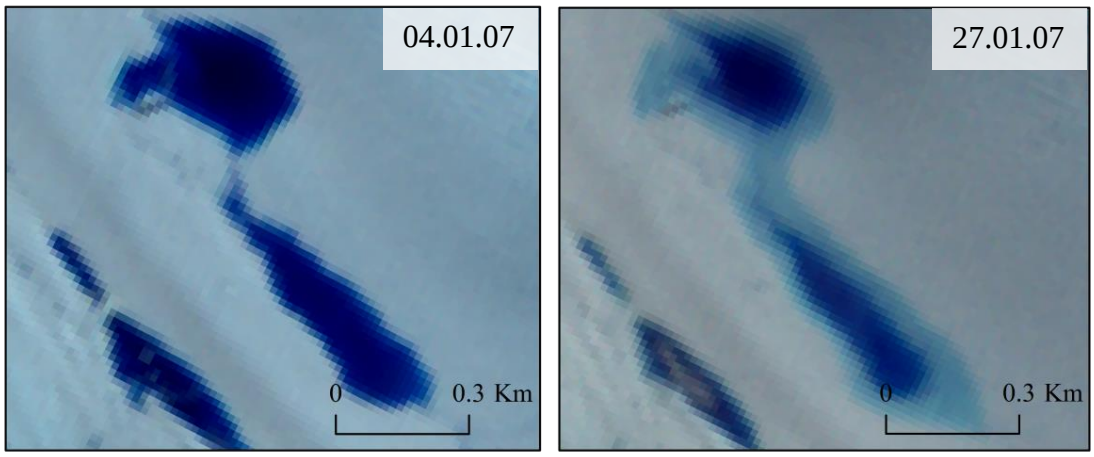

Figure 5.15: ASTER image of a lake shrinking mid-season in January 2007, located on the floating ice shelf of Langhovde Glacier.

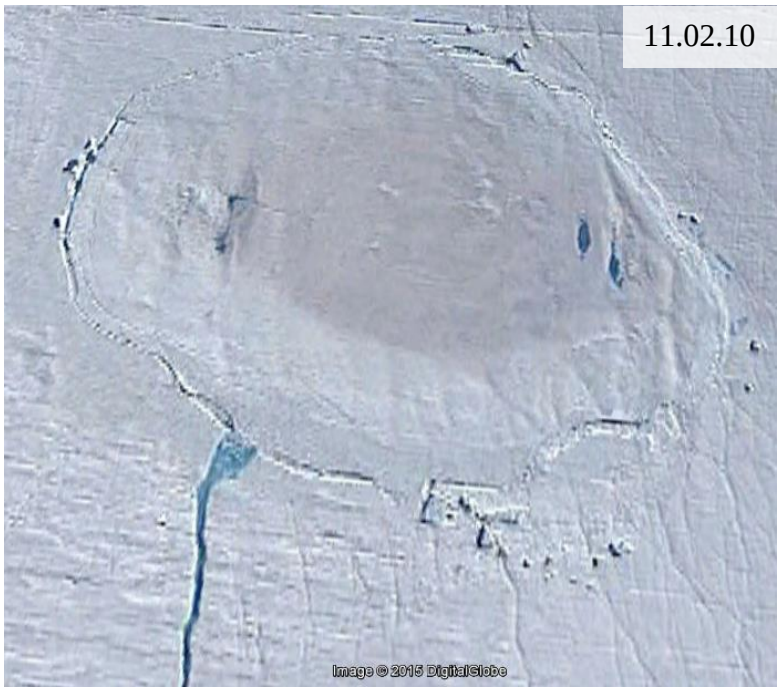

Figure 5.16: A DigitalGlobe image (Google Earth) from 2010 identifies an unusual fracture from a former lake.

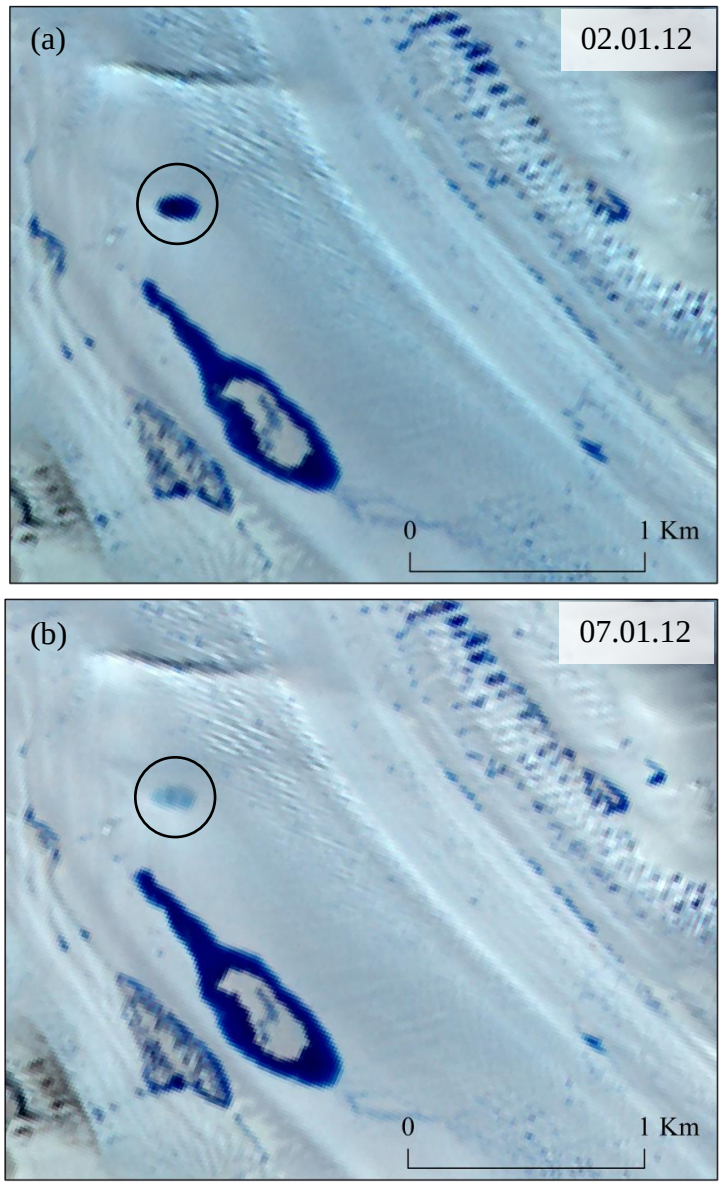

Figure 5.17: Despite lakes in the surrounding area growing, a lake on the floating ice shelf disappears within 5 days in 2012 (ASTER images).

5.4.3 Draining Supraglacially

Supraglacial channels are observed on the surface of Langhovde Glacier. As mentioned previously they closely follow the surface topography, often initiating from the same point and terminating from the same point each year. They are present up to 15 km inland (630 m a.s.l.), and reach lengths of 3.5 km (Figure 5.10). We observed two different types of feature which have varying potential to affect SGL evolution. Some initiate from SGLs (Figure 5.18a) and form sinuous drainage networks, following the local topographic slope, and rerouting meltwater to other SGLs and to the crevasses on

the floating ice shelf. Although these channels are fed by SGLs, there were no observations of fully drained lakes as a result. Conversely, others form irrespective of an SGL, and these thin meltwater features lie static over the melt season (Figure 5.18b). They are not fed by a supply of water and therefore remain shallow (interpreted from their lighter blue tones) and thin, unable to reroute water across the ice surface.

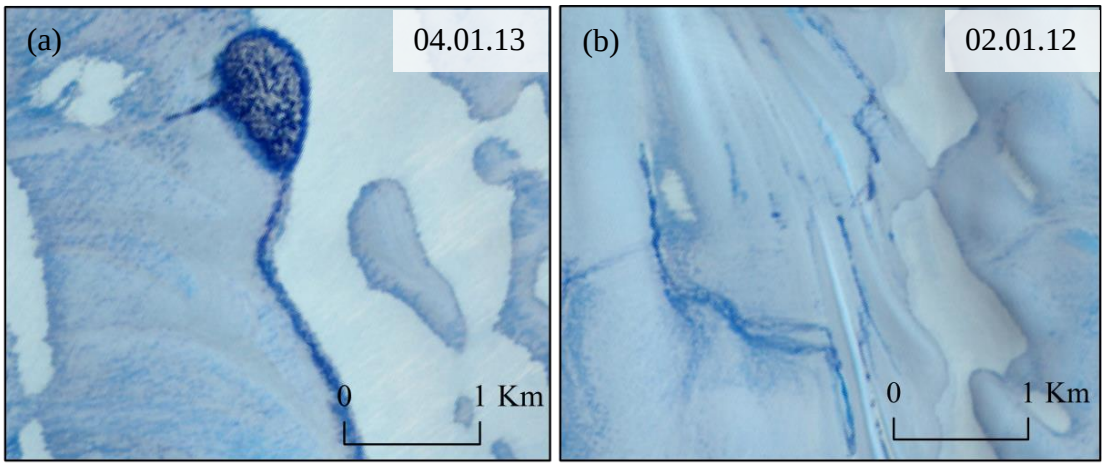

Figure 5.18: Examples of surface channel behaviours. a) A surface channel fed by a lake at higher elevation. b) Thin, linear meltwater features which form irrespective of SGLs.

Discussion

6.1 Annual and Inter-annual Variability

A typical SGL season on Langhovde Glacier is from late November to mid-February. A typical season for supraglacial channels is shorter, from early December to the end of January. This is due to channel morphology (Figure 5.8). A long, thin, and presumably shallow (light blue in colour) channel has a greater surface area in contact with glacier ice and the atmosphere, leaving them more vulnerable to cooler surface temperatures compared to a wide and deep (dark blue in colour) SGL (Rippin et al., 2015). The lag before supraglacial channels develop possibly also reflects the time before SGLs are able to overtop their edges and drain across the surface. Similar to the GrIS (Johannson et al., 2012), there are significant correlations between the four measured variables (N_{total}, A_{total}, A_{mean}, and C_{total}) on Langhovde Glacier (Figure 5.3). For example, if there was an increase in the number of lakes, one would expect an increase in the number of surface channels, and vice versa. As expected, the principle forcing mechanism is surface air temperature, which governs melt factors (i.e. incoming shortwave and longwave radiation, and sensible heat flux) and, in turn, the four measured variables (Bartholomew et al., 2010). Statistical plots (Figure 5.4) demonstrate the temperature thresholds required before lakes and channels are able to form. According to the daily mean surface air temperatures retrieved from Syowa research station, this threshold can be as low as -5ºC. For example, on the 27th November 2011, lakes appeared when daily mean surface air temperatures were ~ -4.3ºC. Further analysis of the temperature record showed minus temperatures at hourly intervals also (this was checked as although the daily mean could be minus, there may have been times during the day when temperatures reached positive). As a result, we suggest that local effects may result in the station (located 20 km south on East Ongul Island, Figure 4.4) being much windier and cooler than the glacier.

Once a threshold for SGL and channel inception has been reached, SGLs and channels are very sensitive to surface air temperature increase (Figure 5.4). This is in line with previous studies on the GrIS (Howat et al., 2010; Carr et al., 2013) and the EAIS (Kingslake et al. 2015; Trusel et al., 2012). A very small increase in the average daily surface air temperature can lead to a relatively large increase in the N_{total}, A_{total}, A_{mean}, and C_{total}; hence why lake inception and growth at the beginning of the melt season is so rapid (Figure 5.2). A number of locational factors and feedback mechanisms have

been discussed in previous research to explain the sensitivity of SGLs and channels to surface air temperatures (Bartholomew et al., 2010). Specific to the Dronning Maud Land region, blue-ice has been considered a key factor in enhancing surface melt (Liston and Winther, 2005). These regions typically consist of large ice grains and low albedos, which can absorb more solar radiation than snow or typical ice surfaces (Liston and Winther, 2005). Non-blue ice regions usually have a higher threshold for melting to occur, as incoming solar radiation needs to be greater to overcome surface reflectance (Winther et al., 2001). Once SGLs do form, albedo feedback mechanisms will enhance melt (Tedesco et al., 2011). The reduced albedo favours melting at a rate greater than surface air temperature increase (Luthje et al., 2006). This, alongside lake-bottom ablation which involves greater melting at the base and sides of a lake due to the higher thermal conductivity of water, are plausible reasons for the sensitivity of SGLs to surface air temperatures (once a threshold temperature has been reached) (Box and Ski, 2007; Georgiou et al., 2009). This sensitivity of SGLs and channels is concerning in light of future climate change (Clason et al., 2014; Fitzpatrick et al., 2014). Based on these observations, one would expect to see a nonlinear relationship between N_{total}, A_{total}, A_{mean}, and C_{total} following projected surface air temperature increases.

6.2 Supraglacial Lake Characteristics

SGLs are observed on both the floating ice shelf and the grounded ice of Langhovde Glacier (Figure 5.9). They are observed up to 18 km inland (670 m.a.s.l.), which is the highest that they have ever been documented on the EAIS. The precise location of SGLs on Langhovde Glacier is likely related to surface topography, with lakes favouring low surface gradients (i.e. not between 100 and 380 m a.s.l. where surface slope is steeper). Similar to lakes described on the GrIS (Echelmeyer et al., 1991) those that occupy the same depressions each year are usually located on the grounded ice (Figure 5.9). They are likely a reflection of the interaction between subglacial topography and ice flow (Sergienko, 2013; Echelmeyer et al., 1991). Therefore, alongside climate forcing, internal processes (e.g. ice-flow physics and bedrock features) will help determine the distribution, geometry and volume of lakes (Banwell et al., 2014). In contrast, lakes observed on the floating ice shelf will be influenced by a different set of processes. They are not defined by the bedrock topography, and possibly arise from surface and basal crevasses (McGrath et al., 2012). The flexure and fracturing of the floating ice at

Langhovde Glacier will cause inter-annual variations in ice surface depressions for meltwater to accumulate in each year (e.g. MacAyeal et al., 2013).

It is interesting to note the existence of lakes which show characteristics of part-grounded and part-floating (Figure 5.9 inset). It is possible that these lie directly over the grounding line position, and are controlled by both a bed perturbation and the advection of ice once it begins to float. If further research is able to confirm that these types of lakes do lie over the grounding line, it might be possible that the characteristics of SGLs (i.e. whether they remain stationary, appear randomly, or initiate from the same point and elongate) can be used to help determine grounding lines of similar outlet glaciers.

The existence and behaviour of SGLs on Langhovde Glacier has potential to impact on the surface energy balance. Across the entire glacier, lakes that refreeze (Figure 5.12; 5.13) and release latent heat at the end of the ablation season may influence temperature distribution and thermodynamics in the upper layers of glacier ice (Tedesco et al., 2012). The refreezing of water can modify the snowpack energy budget, morphology, density and isotopic signature (Cuffey end Peterson, 2010). Conversely, observations of SGLs disappearing on the ice shelf may have the potential to impact on the ice shelf (and potentially sheet) dynamics. At present, draining SGLs have not been reported on the EAIS, despite their prevalence on the AP and GrIS. This study has revealed a number of occasions where SGLs have disappeared despite above freezing temperatures (and SGLs growing elsewhere) (Figure 5.14; 5.15; 5.17). During peak SGL season, certain lakes were observed shrinking, displaying very different characteristics to lakes that refreeze at the end of the ablation season (i.e. these lakes shrunk from the outside-in rather than refreezing from the inside-outwards) (Selmes et al., 2011). In further support is a circular feature observed in high-resolution DigitalGlobe imagery (Figure 5.16). The feature shows similarities to ice dolines (see Section 2.4.2) described on the Larsen C ice shelf AP (Figure 6.1) (Bindschadler et al., 2002) and Amery ice shelf East Antarctica (Fricker et al., 2002). These large oval-shaped depressions are often observed on ice shelves, where meltwater ponds have drained through the ice (Glasser and Scambos, 2008).

Draining SGLs and water-filled crevasses can have a major effect on ice shelf dynamics (Sergienko and MacAyeal, 2005). Meltwater that can propagate to the ice-shelf base by hydrofracture will decrease the stability of the ice shelf and promote calving and/or disintegration (Banwell et al., 2014). Consequently, this can reduce the buttressing

forces that usually reduce ice flow above the grounding line (Scambos et al., 2004), causing an acceleration of ice upstream (Glasser et al., 2011). Although it is not certain whether the SGLs on Langhovde are able to drain the full ice-thickness, there are a number of occasions where observations of SGL disappearance are followed by a calving event (Figure 5.14). A relationship between SGLs and calving rate would be in line with previous research on this glacier, which notes sporadic calving events that are weakly correlated with surface air temperature and sea ice concentrations (Fukuda et al., 2014). Further research should focus on confirming that these lakes are able to drain to the sub-shelf ocean (and not just englacially), and then test what their impact is on ice shelf stability, and even ice velocity up-glacier. If current warming trends prevail, a greater number and size of SGLs is expected (section 6.1). Subsequently, if water-driven fracture propagation is confirmed as the likely mechanism for SGL disappearance observed in this study, we might expect to see more of these events on Langhovde Glacier in the future (Banwell et al., 2013).

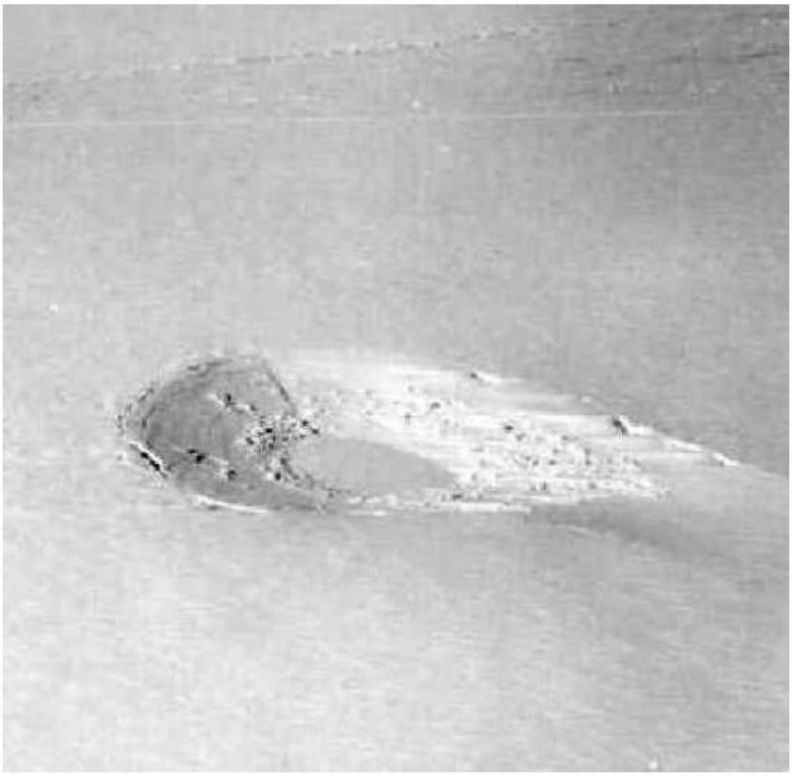

Figure 6.1: Aerial photograph of an ice doline on the Larsen Ice Shelf, from Bindschadler et al. (2002).

6.3 Supraglacial Channel Characteristics

On Langhovde Glacier, supraglacial channels are observed coinciding with SGL evolution. Surface channels have been documented elsewhere in East Antarctica,

namely the Nivlisen ice shelf (Kingslake et al., 2014). However, they have not been documented as far inland on the grounded ice sheet as we detect. Sinuous, dynamic channels that were observed instigating from SGLs (Figure 5.18a) and connecting SGLs to crevasses closely resemble those described by Kingslake et al. (2014); and a similar initiation mechanism via the turbulent dissipation of heat is assumed (Tedesco et al., 2013). However, the channels on Langhovde Glacier were not as long as those described by Kingslake et al. (2014). They documented >70 km long channels across the Nivlisen ice shelf, whereas surface channels on Langhovde Glacier reached no more than 3.5 km. Nevertheless, they behaved in a similar way, by initiating from a lake and routing water across the surface. Kingslake et al. (2014) modelled 'unstable drainage', whereby the discharge from an SGL increases with time, presumably from increased channel incision. This process results in a lake fully draining. However, a complete lake drainage event via surface flow was not observed on Langhovde Glacier. Although channels initiated from SGLs, there were no observations of a fully-drained lake as a consequence. Instead, these observations resemble the 'stable drainage' modelled by Kingslake et al. (2014). This refers to lake bed ablation exceeding channel incision and, therefore, a lake is not completely emptied. As 'unstable drainage' is considered a product of greater initial lake area and input (Kingslake et al., 2014), which we expect to see if warming temperatures prevail (section 6.1), observations of 'unstable drainage' may emerge in the future.

The presence of surface channels may have the potential to influence the transient behaviour of the subglacial environment. As documented in Greenland, channels can connect lakes to moulins on the glacier surface, thereby supplying water to the ice/bed interface (Das et al., 2008). The resolution of imagery in this study was not sufficient to identify moulins on the glacier surface with confidence; however, it was interesting to note that channels often terminate in the same location throughout the melt season (Figure 5.10). Each year, the supraglacial channels on Langhovde Glacier follow the same route and terminate at the same point. Although a number of factors could also cause this (i.e. insufficient water supply), it may be possible that these channels are reaching moulins, and it therefore follows that the water would be draining into the glacier, and perhaps to the bed. Considering the effects of meltwater routing to the base of the GrIS, it is important to discern why these channels terminate so abruptly on Langhovde Glacier.

The second form of linear meltwater feature observed were those that did not initiate from an SGL. They were very thin, linear melt features that simply formed in isolation (Figure 5.18b). Their static nature and consistency in length and position suggested a thin lake, similar to those described by Glasser and Scambos (2008) on the Larsen C ice shelf. It is unlikely that these features have a considerable effect on the surface of the glacier, considering their size and isolation from SGLs.

6.4 Potential Future Implications

Based on these findings, we would expect to see increased lake incidence and drainage in a warmer environment on both the floating and grounded ice of East Antarctica. Lake drainage and meltwater routing could therefore be very important in this region in the near future. Based on research in Greenland (Zwally et al., 2002; Das et al., 2008), we would expect to see transient acceleration and ice sheet uplift in response to SGLs draining on the grounded ice. However, this is likely to be on a diurnal scale, and it would be interesting to see how quickly the subglacial system begins to mediate the flow of water. The subglacial environment of East Antarctica is likely to be inefficient and not channelized, based on limited availability of supraglacial melt compared to Greenland (Trusel et al., 2012). Based on this assumption, and if lake drainage events are more prevalent in the future, we might expect to see a dramatic initial increase in ice motion/uplift along the East Antarctic coastline during summer seasons (Schoof, 2010). Until the system is able to channelize and manage subglacial meltwater flow efficiently, like we believe is beginning to happen in Greenland, the pulses of meltwater that may potentially reach the subglacial system of East Antarctica are likely to temporarily increase ice stream and outlet glacier velocity. However, in light of recent research on the decadal characteristics of the subglacial environment along a land-terminating sector of Greenland (Tedstone et al., 2015), we might expect to see the subglacial drainage system adapt to meltwater supply in the long-term.

The appearance and disappearance of SGLs observed on the floating ice shelf of Langhovde present an additional concern for the coastline and future of East Antarctica. As shown in this study and others (Tedesco and Monaghan, 2009), little atmospheric warming is necessary to dramatically increase the areal extent of surface melting. As modelled by DeConto and Pollard (2016), surface meltwater-enhanced calving via hydrofracture can aid in ice shelf disintegration and an increase in seaward ice flux.

Consequently, increased open-ocean warming and warm-water incursions into the ice shelf cavity can initiate grounding line retreat. This is particularly concerning as the EAIS includes more than two-thirds of the total volume of Antarctic ice grounded below sea level (Fretwell et al., 2013), which may be vulnerable to marine ice sheet instability (Schoof, 2007). The EAIS is characterised by deep subglacial basins with marine-terminating, reverse-sloped outlet troughs (some up to 1500m deep) (DeConto and Pollard, 2016). Large parts of the East Antarctic coastline are therefore vulnerable to runaway marine ice shelf instability, with a potential trigger mechanism being increased supraglacial meltwater on the ice shelves.

6.5 RACMO2.3

This study relied strongly on high resolution imagery (ASTER and Landsat-7) to easily discern lake boundaries and identify lake characteristics. RACMO2.3 is a regional climate model that can simulate surface air temperature and meltwater runoff based on input parameters (Van Wessem et al., 2014). Its 2000-2013 output for Langhovde Glacier was compared with this study's results, to determine its reliability in diagnostic and prognostic modelling on outlet glaciers. Similar to results by Barrand et al. (2013) for RACMO2, RACMO2.3 produced reliable estimates of inter-annual melt variability for Langhovde glacier (Figure 5.5). It was able to distinguish between a relatively high melt year (2012/13) and a relatively low melt year (2007/08), consistent with observations. However, on an annual scale, there were great discrepancies in the timing of the seasonal melt cycle (Figure 5.6). This is largely due to its weak ability in replicating surface air temperatures similar to station data (Figure 5.7). RACMO2.3 produced cooler temperatures (even with applied lapse rates) compared to station readings, which meant it will have also underestimated surface melt generated. This can largely be due to its crude representation of the coastal climate, based on its 27 km grid cell. The resolution is too low for Langhovde Glacier (Figure 4.10), and therefore it does not accurately represent the topography (merging its entire elevation to 240 m) and atmospheric flow. Similar discrepancies have been noted in locational research on the AP (Barrand et al., 2013) and for Terre Adelie, East Antarctica (Lenaerts et al., 2012). Future runs which can utilise the most recent advance in model resolution (5.5 km) (Van Wessem et al., 2015), alongside more detailed DEMs, will further improve the use of RACMO2.3 in constraining surface melt and air temperature on outlet glaciers such as Langhovde.

Conclusions

In this study, 7,990 SGLs and 855 surface channels were digitized between 2000 and 2013 at Langhovde Glacier, East Antarctica. The total number of lakes, total lake area, mean lake area, and number of surface channels in each satellite image (n = 153) were calculated. These results were analysed alongside meteorological readings and previous SGL studies to produce the following key conclusions:

1. **Supraglacial lakes exist on the grounded and floating section of the glacier and there is strong annual and inter-annual variability in their evolution between 2000 and 2013.**

This study provides the first detailed multi-year study of SGL evolution on an East Antarctic outlet glacier, documenting lake inception, development, and demise over 13 ablation seasons. In each scene, N_{total}, A_{total}, and A_{mean}, are significantly correlated with one another. In addition, all variables show a significant correlation with daily surface air temperatures. SGLs are very sensitive to small increases in surface air temperature, with peak N_{total}, A_{total}, and A_{mean} documented soon after a threshold has been reached. This is likely due to feedback mechanisms such as melt-albedo feedback and lake-bottom ablation. If current warming trends continue, we might expect to see an exponential increase in N_{total}, A_{total}, and A_{mean} for each temperature increment, based on these feedback mechanisms.

2. **There are spatiotemporal trends in the location of SGLs on Langhovde Glacier.**

SGLs are shown to exist up to 670 m a.s.l. (18 km inland) on the outlet glacier, the highest that SGLs have ever been reported on East Antarctica. The location of SGLs is partly related to topographic slope, with lakes favouring the low and high elevations which have low slope gradient. Lakes on the grounded ice occupy the same surface depressions each year, likely a result of subglacial topography (Echelmeyer et al., 1991). Lakes on the floating ice shelf occupy different lake basins each year, with the inter-annual variability in the flexure and fracturing of the shelf helping to develop new undulations for water to accumulate. A couple of lakes are observed both initiating from the same basin, and advecting with ice flow each year. They are possibly located directly over the grounding line, and may offer a new means of identifying grounding line positions on glaciers where SGLs are prevalent.

3. There are spatiotemporal trends in the number and evolution of supraglacial channels on Langhovde Glacier

Channel-like features on Langhovde Glacier have a shorter ablation season compared to SGLs, most likely due to their shape and size which leaves them more vulnerable to surface air temperature fluctuations and freezing. Two types of linear meltwater feature are identified on the glacier: sinuous channels and thin standing bodies of water. The former are observed draining from SGLs, connecting SGLs, and routing water across the ice surface. There were no observations of channels draining an SGL completely (as observed in Greenland), however, if the modelled parameters necessary for this to happen are as Kingslake et al. (2015) suggests (i.e. greater initial lake area), we might expect to see this occurring if warming temperatures prevail. The second form of linear feature were those that formed irrespective of SGLs, and appeared much shallower (light blue compared to dark blue), similar to a thin lake (Glasser and Scambos, 2008). Although moulins were not possible to discern in satellite imagery, it was noted how channels often terminate in the same positions over the melt season, each year. Further research should focus on determining why these channels terminate where they do, and whether they are able to access the en- or sub-glacial environment.

4. SGLs were observed freezing, possibly draining through-ice, and draining supraglacially

SGLs on Langhovde Glacier refreeze at the end of the ablation season. However, mid-season there was a number of occasions where lakes on the floating ice shelf have shown a different mechanism for areal decline. Observations of lakes shrinking, despite positive air temperatures and lakes growing elsewhere, suggests potential for lakes to drain through-ice. A doline-type feature observed in high-resolution imagery on the floating ice shelf shows similarities to depressions caused by the fracture propagation of lakes on the AP, and thus would support this theory. This may be the reason for sporadic calving events documented on Langhovde Glacier (Fukuda et al. 2014). Further research should focus on confirming whether these disappearing lakes are, in fact, able to drain via hydrofracture. If this can be confirmed, we need to consider how warming temperatures may affect the prevalence of these events, and what impact this may have on the stability of the ice shelf.

From this combined analysis, the idea that East Antarctica is not vulnerable now (or in the near future) to the hydrological changes experienced in Greenland and the AP can

be questioned. Future research should focus on using higher resolution imagery to try and capture possible drainage events and determine their impact on ice shelf stability and transient variations in ice velocity on Langhovde Glacier. Considering the role of SGLs in causing seasonal variations in ice velocity in Greenland, it would also be useful to model what lake volume and temperature thresholds are required for SGLs to drain via fracture propagation on the grounded ice of East Antarctica. This study suggests that similar SGL and channel activities are likely at other outlet glaciers of the EAIS, and investigations into their prevalence and potential to generate seasonal change in ice sheet dynamics across the entire coastline are required.

References

Alley, R. B., & Whillans, I. M. (1984). Response of the East Antarctica ice sheet to sea-level rise. *Journal of Geophysical Research: Oceans (1978–2012)*,*89*(C4), 6487-6493.

Alley, R. B., Clark, P. U., Huybrechts, P., & Joughin, I. (2005). Ice-sheet and sea-level changes. *science*, *310* (5747), 456-460.

Arnold, N. (2010). A new approach for dealing with depressions in digital elevation models when calculating flow accumulation values. *Progress in Physical Geography*, *34*(6), 781-809.

Banwell, A. F., Arnold, N. S., Willis, I. C., Tedesco, M., & Ahlstrøm, A. P. (2012). Modeling supraglacial water routing and lake filling on the Greenland Ice Sheet. *Journal of Geophysical Research: Earth Surface (2003–2012)*, *117*(F4).

Banwell, A. F., Willis, I. C., & Arnold, N. S. (2013). Modeling subglacial water routing at Paakitsoq, W Greenland. *Journal of Geophysical Research: Earth Surface*, *118*(3), 1282-1295.

Banwell, A. F., Caballero, M., Arnold, N. S., Glasser, N. F., Cathles, L. M., & MacAyeal, D. R. (2014). Supraglacial lakes on the Larsen B ice shelf, Antarctica, and at Paakitsoq, West Greenland: a comparative study. *Annals of Glaciology*, *55*(66), 1-8.

Barrand, N. E., Hindmarsh, R. C., Arthern, R. J., Williams, C. R., Mouginot, J., Scheuchl, B., Rignot, E., Ligtenberg, S.R.M., van den Broeke, M.R., Edwards, T.L., Cook, A.L., & Simonsen, S. B. (2013). Computing the volume response of the Antarctic Peninsula ice sheet to warming scenarios to 2200. *Journal of Glaciology*, *59*(215), 397-409.

Bartholomew, I., Nienow, P., Mair, D., Hubbard, A., King, M. A., & Sole, A. (2010). Seasonal evolution of subglacial drainage and acceleration in a Greenland outlet glacier. *Nature Geoscience*, *3*(6), 408-411.

Bartholomew, I., Nienow, P., Sole, A., Mair, D., Cowton, T., Palmer, S. and Wadham, J (2011). Supraglacial forcing of subglacial drainage in the ablation zone of the Greenland ice sheet. *Geophysical Research Letters*, 38(8).

Bartholomew, I., Nienow, P., Sole, A., Mair, D., Cowton, T. and King, M.A. (2012). Short-term variability in Greenland Ice Sheet motion forced by time-varying meltwater drainage: Implications for the relationship between subglacial drainage system behavior and ice velocity. *Journal of Geophysical Research: Earth Surface*, 117(F3).

Bindschadler, R., Choi, H., Wichlacz, A., Bingham, R., Bohlander, J., Brunt, K., ... & Young, N. (2011). Getting around Antarctica: new high-resolution mappings of the grounded and freely-floating boundaries of the Antarctic ice sheet created for the International Polar Year. *The Cryosphere*.

Bøggild, C. E., Brandt, R. E., Brown, K. J., & Warren, S. G. (2010). The ablation zone in northeast Greenland: ice types, albedos and impurities. *Journal of Glaciology*, *56*(195), 101-113.

Box, J.E. (1997). Melt pond depth variations and albedo in the Jacobshavn ablation region of the Greenland ice sheet. [Abstract U21A-19.] EOS Trans. AGU, 78(46).

Box, J. E., & Ski, K. (2007). Remote sounding of Greenland supraglacial melt lakes: implications for subglacial hydraulics. *Journal of glaciology*, *53*(181), 257-265.

Carr, J. R., Vieli, A., & Stokes, C. (2013). Influence of sea ice decline, atmospheric warming, and glacier width on marine-terminating outlet glacier behavior in northwest Greenland at seasonal to interannual timescales. *Journal of Geophysical Research: Earth Surface*, *118*(3), 1210-1226.

Clason, C. C., Mair, D. W. F., Nienow, P. W., Bartholomew, I. D., Sole, A., Palmer, S., & Schwanghart, W. (2014). Modelling the transfer of supraglacial meltwater to the bed of Leverett Glacier, southwest Greenland. *The Cryosphere Discussions*, *8*(4), 4243-4280.

Cuffey, K. M., & Paterson, W. S. B. (2010). *The physics of glaciers*. Academic Press.

Darnell, K. N., Amundson, J. M., Cathles, L. M., & MacAyeal, D. R. (2013). The morphology of supraglacial lake ogives. *Journal of Glaciology*, *59*(215), 533-544.

Das, S. B., Joughin, I., Behn, M. D., Howat, I. M., King, M. A., Lizarralde, D., & Bhatia, M. P. (2008). Fracture propagation to the base of the Greenland Ice Sheet during supraglacial lake drainage. *Science*, *320*(5877), 778-781.

DeConto, R.M. and Pollard, D. (2016). Contribution of Antarctica to past and future sea-level rise. *Nature*, *531*(7596), pp.591-597.

Domack, E., Duran, D., Leventer, A., Ishman, S., Doane, S., McCallum, S., ... & Prentice, M. (2005). Stability of the Larsen B ice shelf on the Antarctic Peninsula during the Holocene epoch. *Nature*, *436*(7051), 681-685.

Echelmeyer, K., & Harrison, W. (1990). Jakobshavns Isbrae, West Greenland: Seasonal variations in velocity-or lack thereof. *Journal of Glaciology*, *36*.

Echelmeyer, K., Clarke, T. S., & Harrison, W. D. (1991). Surficial glaciology of Jakobshavns Isbræ, West Greenland. I: Surface morphology. *Journal of Glaciology*, *37*(127), 368-382.

Enderlin, E.M., Howat, I.M., Jeong, S., Noh, M.J., Angelen, J.H. and Broeke, M.R. (2014). An improved mass budget for the Greenland ice sheet. *Geophysical Research Letters*, *41*(3), 866-872.

Fitzpatrick, A. A. W., Hubbard, A. L., Box, J. E., Quincey, D. J., Van As, D., Mikkelsen, A. P. B., ... & Jones, G. A. (2014). A decade (2002–2012) of supraglacial lake volume estimates across Russell Glacier, West Greenland.*The Cryosphere*, *8*(1), 107-121.

Fretwell, P., Pritchard, H.D., Vaughan, D.G., Bamber, J.L., Barrand, N.E., Bell, R., Bianchi, C., Bingham, R.G., Blankenship, D.D., Casassa, G. and Catania, G. (2013). Bedmap2: improved ice bed, surface and thickness datasets for Antarctica. *The Cryosphere*, *7*(1).

Fricker, H. A., & Scambos, T. (2009). Connected subglacial lake activity on lower Mercer and Whillans ice streams, West Antarctica, 2003–2008. *Journal of Glaciology*, *55*(190), 303-315.

Fukuda, T. (2014) Variations in the terminus position, ice velocity and surface elevation of the Langhovde Glacier, East Antarctica. Unpublished PhD thesis. Hokkaido University

Fukuda, T., Sugiyama, S., Sawagaki, T., & Nakamura, K. (2014). Recent variations in the terminus position, ice velocity and surface elevation of Langhovde Glacier, East Antarctica. *Antarctic Science*, *26*(06), 636-645.

Georgiou, S., Shepherd, A., McMillan, M., & Nienow, P. (2009). Seasonal evolution of supraglacial lake volume from ASTER imagery. *Annals of Glaciology*, *50*(52), 95-100.

Glasser, N. F., & Scambos, T. A. (2008). A structural glaciological analysis of the 2002 Larsen B ice-shelf collapse. *Journal of Glaciology*, *54*(184), 3-16.

Glasser, N. F., Kulessa, B., Luckman, A., Jansen, D., King, E. C., Sammonds, P. R., ... & Jezek, K. C. (2009). Surface structure and stability of the Larsen C ice shelf, Antarctic Peninsula. *Journal of Glaciology*, *55*(191), 400-410.

Glasser, N. F., Scambos, T. A., Bohlander, J., Truffer, M., Pettit, E., & Davies, B. J. (2011). From ice-shelf tributary to tidewater glacier: continued rapid recession, acceleration and thinning of Röhss Glacier following the 1995 collapse of the Prince Gustav Ice Shelf, Antarctic Peninsula. *Journal of Glaciology*, *57*(203), 397-406.

Glasser, N. F., & Gudmundsson, G. H. (2012). Longitudinal surface structures (flowstripes) on Antarctic glaciers. *The Cryosphere*, *6*(2), 383-391.

Hall, A., & Visbeck, M. (2002). Synchronous variability in the Southern Hemisphere atmosphere, sea ice, and ocean resulting from the Annular Mode*.*Journal of Climate*, *15*(21), 3043-3057.

Haran, T., J. Bohlander, T. Scambos, T. Painter, and M. Fahnestock. 2014. *MODIS Mosaic of Antarctica 2008-2009 (MOA2009) Image Map, Version 1*. [indicate subset used]. Boulder, Colorado USA. NSIDC: National Snow and Ice Data Center. http://dx.doi.org/10.7265/N5KP8037. [Date Accessed].

Hambrey, M. J., & Dowdeswell, J. A. (1994). Flow regime of the Lambert Glacier-Amery Ice Shelf system, Antarctica: structural evidence from Landsat imagery. *Annals of Glaciology*, *20*(1), 401-406.

Hoffman, M. J., Catania, G. A., Neumann, T. A., Andrews, L. C., & Rumrill, J. A. (2011). Links between acceleration, melting, and supraglacial lake drainage of the western Greenland Ice Sheet. *Journal of Geophysical Research: Earth Surface (2003–2012)*, *116*(F4).

Howat, I. M., Box, J. E., Ahn, Y., Herrington, A., & McFadden, E. M. (2010). Seasonal variability in the dynamics of marine-terminating outlet glaciers in Greenland. *Journal of Glaciology*, *56*(198), 601-613.

Hubbard, B. and Nienow, P. (1997). Alpine subglacial hydrology. *Quaternary Science Reviews*, *16*(9), 939-955.

Iken, A. and Bindschadler, R.A. (1986). Combined measurements of subglacial water pressure and surface velocity of Findelengletscher, Switzerland: conclusions about drainage system and sliding mechanism. *Journal of Glaciology*, *32*(110), 101-119.

Johannson, M.A., Jansson, P., & Brown, I.A. (2012) Characteristics of supra-glacial lakes on the south-west Greenland Ice Sheet, Manuscript. Unpublished PhD thesis. Stockholm University

Johansson, A. M., Jansson, P., & Brown, I. A. (2013). Spatial and temporal variations in lakes on the Greenland Ice Sheet. *Journal of hydrology*, *476*, 314-320.

Joughin, I., Das, S. B., King, M. A., Smith, B. E., Howat, I. M., & Moon, T. (2008). Seasonal speedup along the western flank of the Greenland Ice Sheet.*Science*, *320*(5877), 781-783.

Joughin, I., Das, S. B., Flowers, G. E., Behn, M. D., Alley, R. B., King, M. A., ... & Van Angelen, J. H. (2013). Influence of ice-sheet geometry and supraglacial lakes on seasonal ice-flow variability. *The Cryosphere*, *7*(4), 1185-1192.

Kääb, A. (2002). Monitoring high-mountain terrain deformation from repeated air-and spaceborne optical data: examples using digital aerial imagery and ASTER data. *ISPRS Journal of Photogrammetry and remote sensing*, *57*(1), 39-52.

King, M. A., Bingham, R. J., Moore, P., Whitehouse, P. L., Bentley, M. J., & Milne, G. A. (2012). Lower satellite-gravimetry estimates of Antarctic sea-level contribution. *Nature*, *491*(7425), 586-589.

Kingslake, J., & Sole, A. (2015). Modelling channelized surface drainage of supraglacial lakes. *Journal of Glaciology*, *61*(225), 185-199.

Koenig, L., Forster, R., Brucker, L., & Miller, J. (2015). Remote sensing of accumulation over the Greenland and Antarctic ice sheets. *Remote Sensing of the Cryosphere*, 157-186.

Konzelman, T. (1995). Variations of ablation, albedo and energy balance at the tnargin of the Greenland ice sheet, Kronprins Christian Land, eastern north Greenland. *Journal of Glaciology*, *41*(137).

Lampkin, D. J., & VanderBerg, J. (2011). A preliminary investigation of the influence of basal and surface topography on supraglacial lake distribution near Jakobshavn Isbrae, western Greenland. *Hydrological Processes*, *25*(21), 3347-3355.

Leeson, A. A., Shepherd, A., Palmer, S., Sundal, A., & Fettweis, X. (2012). Simulating the growth of supraglacial lakes at the western margin of the Greenland ice sheet. *The Cryosphere*, *6*(5), 1077-1086.

Leeson, A. A., Shepherd, A., Sundal, A. V., Johansson, A. M., Selmes, N., Briggs, K., ... & Fettweis, X. (2013). A comparison of supraglacial lake observations derived from MODIS imagery at the western margin of the Greenland ice sheet. *Journal of Glaciology*, *59*(218), 1179-1188.

Leeson, A. A., Shepherd, A., Briggs, K., Howat, I., Fettweis, X., Morlighem, M., & Rignot, E. (2014). Supraglacial lakes on the Greenland ice sheet advance inland under warming climate. *Nature Climate Change*.

Lenaerts, J. T. M., Den Broeke, M. R., Berg, W. J., Meijgaard, E. V., & Kuipers Munneke, P. (2012). A new, high-resolution surface mass balance map of Antarctica (1979–2010) based on regional atmospheric climate modeling.*Geophysical Research Letters*, *39*(4).

Leprince, S., Ayoub, F., Klinger, Y., & Avouac, J. P. (2007, July). Co-registration of optically sensed images and correlation (COSI-Corr): An operational methodology for ground deformation measurements. In *Geoscience and Remote Sensing Symposium, 2007. IGARSS 2007. IEEE International* (pp. 1943-1946).

Liang, Y. L., Colgan, W., Lv, Q., Steffen, K., Abdalati, W., Stroeve, J., ... & Bayou, N. (2012). A decadal investigation of supraglacial lakes in West Greenland using a fully automatic detection and tracking algorithm. *Remote Sensing of Environment*, *123*, 127-138.

Liston, G. E., & Winther, J. G. (2005). Antarctic surface and subsurface snow and ice melt fluxes. *Journal of Climate*, *18*(10), 1469-1481.

Liu, S., Ding, Y., Shangguan, D., Zhang, Y., Li, J., Han, H., ... & Xie, C. (2006). Glacier retreat as a result of climate warming and increased precipitation in the Tarim river basin, northwest China. *Annals of Glaciology*,*43*(1), 91-96.

Luckman, A., Elvidge, A., Jansen, D., Kulessa, B., Kuipers Munneke, P., King, J., & Barrand, N. E. (2014). Surface melt and ponding on Larsen C Ice Shelf and the impact of foehn winds. *Antarctic Science*, *26*(06), 625-635.

Lüthje, M., Pedersen, L. T., Reeh, N., & Greuell, W. (2006). Modelling the evolution of supraglacial lakes on the West Greenland ice-sheet margin.*Journal of Glaciology*, *52*(179), 608-618.

MacAyeal, D. R., Scambos, T. A., Hulbe, C. L., & Fahnestock, M. A. (2003). Catastrophic ice-shelf break-up by an ice-shelf-fragment-capsize mechanism.*Journal of Glaciology*, *49*(164), 22-36.

MacAyeal, D. R., & Sergienko, O. V. (2013). The flexural dynamics of melting ice shelves. *Annals of Glaciology*, *54*(63), 1-10.

Marshall, S. J. (2006). Modelling glacier response to climate change. *Glacier Science and Environmental Change*, 163-173.

McGrath, D., Steffen, K., Rajaram, H., Scambos, T., Abdalati, W., & Rignot, E. (2012). Basal crevasses on the Larsen C Ice Shelf, Antarctica: Implications for meltwater ponding and hydrofracture. *Geophysical Research Letters*, *39*(16).

McMillan, M., Nienow, P., Shepherd, A., Benham, T., & Sole, A. (2007). Seasonal evolution of supra-glacial lakes on the Greenland Ice Sheet. *Earth and Planetary Science Letters*, *262*(3), 484-492.

Mernild, S. H., Liston, G. E., Steffen, K., & Chylek, P. (2010). Meltwater flux and runoff modeling in the ablation area of Jakobshavn Isbræ, West Greenland.*Journal of Glaciology*, *56*(195), 20-32.

Mellor, M. (1960). Temperature gradients in the Antarctic ice sheet. *Journal of Glaciology*, *3*, 773-782.

Miles, B. W. J., Stokes, C. R., Vieli, A., & Cox, N. J. (2013). Rapid, climate-driven changes in outlet glaciers on the Pacific coast of East Antarctica.*Nature*, *500*(7464), 563-566.

Moon, T., & Joughin, I. (2008). Changes in ice front position on Greenland's outlet glaciers from 1992 to 2007. Journal of Geophysical Research: Earth Surface (2003-2012), 113 (F2)

Morriss, B. F., Hawley, R. L., Chipman, J. W., Andrews, L. C., Catania, G. A., Hoffman, M. J., ... & Neumann, T. A. (2013). A ten-year record of supraglacial lake evolution and rapid drainage in West Greenland using an automated processing algorithm for multispectral imagery. *The Cryosphere*, *7*(6), 1869-1877.

Nienow, P., Sharp, M. and Willis, I. (1998). Seasonal changes in the morphology of the subglacial drainage system, Haut Glacier d'Arolla, Switzerland. *Earth Surface Processes and Landforms*, *23*(9),.825-843.

Parizek, B. R., & Alley, R. B. (2004). Implications of increased Greenland surface melt under global-warming scenarios: ice-sheet simulations. *Quaternary Science Reviews*, *23*(9), 1013-1027.

Paul, F., Huggel, C., & Kääb, A. (2004). Combining satellite multispectral image data and a digital elevation model for mapping debris-covered glaciers.*Remote Sensing of Environment*, *89*(4), 510-518.

Paul, F., & Andreassen, L. M. (2009). A new glacier inventory for the Svartisen region, Norway, from Landsat ETM+ data: challenges and change assessment.*Journal of Glaciology*, *55*(192), 607-618.

Phillips, T., Rajaram, H., & Steffen, K. (2010). Cryo-hydrologic warming: A potential mechanism for rapid thermal response of ice sheets. *Geophysical Research Letters*, *37*(20).

Picard, G., & Fily, M. (2006). Surface melting observations in Antarctica by microwave radiometers: Correcting 26-year time series from changes in acquisition hours. *Remote sensing of environment*, *104*(3), 325-336.

Pudsey, C. J., & Evans, J. (2001). First survey of Antarctic sub–ice shelf sediments reveals mid-Holocene ice shelf retreat. *Geology*, *29*(9), 787-790.

Rack, W., & Rott, H. (2004). Pattern of retreat and disintegration of the Larsen B ice shelf, Antarctic Peninsula. *Annals of Glaciology*, *39*(1), 505-510.

Rastner, P., Bolch, T., Notarnicola, C., & Paul, F. (2014). A comparison of pixel-and object-based glacier classification with optical satellite images.*Selected Topics in Applied Earth Observations and Remote Sensing, IEEE Journal of*, *7*(3), 853-862.

Raymond, C. F., & Nolan, M. A. T. T. (2000). Drainage of a glacial lake through an ice spillway. *IAHS publication*, 199-210.

Rignot, E., & Jacobs, S. S. (2002). Rapid bottom melting widespread near Antarctic ice sheet grounding lines. *Science*, *296*(5575), 2020-2023.

Rignot, E., Velicogna, I., Van den Broeke, M. R., Monaghan, A., & Lenaerts, J. T. M. (2011). Acceleration of the contribution of the Greenland and Antarctic ice sheets to sea level rise. *Geophysical Research Letters*, *38*(5).

Rippin, D. M., Pomfret, A., & King, N. (2015). High resolution mapping of supra-glacial drainage pathways reveals link between micro-channel drainage density, surface roughness and surface reflectance. Earth Surface Processes and Landforms.

Röthlisberger, H. (1972). Water pressure in intra-and subglacial channels.Journal of Glaciology, 11(62), 177-203.

Rothlisberger, H. and Lang, H. (1987). Glacial hydrology. Glacio-Fluvial Sediment Transfer: An Alpine Perspective. John Wiley and Sons, New York New York. 207-284.

Scambos, T. A., Dutkiewicz, M. J., Wilson, J. C., & Bindschadler, R. A. (1992). Application of image cross-correlation to the measurement of glacier velocity using satellite image data. *Remote Sensing of Environment*, *42*(3), 177-186.

Scambos, T. A., Hulbe, C., Fahnestock, M., & Bohlander, J. (2000). The link between climate warming and break-up of ice shelves in the Antarctic Peninsula. *Journal of Glaciology*, *46*(154), 516-530.

Scambos, T. A., Bohlander, J. A., Shuman, C. U., & Skvarca, P. (2004). Glacier acceleration and thinning after ice shelf collapse in the Larsen B embayment, Antarctica. *Geophysical Research Letters*, *31*(18).

Scambos, T. A., Haran, T. M., Fahnestock, M. A., Painter, T. H., & Bohlander, J. (2007). MODIS-based Mosaic of Antarctica (MOA) data sets: Continent-wide surface morphology and snow grain size. *Remote Sensing of Environment*,*111*(2), 242-257.

Schoof, C. (2007). Cavitation on deformable glacier beds. *SIAM Journal on Applied Mathematics*, *67*(6), pp.1633-1653.

Schoof, C. (2010). Ice-sheet acceleration driven by melt supply variability.*Nature*, *468*(7325), 803-806.

Selmes, N., Murray, T., & James, T. D. (2011). Fast draining lakes on the Greenland Ice Sheet. *Geophysical Research Letters*, *38*(15).

Sergienko, O., & Macayeal, D. R. (2005). Surface melting on Larsen ice shelf, Antarctica. *Annals of Glaciology*, *40*(1), 215-218.

Sergienko, O. V. (2013). Glaciological twins: basally controlled subglacial and supraglacial lakes. *Journal of Glaciology*, *59*(213), 3-8.

Shannon, S. R., Payne, A. J., Bartholomew, I. D., van den Broeke, M. R., Edwards, T. L., Fettweis, X., ... & Zwinger, T. (2013). Enhanced basal lubrication and the contribution of the Greenland ice sheet to future sea-level rise. *Proceedings of the National Academy of Sciences*, *110*(35), 14156-14161.

Shepherd, A., Wingham, D., Payne, T., & Skvarca, P. (2003). Larsen ice shelf has progressively thinned. *Science*, *302*(5646), 856-859.

Shepherd, A., Wingham, D., Wallis, D., Giles, K., Laxon, S., & Sundal, A. V. (2010). Recent loss of floating ice and the consequent sea level contribution.*Geophysical Research Letters*, *37*(13).

Sneed, W. A., & Hamilton, G. S. (2007). Evolution of melt pond volume on the surface of the Greenland Ice Sheet. *Geophysical Research Letters*, *34*(3).

Sole, A. J., Mair, D. W. F., Nienow, P. W., Bartholomew, I. D., King, M. A., Burke, M. J., & Joughin, I. (2011). Seasonal speedup of a Greenland marine-terminating outlet glacier forced by surface melt–induced changes in subglacial hydrology. *Journal of Geophysical Research: Earth Surface (2003–2012)*,*116*(F3).

Sole, A., Nienow, P., Bartholomew, I., Mair, D., Cowton, T., Tedstone, A., & King, M. A. (2013). Winter motion mediates dynamic response of the Greenland Ice Sheet to warmer summers. *Geophysical Research Letters*, *40*(15), 3940-3944.

Speirs, J. C., Steinhoff, D. F., McGowan, H. A., Bromwich, D. H., & Monaghan, A. J. (2010). Foehn Winds in the McMurdo Dry Valleys, Antarctica: The Origin of Extreme Warming Events*. *Journal of Climate*, *23*(13), 3577-3598.

Stammerjohn, S. E., Martinson, D. G., Smith, R. C., Yuan, X., & Rind, D. (2008). Trends in Antarctic annual sea ice retreat and advance and their relation to El Niño–Southern Oscillation and Southern Annular Mode variability. *Journal of Geophysical Research: Oceans (1978–2012)*, *113*(C3).

Steffen, K., & Box, J. (2001). Surface climatology of the Greenland ice sheet- Greenland Climate Network 1995-1999. *Journal of Geophysical Research. D. Atmospheres*, *106*, 33.

Steffen, K., Nghiem, S. V., Huff, R., & Neumann, G. (2004). The melt anomaly of 2002 on the Greenland Ice Sheet from active and passive microwave satellite o

Stroeve, J., Nolin, A., & Steffen, K. (1997). Comparison of AVHRR-derived and in situ surface albedo over the Greenland ice sheet. *Remote Sensing of Environment*, *62*(3), 262-276.

Sugiyama, S., Sawagaki, T., Fukuda, T., & Aoki, S. (2014). Active water exchange and life near the grounding line of an Antarctic outlet glacier. *Earth and Planetary Science Letters*, *399*, 52-60.

Sundal, A. V., Shepherd, A., Nienow, P., Hanna, E., Palmer, S., & Huybrechts, P. (2009). Evolution of supra-glacial lakes across the Greenland Ice Sheet.*Remote Sensing of Environment*, *113*(10), 2164-2171.

Tedesco, M. (2007). Snowmelt detection over the Greenland ice sheet from SSM/I brightness temperature daily variations. *Geophysical Research Letters*,*34*(2).

Tedesco, M., & Monaghan, A. J. (2009). An updated Antarctic melt record through 2009 and its linkages to high-latitude and tropical climate variability.*Geophysical Research Letters*, *36*(18).

Tedesco, M., & Steiner, N. (2011). In-situ multispectral and bathymetric measurements over a supraglacial lake in western Greenland using a remotely controlled watercraft. *The Cryosphere*, *5*(2), 445-452.

Tedesco, M., Fettweis, X., Van den Broeke, M. R., Van de Wal, R. S. W., Smeets, C. J. P. P., van de Berg, W. J., ... & Box, J. E. (2011). The role of albedo and accumulation in the 2010 melting record in Greenland.*Environmental Research Letters*, *6*(1), 014005.

Tedesco, M., Lüthje, M., Steffen, K., Steiner, N., Fettweis, X., Willis, I., ... & Banwell, A. (2012). Measurement and modeling of ablation of the bottom of supraglacial lakes in western Greenland. *Geophysical Research Letters*, *39*(2).

Tedesco, M., Willis, I. C., Hoffman, M. J., Banwell, A. F., Alexander, P., & Arnold, N. S. (2013). Ice dynamic response to two modes of surface lake drainage on the Greenland ice sheet. *Environmental Research Letters*, *8*(3), 034007.

Tedstone, A.J., Nienow, P.W., Gourmelen, N., Dehecq, A., Goldberg, D. and Hanna, E. (2015). Decadal slowdown of a land-terminating sector of the Greenland Ice Sheet despite warming. *Nature*, *526*(7575), pp.692-695.

Torinesi, O., Fily, M., & Genthon, C. (2003). Variability and trends of the summer melt period of Antarctic ice margins since 1980 from microwave sensors. *Journal of Climate*, *16*(7), 1047-1060.

Trusel, L. D., Frey, K. E., & Das, S. B. (2012). Antarctic surface melting dynamics: Enhanced perspectives from radar scatterometer data. *Journal of Geophysical Research: Earth Surface (2003–2012)*, *117*(F2).

Trusel, L. D., Frey, K. E., Das, S. B., Munneke, P. K., & Broeke, M. R. (2013). Satellite-based estimates of Antarctic surface meltwater fluxes. *Geophysical Research Letters*, *40*(23), 6148-6153.

Van den Broeke, M. R., & Van Lipzig, N. P. M. (2003). Factors Controlling the Near-Surface Wind Field in Antarctica*. *Monthly Weather Review*, *131*(4), 733-743.

van den Broeke, M. (2005). Strong surface melting preceded collapse of Antarctic Peninsula ice shelf. *Geophysical Research Letters*, *32*(12).

Van Der Veen, C. J. (2007). Fracture propagation as means of rapidly transferring surface meltwater to the base of glaciers. *Geophysical Research Letters*, *34*(1).

Van Wessem, J. M., Reijmer, C. H., Morlighem, M., Mouginot, J., Rignot, E., Medley, B., ... & Van Meijgaard, E. (2014). Improved representation of East Antarctic surface mass balance in a regional atmospheric climate model.*Journal of Glaciology*, *60*(222), 761-770.

Vaughan, D. G., & Doake, C. S. M. (1996). Recent atmospheric warming and retreat of ice shelves on the Antarctic Peninsula.

Weertman, J. (1973). Can a water-filled crevasse reach the bottom surface of a glacier. *IASH Publ*, *95*, 139-145.

Wessels, R. L., Kargel, J. S., & Kieffer, H. H. (2002). ASTER measurement of supraglacial lakes in the Mount Everest region of the Himalaya. *Annals of Glaciology*, *34*(1), 399-408.

Winther, J.G., Jespersen, M.N. and Liston, G.E., 2001. Blue-ice areas in Antarctica derived from NOAA AVHRR satellite data. *Journal of Glaciology*,*47*(157), pp.325-334.

Zwally, H. J., Abdalati, W., Herring, T., Larson, K., Saba, J., & Steffen, K. (2002). Surface melt-induced acceleration of Greenland ice-sheet flow.*Science*, *297*(5579), 218-222.